ELECTROCHEMICAL IMMUNOSENSOR FOR DETERMINATION OF LEPTOSPIRAL LIPL32 PROTEIN

Mr. Zunpitch Kwanyuen

A Thesis Submitted in Partial Fulfillment of the Requirements

for the Degree of Master of Science Program in Biomedical Engineering

Faculty of Engineering

Chulalongkorn University

Academic Year 2015

อิมมูโนเซนเซอร์ชนิดไฟฟ้าเคมีสำหรับการตรวจวัดโปรตีน LipL32 ของเชื้อเลปโตสไปรา

นายสัณห์พิชญ์ ขวัญยืน

วิทยานิพนธ์นี้เป็นส่วนหนึ่งของการศึกษาตามหลักสูตรปริญญาวิทยาศาสตรมหาบัณฑิต
สาขาวิชาวิศวกรรมชีวเวช
คณะวิศวกรรมศาสตร์ จุฬาลงกรณ์มหาวิทยาลัย
ปีการศึกษา 2558

Thesis Title	ELECTROCHEMICAL IMMUNOSENSOR FOR DETERMINATION OF LEPTOSPIRAL LIPL32 PROTEIN
By	Mr. Zunpitch Kwanyuen
Field of Study	Biomedical Engineering
Thesis Advisor	Associate Professor Seeroong Prichanont, Ph.D.
Thesis Co-Advisor	Assistant Professor Kanitha Patarakul, Ph.D.

Accepted by the Faculty of Engineering, Chulalongkorn University in Partial Fulfillment of the Requirements for the Master's Degree

.....Dean of the Faculty of Engineering

(Professor Dr. Bundhit Eua-arporn, Ph.D.)

THESIS COMMITTEE

.....Chairman

(Associate Professor Mana Sriyudthsak, Ph.D.)

.....Thesis Advisor

(Associate Professor Seeroong Prichanont, Ph.D.)

.....Thesis Co-Advisor

(Assistant Professor Kanitha Patarakul, Ph.D.)

.....External Examiner

(Lerdluck Kaewvimol, Ph.D.)

สัณห์พิชญ์ ขวัญยืน : อิมมูโนเซนเซอร์ชนิดไฟฟ้าเคมีสำหรับการตรวจวัดโปรตีน LipL32 ของเชื้อเลปโตสไปรา (ELECTROCHEMICAL IMMUNOSENSOR FOR DETERMINATION OF LEPTOSPIRAL LIPL32 PROTEIN) อ.ที่ปรึกษาวิทยานิพนธ์หลัก: รศ. ดร.สีรุ้ง ปรีชานนท์, อ.ที่ปรึกษาวิทยานิพนธ์ร่วม: ผศ. ดร. พญ.กนิษฐา ภัทรกุล, 131 หน้า.

LipL32 เป็นโปรตีนพื้นผิวเซลล์ที่มีอยู่เฉพาะบนเซลล์แบคทีเรียสายพันธุ์ *Leptospira* ชนิดก่อโรคเท่านั้น ซึ่งเป็นสาเหตุของโรคฉี่หนู เนื่องจากโรคฉี่หนูเป็นโรคที่เกิดจากสัตว์ที่มีความสำคัญระดับนานาชาติแต่อุปกรณ์ในการตรวจวินิจฉัยยังไม่มีประสิทธิภาพ และ/หรือไม่สามารถเข้าถึงพื้นที่กันดารห่างไกลซึ่งเป็นพื้นที่หลักที่ได้รับผลกระทบได้ ความจำเป็นในการสร้างอิมมูโนเซนเซอร์เพื่อตรวจจับโรคนี้จึงค่อนข้างชัดเจน ในงานนี้ อิมมูโนเซนเซอร์สำหรับการตรวจวัดโปรตีน LipL32 ได้ถูกสร้างขึ้น ปรัสเซียน บลู ได้ถูกนำมาผสมเข้ากับ Graphene-PEDOT:PSS เป็นสารผสม กราฟีน-ปรัสเซียน บลู (GPB) สารผสมนี้ถูกนำไปหยดเคลือบลงบนอิเล็กโทรดคาร์บอนพิมพ์สกรีน (SPCE) ซึ่งต่อมาถูกนำมาเคลือบด้วยไคโตซาน (CS) และอนุภาคทองชนิดห่อหุ้มด้วยซิเตรต (cAuNPs) อิเล็กโทรดที่ถูกปรับปรุงแล้วนี้ก็ถูกนำมาปรับปรุงเพิ่มเติมด้วยการบ่มกับ *Staphylococcal* Protein A และแอนติบอดี้ชนิดจับกับ LipL32 (Ab) เพื่อการตรวจจับ LipL32 ที่ไวยิ่งขึ้น จากนั้นซีรั่มอัลบูมินจากวัว (BSA) ถูกนำมาใช้เคลือบชั้นบนสุดของอิเล็กโทรดเพื่อป้องกันการจับกันอย่างไม่จำเพาะของอิเล็กโทรดกับชีวโมเลกุลอื่นๆที่ไม่เกี่ยวข้อง อิเล็กโทรดที่ถูกปรับแต่งจนมีประสิทธิภาพสูงสุดสามารถนำมาใช้ตรวจจับ LipL32 ได้โดยมีระยะการตรวจวัดที่ให้ค่าเป็นเส้นตรงบริเวณ 50 ถึง 200 นาโนกรัม/มล. และ 250 ถึง 600 นาโนกรัม/มล. มีลิมิตของการตรวจจับเท่ากับ 54.98 นาโนกรัม/มล. โดยมีค่าเบี่ยงเบนมาตรฐานของการผลิตอิเล็กโทรดซ้ำที่ 8.254 นอกจากนั้น การทดสอบกับเซลล์ *Leptospira interrogans* ชนิดมีชีวิตแบบที่ยังคงสภาพและแบบที่ถูก sonicated ได้ผลการทดสอบว่ามีระยะการตรวจวัดที่ให้ค่าเป็นเส้นตรงบริเวณ 10 ถึง 100 เซลล์/มล. และลิมิตของการตรวจจับเท่ากับ 44.29 เซลล์/มล. และ 77.25 เซลล์/มล. ตามลำดับ ความเสถียรของอิเล็กโทรดก็อยู่ในระดับที่น่าพอใจเช่นกัน โดยมีการลดลงของสัญญาณกระแสตอบสนองเพียง 6.79% หลังการเก็บรักษาในสภาวะแห้งที่ 4 องศาเซลเซียสเป็นเวลา 3 สัปดาห์

สาขาวิชา วิศวกรรมชีวเวช ลายมือชื่อนิสิต .....

ปีการศึกษา 2558 ลายมือชื่อ อ.ที่ปรึกษาหลัก .....

ลายมือชื่อ อ.ที่ปรึกษาร่วม .....

5670422621 : MAJOR BIOMEDICAL ENGINEERING

KEYWORDS: GRAPHENE-BASED ELECTROCHEMICAL SENSOR / ELECTROCHEMICAL BIOSENSER / LEPTOSPIRA SPP. / LIPL32 / IMMUNOSENSOR

ZUNPITCH KWANYUEN: ELECTROCHEMICAL IMMUNOSENSOR FOR DETERMINATION OF LEPTOSPIRAL LIPL32 PROTEIN. ADVISOR: ASSOC. PROF. SEEROONG PRICHANONT, Ph.D., CO-ADVISOR: ASST. PROF. KANITHA PATARAKUL, Ph.D., 131 pp.

LipL32 is a surface membrane protein present only on pathogenic *Leptospira* species, which are the cause of Leptospirosis disease. As this zoonotic disease is of global importance but current diagnostic tools are still ineffective and/or inaccessible to rural areas which are affected, the need to develop an immunosensor for its detection is clear. In this work, an immunosensor for LipL32 protein was developed. Prussian blue was mixed with Graphene-PEDOT:PSS, creating Graphene-Prussian blue composite (GPB). The GPB was drop-casted on screen-printed carbon electrode (SPCE) which was later coated by Chitosan (CS) and citrate-capped gold nanoparticles (cAuNPs). The modified electrode was then further incubated with *Staphylococcal* protein A (PrA) and anti-LipL32 antibodies (Ab) for more sensitivity in LipL32 detection. Bovine Serum Albumin (BSA) then was used to coat the topmost layer to prevent non-specific binding of the electrode to unrelated biomolecules. The optimum electrode obtained could be used to detect LipL32 in a linear range of 50 to 200 ng ml^{-1} and 250 to 600 ng ml^{-1}, lower detection limit of 54.98 ng ml^{-1} with RSD of reproducibility at 8.254. Furthermore, tests with intact and sonicated *Leptospira interrogans c*ells resulted in linear range of 10 to 100 cells ml^{-1}, lower detection limit of 44.29 cells ml^{-1} and 77.25 cells ml^{-1}. The stability of the fabricated electrode also satisfactory, with only 6.79% drop in residual response current after three weeks of storage at 4°C in dried form.

Field of Study: Biomedical Engineering Student's Signature .....

Academic Year: 2015 Advisor's Signature .....

Co-Advisor's Signature .....

ACKNOWLEDGEMENTS

The author would like to thank many people. Firstly, Assoc.Prof. Dr. Seeroong Prichanont, who has been a really, really great advisor. Without her guidance this thesis could never happen. Asst. Prof. Dr. Kanitha Patarakul for providing a lot of antibody and antigen without ever collecting a fee, who has also been a great advisor and supporter for this work. My friends who lent me help in serious time of need. Part of me that never let me give up. Anonymous people on the internet who released DRM-free electrochemical textbooks for students like me to study on. And last but not least, my family who has always been supportive and encouraging about my decisions in life. I am truly grateful.

CONTENTS

Page

Page

Page

Page

Page

Page

Abbreviations

α	=	Alpha
β	=	Beta
δ	=	Delta
ε	=	Epsilon
γ	=	Gamma
λ	=	Lambda
Γ	=	Electrode surface coverage
°C	=	Degree Celsius
%RSD	=	Percentage of relative standard deviation
µA	=	Microampere
µL	=	Microliter
A	=	Ampere
Ab	=	Antibody
AFM	=	Atomic force microscopy
AFP	=	Alfa-fetoprotein
Ag	=	Antigen
Ag/AgCl	=	Silver/silver chloride
BG	=	Berlin green
BSA	=	Bovine serum albumin
cAuNP	=	Citrate-capped gold nanoparticles
cm^2	=	Square centimeter
cTNT	=	Cardiac troponin T
C	=	Concentration of diffusion material
CEA	=	Carcinogenic embryonic antigen
CS	=	Chitosan
CV	=	Cyclic voltammetry
C/mol	=	Coulomb per mole
DNA	=	Deoxyribonucleic acid
et al.	=	And other

etc.	=	And so on...
ex.	=	Example
ELISA	=	Enzyme-linked immunosorbent assay
EMJH	=	Ellinghausen–McCullough–Johnson–Harris medium
ES	=	Everitt's salt
fg	=	Femtogram
F	=	Faraday's constant
Fab	=	Fragment antigen binding
Fc	=	Fragment crystallizable of antibody
$FeCl_3$	=	Ferric chloride
FDA	=	Food and drug administration
g	=	Gram
g/mol	=	Gram per mole
GO	=	Graphene oxide
GPB	=	Graphene PEDOT:PSS Prussian blue
GR	=	Graphene
H	=	Heavy chains
$HAuCl_4.3H2O$	=	Chloroauric acid
hrs	=	Hours
IgA	=	Immunoglobulin A
IgD	=	Immunoglobulin D
IgE	=	Immunoglobulin E
IgG	=	Immunoglobulin G
IgM	=	Immunoglobulin M
IL-6	=	Interleukine-6
ITO	=	Indium Tin Oxide
IUPAC	=	International union of pure and applied chemistry
kDa	=	Kilodalton
KCL	=	Potassium chloride
$K_4[Fe(CN)_6]$	=	Patassium ferrocyanide

L	=	Light chains
LoB	=	Limit of blank
LoD	=	Limit of detection
LSPR	=	Localized Surface Plasmon Resonance
m	=	Meter
mg	=	Milligram
mL	=	Milliliter
mg/mL	=	Milligram per milliliter
mol	=	Mole
mM	=	Millimolar
mV	=	Millivolt
M	=	Molar
MAT	=	Microscopic agglutination test
ng	=	Nanogram
ng/mL	=	Nanogram per milliliter
NaOH	=	Sodium hydroxide
$Na_3C_6H_5O_7$	=	Trisodium citrate
NFDM	=	Non-fat dairy milk
O	=	Oxidized
pg	=	Picogram
PB	=	Prussian blue
PBS	=	Phosphate buffer saline
PB-GR	=	Prussian blue-graphene
PCR	=	Polymerase chain reaction
PEDOT:PSS	=	Poly(3,4-ethylenedioxythiophene) polystyrene sulfonate
PEI	=	Polyethylenimine
PrA	=	Staphyloccocal protein A
PW	=	Prussian white
QCM	=	Quartz crystal microbalance
R	=	Reduced

s	=	Second
spp.	=	Species
SAW	=	Surface acoustic waves
SCE	=	Standard calomel electrode
SEM	=	Scanning electron microscope
SPE	=	Screen-printed electrode
SPEC	=	Screen-printed carbon electrode
SPR	=	Surface Plasmon Resonance
SWCNT	=	Single-walled carbon nanotube
S/cm	=	Siemens per centimeter
t	=	Time
T	=	Temperature
TPa	=	Terrapascal
v/v	=	Volume by volume
V	=	Volt
WHO	=	World health organization
x	=	Distance from electrode surface

Chapter 1

Introduction

1.1. Leptospirosis

Fast, reliable, and efficient pathogen detection for diagnostic purpose has always been a high priority for healthcare workers. Some diseases are hard to differentiate from others, and one of them is known as Leptospirosis, which has been recorded as one of the most widespread zoonotic (animal-to-human) disease [1].

Leptospirosis is an infectious disease caused from direct contact with soil or water that is contaminated with pathogenic spirochetes of the genus *Leptospira*. Inexperienced or untrained physicians with no access to specialized laboratory may prone to misdiagnose its symptoms as other febrile or hemorrhagic diseases such as influenza or dengue fever diseases. As confirmed by a study in 2004 that a clinical-based diagnosis of Leptospirosis was correct only 143 cases out of 700 suspected cases, or around 20 percent [2].

After the infection and incubation period, some patients may not display any symptoms at all. Ninety percents of patients that show symptoms usually fully healed of disease after passing the first phase of febrile or hemorrhagic Leptospirosis. Nevertheless, the remaining 10% will proceed onto developing severe Leptospirosis which is the second phase, known as Weil's Disease, which would cause high mortality rates from serious complications such as severe lung injury, heart failure, pulmonary oedema (excessive fluid retention), acute renal failure, respiratory failure, internal bleeding, and death [3, 4].

Global burden of this disease is around 300,000 to 500,000 cases per year, with highest death rate per year at 30% [5]. In Thailand, a National Disease Surveillance (Report 506) statistic for Leptospirosis in 2012 by Bureau of Epidemiology shows there was 4,130 diagnosed patients countrywide, calculated as 6.50 patients per 100,000 population, with 60 deaths resulting in mortality rate of 0.09 per 100,000 population. By district, Ranong had the highest number of patient, at 227.73 patients per 100,000 population. The highest percentages of patients' occupation countrywide are in agricultural sector, common services, and students at 58.5%, 19.9%, and 10.2% respectively [6]. Recent endemic outbreak of Leptospirosis in Southeast Asia has also raised awareness of the need to improve rapid Leptospirosis diagnostic method further [7]. Furthermore, climate change, flooding, and extended urbanization also result in upsurge of *Leptospira* infections, and enhanced surveillance for

Leptospirosis is strongly suggested to reduce burden of this disease [8].

These information implies this disease is on the uptrend, especially in the tropical zone such as Southeast Asia, and those who suffer the most from this disease are of the low-income household in rural areas who have little to no access to specialized physicians or laboratories. Therefore, diagnostic kits which is reliable, accurate, inexpensive, accessible even in remote areas, and easy to operate need to be developed and utilized to subside suffering and death caused by this disease.

LipL32 outer membrane protein is a protein present only in pathogenic species of *Leptospira* and can also be used to detect whole-cell *Leptospira*, thus it can be used as the antigen for this application [9].

1.1.1. Problems in Leptospirosis diagnosis

There are various tests that can be used to diagnose Leptospirosis ranging from direct examination, blood cultures, urine tests, direct probing on DNA by polymerase chain reaction (PCR), to serological diagnosis. Howver, these methods require appropriate laboratory support in general, which make laboratory diagnosis of Leptospirosis a confusing topic for personnel involved [10].

Standard method for culturing of *Leptospira* for diagnostic test is to drop 100-200 µL of whole blood into Ellinghausen–McCullough–Johnson–Harris (EMJH) medium supplemented with 3% rabbit serum and 0.1% agarose [11, 12], some serotypes are even more fastidious and require more specific nutrients to grow. All of these are costly reagents. Moreover, growth of *Leptospira* is relatively slow, having best doubling time of about 6-8 hours. It grows very slowly to the point that by the time of culture confirmation, which take about 5-10 days to complete, antibodies level in patient would already high enough for serological confirmation, such as Microscopic Agglutination Test (MAT) test [13].

Also in counting cultured *Leptospira*, the current standard is using Petroff-Hausser counting chamber and dark-field microscope, which is time-consuming, laborious, and prone to error of operator as recognition of leptospires is difficult. Due to it being thin and small, unrelated materials such as fibrin and protein threads may easily be mistaken as leptospires [14, 15].

For MAT, the test cannot be conducted in the first week after infection due to the amount of antibody has not yet risen to the detectable level [16]. After patient's antibody has risen to considerable level, the test has to be conducted with every type of known endemic *Leptospira* serovars to test of patient's antibody agglutination to the *Leptospira* antigen samples. Furthermore, MAT test must conducted at least two times to compare with each other to see if the antibody level has risen at least 4 fold or not, which is the cut-off point for

Leptospira infection confirmation. Therefore, this test require constant maintenance of *Leptospira* spp. which are extremely costly, tedious, and rarely available even in medical centers. This method even considered an unreliable predictor of the infecting serovars in Thailand [17].

Other alternatives are immunostaining and PCR. These tests also require established laboratory, trained lab technicians, and lots of reagents, which are expensive. Each of these tests still requires considerable training, materials and reagents, and equipment, which some distant and impoverished places cannot afford. Even in non-impoverished area that can afford these tests, they are still not favorable because they are time-consuming. Even for experienced physicians, this situation leads to inevitable empirical treatment of suspected early stage Leptospirosis infection to prevent the bacterium from spreading to organs, which would result in onset of second phase that involves organ failure. Therefore, successful direct detection of the *Leptospira* bacterium would create a way to circumvent these cumbersome detection methods, as it can confirm Leptospirosis during any stage of infection. This is the reason that inspire us to create an immunosensor for detection of antigen (LipL32) which are present only on the surface of the pathogenic *Leptospira* species.

Due to difficulties described above, some hospitals start to apply Enzyme-link Immunosorbent assay (ELISA) as an alternative method of *Leptospira* diagnosis, which is of significantly lower costs and assay time (as low as 30 minutes) [18].

Immunosorbent assay is a biochemical test for measurement of macromolecules by utilizing highly specific interaction between antigen (Ag) and antibody (Ab), and is a subset of biosensors. Or to be more specific, a subset of affinity-based biosensor, which means a biosensor that utilize the bioaffinity between antigen and antibody to create the result [19]. Antibodies are protein produced by immune system of animals and have unique structure which makes them bind to its antigen counterpart specifically. ELISA has been used for myriad of purposes ranging from industrial inspection to clinical analysis [20, 21]

However, even ELISA test can also be affected by lack of quality resources, such as lack of pure water to wash the plates after antibody incubation, or a trained lab technician. Also even ELISA has high specificity due to antibody-antigen selective interaction, and high sensitivity from enzyme-based amplification [22], it still has problems of relatively high reagent consumption, which is a limiting factor for its uses in developing countries [23]. This leads to development of many derivatives of ELISA-based methods with have considerable decrease in reagent usage, and one of the most popular methods is called electrochemical ELISA, or electrochemical immunosensor, which is a subset of biosensors.

1.1.2. Amperometric electrochemical ELISA: A solution

Biosensors are analytical devices that convert biochemical phenomenon into measurable signal via a transducer, and offer the opportunity of rapid, real-time, sensitive, and capable for "point-of-care" diagnostic testing [24]. Its definition, according to IUPAC (1997), is "a device that uses specific biochemical reactions mediated by isolated enzymes, immunosystem, tissues, organelles, or whole cells to detect chemical compounds usually by electrical, thermal, or optical signals." [25]

The idea of developing "rapid point-of-care sensor", has been around since 1995 [26] but with limited success due to material and technology limitations. However, in the past decade there has been rapid development, especially with the discovery of Graphene by Geim and Novoselov in the year 2010, which is one of the most conducting materials known today, giving boost to interests in research and development of biosensor to become more popular [27, 28].

The ultimate goal of this project is to develop an electrode for detection of LipL32, the major outer membrane protein of pathogenic leptospires for potential point-of-care diagnosis of Leptospirosis based on electrochemical immunoassay technique. As stated before, application of carbon screen-printed electrode will contribute to low-cost, easy-to-use, miniaturized, and high sensitivity, while LipL32 will potentially indicate if pathogenic type of *Leptospira* bacterium is present in the sample or not.

Furthermore, the specificity to LipL32 of the developed electrochemical electrode can be adjusted to be specific to other antigen as the situation required by changing the antibodies that are to be immobilized, which is potentially beneficial to medical diagnostic in wider frame.

To the best of our knowledge, there has been no publication of label-free amperometric immunosensor for detection of LipL32 outer membrane protein or *Leptospira* spp. before.

1.2. Objective and Outline of Thesis

1.2.1. Objective

Develop an immunosensor electrode for detection of LipL32 outer membrane protein

1.2.2. Scope of Research

1.2.2.1. Assemble Graphene-PEDOT:PSS/ Prussian blue/Chitosan/cAuNPs/anti-LipL32 antibody nanocomposite film on screen-printed carbon electrode (SPCE) and utilize it as a working electrode in three-electrodes electrochemical cell.

1.2.2.2. Electrochemically characterize the composite film before and after application of LipL32

antigen.

1.2.2.3. Optimize fabrication process:

1.2.2.3.1. Vary number of Graphene-PEDOT:PSS/ Prussian blue layers

1.2.2.3.2. Vary antibody concentration (0-10 µg/ml)

1.2.2.3.3. Fixed parameters are baking time, concentration and volume of Graphene-PEDOT:PSS, concentration of Prussian blue, cycle number of Cyclic voltammetry (CV), concentration of Polyethylenimine (PEI), concentration of BSA.

1.2.2.4. Electrochemically characterize the electrode:

1.2.2.4.1. Cyclic voltammetry

1.2.2.4.1.1. Vary scan rate to determine reversibility

1.2.2.4.1.2. Study effect of electrode modifications on CV

1.2.2.4.2. Amperometry

1.2.2.4.2.1. Detection limit

1.2.2.4.2.2. Calibration curve

1.2.2.4.2.3. Reproducibility

1.2.2.4.2.4. Storage stability

1.2.2.4.3. Fixed parameters are pH, incubation temperature, concentration of antigen. Concentration of antigen will be in the range from of 10 ng/ml to 600 ng/ml.

1.2.2.5. Optimize analytical conditions. (pH 6-8, antibody incubation time)

1.2.2.6. Characterize the physiology of fabricated electrode by Scanning electron microscope

1.2.3. Expected Outcome

1.2.3.1. Attain optimized SPCEs surface modification method that is inexpensive, suitable, and efficient for point-of-care diagnosis.

1.2.3.2. Attain electrode for LipL32 antigen detection for clinical diagnosis with electrochemical method that is accurate, reliable, inexpensive, and can be used in real situation.

Chapter 2

Theories

Every immunoassays are based on the ability of antibodies to form complex with its corresponding antigen, which is a very specific molecular interaction and would result in high sensitivity of immunoassay methods [29, 30]. Immunoassays offer simple, fast, sensitive, and easily automated alternative to golden standard of bacterial culture test and plate counting. One of the most well-known method of immunoassay is called enzyme-linked immunoassay (ELISA), which principles are further adapted for fabrication of immunosensors. Thus, principles of ELISA must first be understood to be able to comprehend how immunosensor systems work.

The theories that are going to be discussed here are guideline of point-of-care immunosensors, ELISA, principles of electrochemical immunosensors, its compositions, modifying materials, and antigen-antibody interaction.

2.1 Point-of-Care immunosensors

Accurate and fast prognosis has always been one of the top priorities in healthcare industry, as patient can hardly heal if diagnosis is wrong and untimely. Current trend of clinical diagnostic has two directions: Centralized, automated laboratories and decentralized, point-of-care testing [31]. In impoverished environment, laboratories by the principle of centralization are not only hindered by environmental factors such as unreliable power supply, hard-to-access location, and poor water quality but also the factor in the laboratory itself such as lack of facility, equipment, funding, and shortage of trained personnel [32].

Hence, in developing countries, decentralized point-of-care testing method has more potential impact over traditional lab-based protocols due to its distributability and lack of restrictions above. Especially when that point-of-care method is inexpensive, easy to use, and requires minimum steps in its utilization. Point-of-care testing can be classified in to three types: In *vivo* (ex. fiber optics), Ex *vivo* (ex. connected to patient's tubing), and In Vitro (entirely not connected to patient), and they are is not something new. The first point-of-care immunoassay principle was first brought to application about half a century ago [33].

By definition, point-of-care testing means testing performed near patients in locations not restricted

only to a laboratory or a hospital [34]. World Health Organization (WHO) and Food and Drug Administration (FDA) had brought about rough guidelines for desirable point-of-care diagnostic apparatuses, especially for less-developed areas as [35, 36]:

- Affordable and equipment-free
- Sensitive (minimal false positive)
- Specific (minimal false negative)
- User- Friendly (easy to operate and requiring little training program)
- Rapid (to ensure proper treatment at the initial visit) and robust
- Deliverable to those who need it
- Automated instrument.
- Need no processing of analyte before testing
- Simple operation prerequisites.
- One-step testing
- Requires minimal maintenance, calibration, interpretation, and calculation.

Nevertheless, application in realistic environment requires even more parameters than those given by WHO and FDA, such as feasibility (can be readily applied in a given condition), and liability (limit of detection, detection range, etc.). One way to improve its feasibility is to make the diagnostic kit simple enough to use even by untrained personnel.

2.2 Enzyme-linked immunosorbent assay (ELISA)

As the name described, ELISA is a test that involves using a substrate consisting of antigen and enzyme-tagged antibody. If these enzymes are present, addition of substrate would generate products, and measurement of this product or by-product of product generation would quantify the amount of antigen present in that respective well [37].

Normally, ELISA test uses 96-welled radioactive-treated polystyrene plate as the substrate. There are two types of ELISA: direct and indirect. Furthermore, choice of applying antibody or antigen onto it leads to two subclasses: direct and indirect ELISA, depending on the objects that generates signal and overall conformation. Note that these terminologies would be used differently in the case of immunosensors.

For normal direct and indirect ELISA, the first immobilized material is the antigen (Ag), as presented in

figure 1 (a) and **figure 1 (b)**. Direct ELISA corresponds to the ones where enzyme tagged antibody (Ab) binds with Ag, while indirect ELISA incorporates another Ab as a linker between Ag and enzyme-tagged Ab.

As for **sandwich** direct and indirect ELISA, **figure 1 (c)** and **figure 1 (d)**, the principles are the same except that the first material to be immobilized are the Ab specific to the Ag. The purpose of "sandwiching" is that the sample does not have to be purified (isolated) before analysis, as the antibodies on the surface would isolate and adhere only to the antigen, which would also make it more sensitive than normal ELISA [38].

However, ELISA has several drawbacks such as bulkiness, power-intensive, and potential false signals from colored samples. Furthermore, it is also labor-intensive, requires specialized knowledge in conducting and handling, and requires a lot of expensive reagents. These problems can pose a barrier for use in point-of-care situation by untrained hands, and electrochemical methods seem to be the most promising alternative [39].

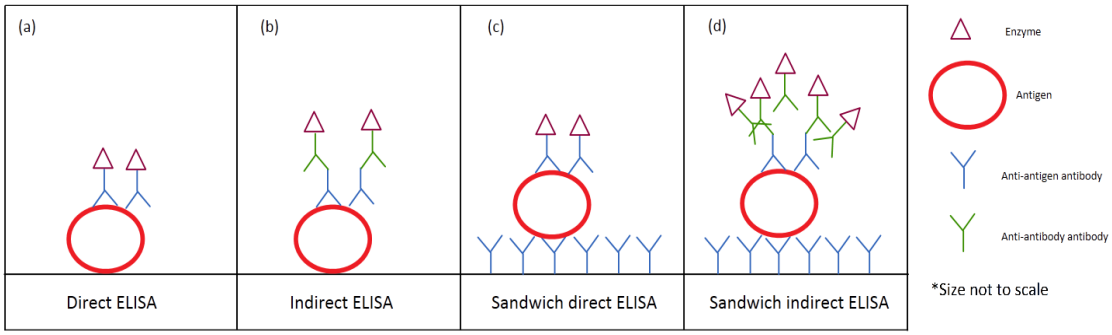

Figure 1: Different types of conventional ELISA, adapted from [38]

2.3 Working Principles of Immunosensor

Immunosensor is a device composed of an antigen or antibody species coupled to a signal transducer, which detects the binding of the complementary species [40]. It is an application of ELISA on transducers which interpret obtained information into quantitative digital form. Its principle is to detect formation of antigen-antibody complexes which will affect generation of transducer's signal, or surface reaction capacity, just like ELISA with a twist. Its primary advantages over ELISA are in its increased sensitivity, lower detection limit, more cost effective, simple and less labor-intensive, reduced usage of expensive reagents, and potential of automation and portability [41].

In general immunosensors, the receptor molecules (antibodies) are immobilized on the working electrode, available for attachment with antigen. They can be classified further into two classes. One is direct (label-free) measurement such as optical, piezoelectric, acoustic bulk-wave based, impedance-based, and non-enzymatic amperometric method, which requires no involvement of secondary antibodies. Another is indirect

(label-based) measurement which applies the second set of antibodies labeled with traceable elements such as fluorophore, enzyme, luminescent compound, and conductive polymer to indicate the presence of antigen [42, 43].

Changed signals (optical, mass-based, and electrochemical) before and after Ab-Ag formation are then measured and interpret by a transducer. Mainly, there are four types of transducers: Optical (optrodes), Calorimetric (thermistors), Mass (piezoelectric), and Electrochemical (electrodes) (see **figure 2**).

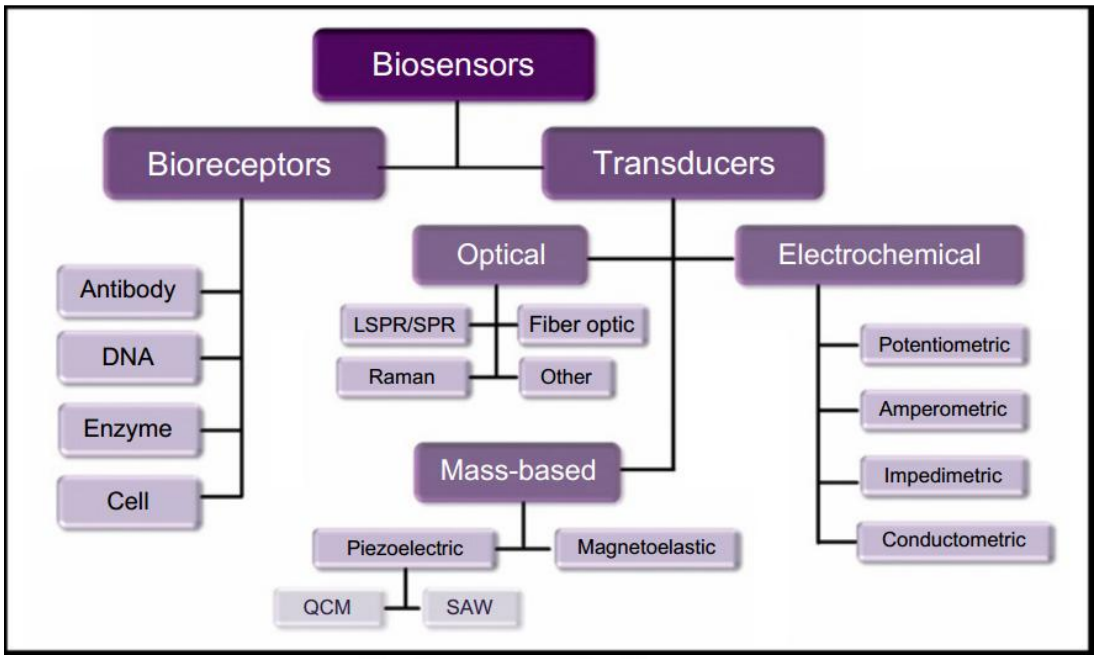

Figure 2: Classification of biosensors according to bioreceptors and transducers [44].

The electrochemical-based immunosensor has advantages over others in its simplicity, fast response, portability, usable in non-transparent media, comparatively inexpensive equipment and operation costs, capability of miniaturization, high sensitivity and selectivity, low power requirement, and low limit of detection (LoD) when compared with other methods, reaching as low as femtomolar levels [44-49]. In addition, electrochemical-based measurement can be developed for both “direct” (label-free) type, as shown in **figure 3 (a)** and “indirect” (label-based) as in **figure 3 (b)** and **figure 3 (c)**.

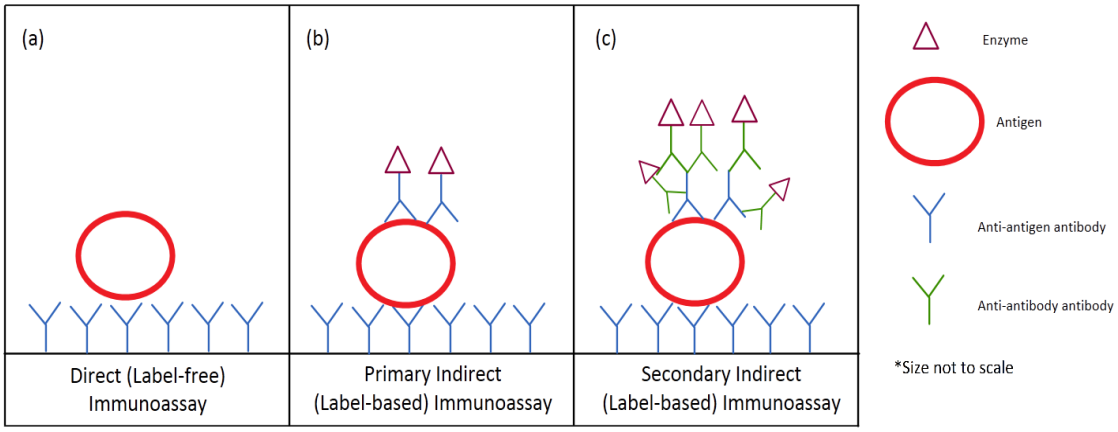

Figure 3: Different types of electrochemical immunosensors. Adapted from [39] and [50]

2.3.1 Electrochemistry

2.3.1.1 Background information

First and foremost, the concept of how current change according to stimulus must be explained. The current is equal to change in charge with time, expressed as:

$$i = \frac{\mathrm{d}Q}{\mathrm{d}t} \tag{1}$$

Where I is faradaic current (unit in amperes, A), t is time in seconds, Q is charge in coulombs given by faraday's law:

$$Q = nFN \tag{2}$$

Where *n* is number of electrons transferred per mole of produced, *F* is Faraday's constant (96,485.3 C/mol), *N* is amount of materials electrolyzed (unit in mol).

Chemical reaction can be either *homogeneous*, occurring in a single phase, and has rate of reaction uniform everywhere in the volume, which would be expressed as:

$$\text{Rate } [\text{mol sec}^{-1}] = \frac{\mathrm{d}N}{\mathrm{d}t} \tag{3}$$

While in electrochemistry and most realistic works, chemical reactions are *heterogeneous*, as it occurs on the electrode surface, which must also take the area, A in cm^2, of the electrode where the reaction occurs into account. Rate of reaction must be normalized for the area of electrode to be able to compare processes that occur at electrode of varying size, using this expression:

$$\text{Rate [mol sec}^{-1}\ \text{cm}^{-2}] = \frac{i}{nFA} = \frac{j}{nF} \quad (4)$$

Where j is current density in unit of ampere per cm^2. As the equation expresses, electrode area is a critical factor to the amount of product created in bulk electrolysis. Now consider the redox reaction at the electrode. Redox reaction can occur both ways, depending on the process of gaining (reduction) or losing electron (oxidation)

$$O + n\,e^- \longleftrightarrow R \quad (5)$$

Unlike classic chemical reaction which rate depends strongly on the temperature as described by Arrhenius equation, electrochemical reaction depends on the electrical potential applied to the electrodes. After the voltage is applied to the electrodes, if the analyte is electroactive, the analyte will undergo redox reaction (whether oxidation or reduction).

In absence of current, the concentrations of two species, Oxidized (O) and reduced (R) are not changed and the relationship to electrode potential can be explained by **Nernst equation**;

$$E = E^{0'} + \frac{RT}{nF}\ln\left(\frac{C_O}{C_R}\right) \quad (6)$$

Where E is equilibrium potential in volts, $E^{0'}$ is the formal potential, R is the gas constant, T is temperature in kelvin unit, n is number of electron transferred per mol of reactant, F is Faraday's constant, C_O is the concentration of the oxidized specie, and C_R is the concentration of the reduced specie. Both concentrations are defined as the concentrations immediately on the electrode surface.

As presented in **figure 4.** There are four factors governing redox reaction rate and current at electrodes: **mass transport** of redox species to and from the electrode surface, **preceding and following reactions** if the redox species is initially unstable after redox reaction or is an intermediate or product that has to be generated from chemical reaction, **surface reactions** where the redox species adsorb itself to the electrode surface, and **kinetics of electron transfer** in the redox reaction at the electrode surface. Of all four steps, the slowest step will be the rate-determining step [51, 52].

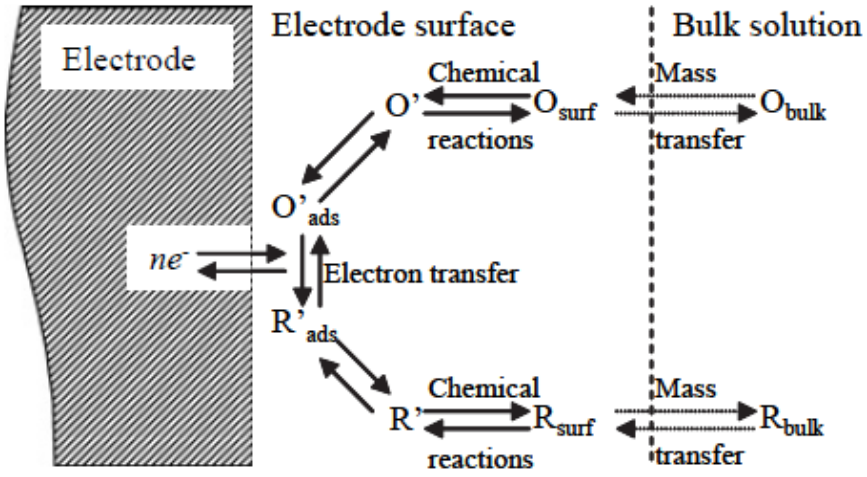

Figure 4: Process involved in an electrode reaction[52]

As for kinetics of redox reaction at the electrode surface, there are commonly four situations [51].

1. At the equilibrium potential (all redox processes are in equilibrium), current density will be zero and no net chemical change. The electrode potential can be calculated from Nernst equation.
2. Close to equilibrium potential, electron transfer will be very slow and will be the rate-determining step, which obeys Butler-Volmer equation.
3. Intermediate overpotential, rate of electron transfer and mass transfer are similar and simple equations will not be obeyed.
4. At very high overpotential, rate of electron transfer increase to a very high level and mass transfer become rate-determining step. Surface concentration of redox species will be zero and only equations related to mass transfer will be applied, which shall be elaborated more below.

As unnecessary problems must be eliminated to reduce complications, the best approach is to maximize every steps and leave only the **mass transport** as the slowest stage because it is the key reaction in electrochemical immunosensing. This can be done by giving the reaction enough driving potential, the chemical reaction must be fast enough if there is any, and the redox reaction must not cause changes on the electrode surface such as adsorption, desorption, or crystallization.

However, as presented by Nernst-Planck equation below, mass transport is not only controlled by **diffusion** (difference in concentration gradient, first term), but also by **migration** (movement of charged species due to potential field, second term), and **convection** (mixing by mechanical force, third term) [52]:

$$J_j(x) = -D_j \frac{\partial C_j(x)}{\partial x} - \frac{z_j F}{RT} D_j C_j \frac{\partial \phi(x)}{\partial x} + C_j v(x) \quad (7)$$

1st term 2nd term 3rd term

Thus, in order to achieve a stable immunosensor environment, we must isolate out as much factor as possible, leaving only the diffusion, the first term, to control mass transport.

This can be achieved by adding the solution with high concentration of inert electrolyte to facilitate charge transfer (eliminate migration) and kept the solution still to eliminate convection. As a result, the mass transfer step is solely controlled by diffusion.

Differences of the resulting current can be used to measure antigen occupation on the electrode surface as occlusion of antigen on the electrode surface would hinder the mass transport of electroactive species, as presented in **figure 5 (b)**.

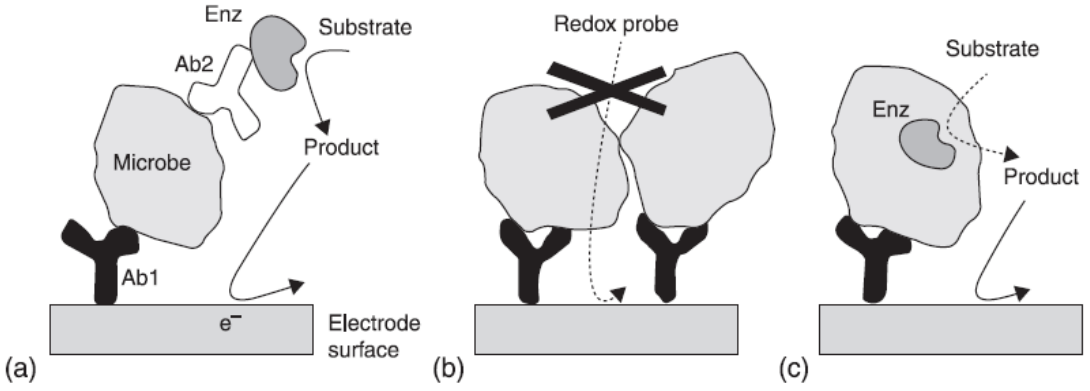

Figure 5: Different types of electrochemical immunosensors. (a) Sandwich (indirect) immunoassay where primary antibody (Ab1) captures microbe (antigen), and got labeled by enzyme-tagged secondary antibody (Ab2). The enzyme label then convert substrate and generate signal. (b) Direct immunoassay; the antigen blocks the sensor surface, (c) Viable (living) cells are captured and given substrate to feed on. The cells then produce enzyme which will convert substrate to product and generate signal [53].

2.3.1.2 Diffusion-controlled Electrochemistry

As difference in concentration between the pre-redox and post-redox species occurred, it will create a driving force of transportation, known as diffusion, to and from the electrode surface. The diffusion of O or R to

the electrode surface and its redox reaction dictates the resulting current. Fick's first law stated that particles will diffuse from higher concentration to lower concentration, formulated as:

$$Flux = \frac{moles}{area\ time} = \frac{dN}{Adt} = -D\left(\frac{\delta C}{\delta x}\right)_{x=0} \quad (8)$$

Where *J* is flux of materials (mol cm^{-2} s^{-1}), *D* is diffusion coefficient, *C* is concentration of diffusing material, and x is distance from the electrode surface. The minus sign means the diffusing species diffuses from concentrated area to area more diluted in the solution. In case of pre-redox diffusion to the electrode, the minus sign is not needed.

Flux can then be converted to current by Faraday's Law of electrochemistry as shown previously in equation (1) and (2). Taking them into account with Fick's first law and we will obtain the relationship between current and molecular flux:

$$i = \frac{dQ}{dt} = -nF\frac{dN}{dt} = -nFA(Flux) = nFAD\left(\frac{\delta C}{\delta x}\right)_{x=0} \quad (9)$$

Additionally, there is Fick's second law for considering concentration of diffusing species with respect to time at the center of volume bound by two planes parallel to electrode surface [51].

$$\frac{\partial \mathbf{c}}{\partial t} = D\frac{\partial^2 \mathbf{c}}{\partial x^2}$$

Where c is concentration of species in the solution. This law is a way to develop more precise theoretical description of experiments as now concentration profile changes with time, c = f(x,t), as presented in **figure 6**.

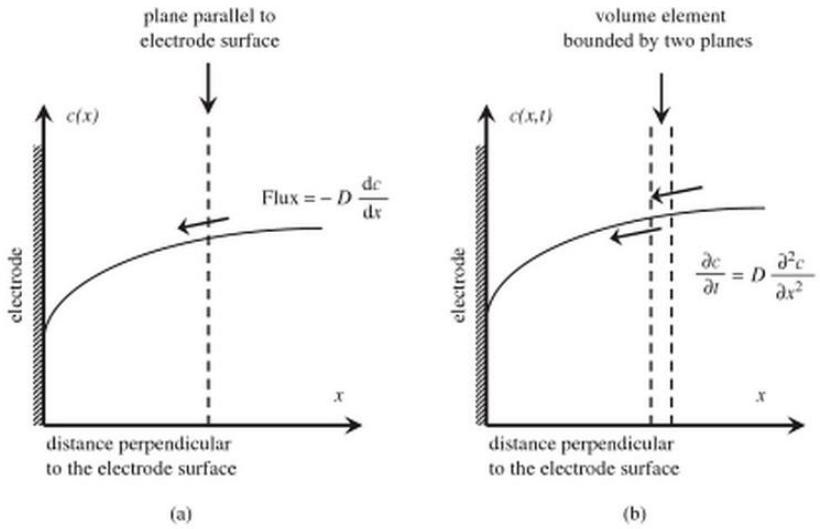

Figure 6: Graphic representation of (a) Fick's first law and (b) Fick's second law. [51]

These two laws can be applied to show the phenomenon at the electrode surface. As transfer of *n* electrons result in one reduced species (R) converted to one oxidized species (O), according to conservation of matter, the influx of O and efflux of R must also equal. Therefore influx of O and efflux of R is related to flux of electrons within the electrode as shown in **figure 7**, and can be expressed as:

$$\frac{j}{nF} = D_{\mathrm{R}}\left(\frac{\partial c_{\mathrm{R}}}{\partial x}\right)_{x=0} = -D_{\mathrm{O}}\left(\frac{\partial c_{\mathrm{O}}}{\partial x}\right)_{x=0}$$

$$j = nFD_{\mathrm{R}}\left(\frac{\partial c_{\mathrm{R}}}{\partial x}\right)_{x=0} = -nFD_{\mathrm{O}}\left(\frac{\partial c_{\mathrm{O}}}{\partial x}\right)_{x=0}$$

Where j is experimental current density in electrode reaction [51].

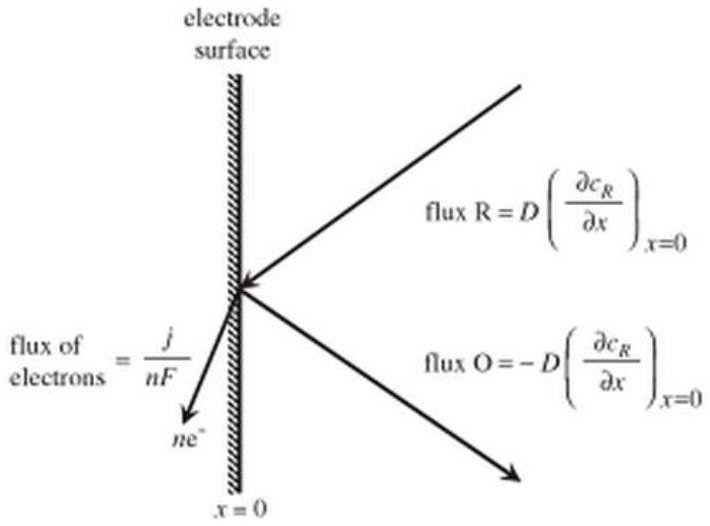

Figure 7: Balance of redox reaction fluxes at the electrode surface [51].

This means positive current density is directly proportional to diffusion coefficient and concentration of reduced species (ready to be oxidized) at a given distance, and vice versa.

Deriving Fick's second law gives Cottrell equation, which predict variation of current in time when a potential step is applied under large overpotential;

$$i(t) = \frac{nFAD^{1/2}C_R}{\pi^{1/2}t^{1/2}} \qquad j = \frac{nFD^{1/2}c_R}{\pi^{1/2}t^{1/2}}$$

, or alternatively

Because at t = 0 there are a lot of R to be oxidized, there would be large current flow initially, but as the concentration gradient becoming smaller, the diffuse layer increases, resulting in current decrease, as presented in **figure 8**.

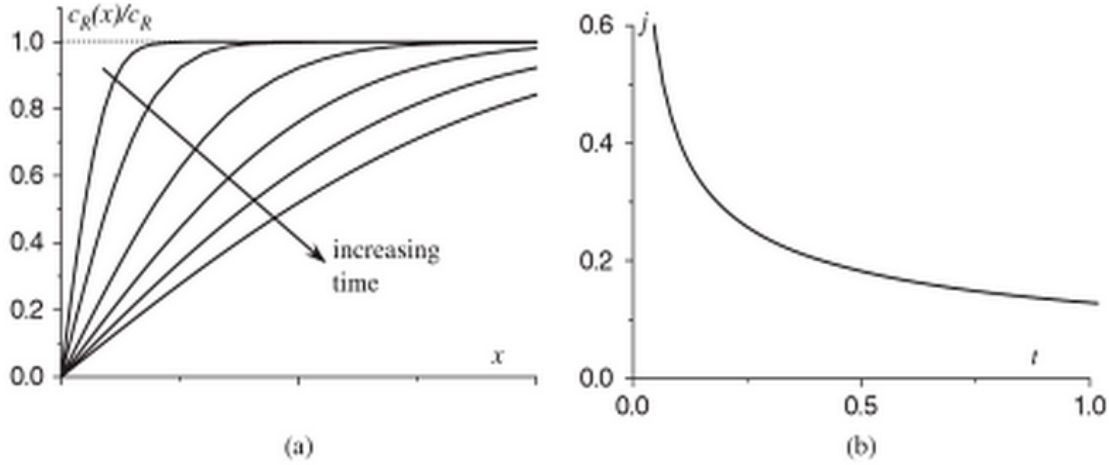

Figure 8: (a) Development of concentration profiles following a potential step from a value where j = 0 to one where the oxidation of R to O is diffusion controlled; (b) the corresponding current density vs time transient [51].

By plotting j vs $t^{1/2}$, if straight line is obtained, then it means the reaction is diffusion controlled. Demonstrating that $jt^{1/2}$ is a constant also confirms that the reaction is diffusion controlled.

Therefore, if less electroactive species can get to the electrode surface, diffusion coefficient will be lowered and diffusion will also be slower due to occlusion of antigen molecules, which will reduce the resulting j (current density), indicating presence of antigen on the electrode surface.

2.3.1.3 Cyclic voltammetry (CV)

First of all, the notations must be defined. By American convention, anodic currents are negative and cathodic currents are positive, while IUPAC convention define anodic currents as positive while cathodic currents are negative, as presented in **figure 9.**

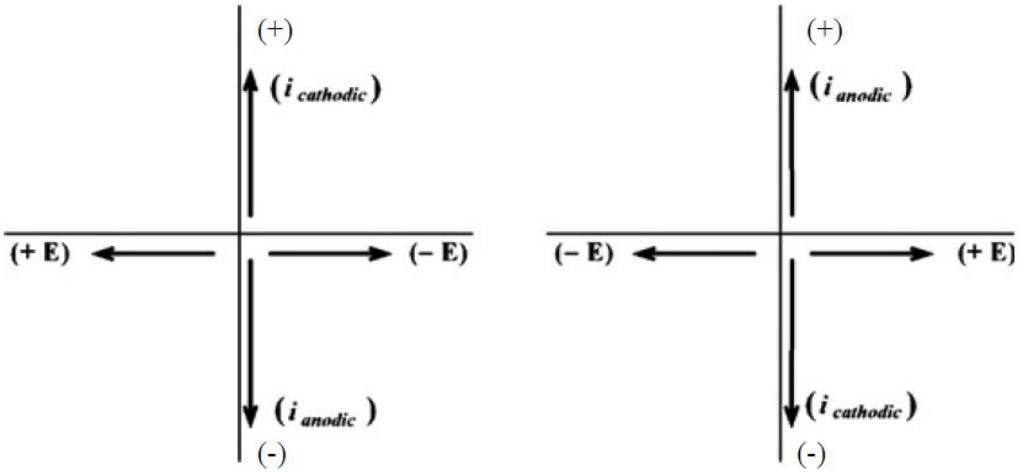

Figure 9: American (left) and IUPAC (right) voltammogram conventions [52].

Cyclic voltammetry is essentially sweeping of voltage back and forth in cycles, as presented in **figure 10 (a)** . Current-voltage curve produced by voltammetric method can be used to determine oxidation peak, reduction peak, reversibility, and what is occurring at a specific voltage, as presented in **figure 10 (b)** [51].

Therefore, cyclic voltammetry is one of the most commonly deployed electrochemical analysis, as it is an excellent method to analyze and characterize an electrochemical system. Choosing waveform is the most important step, as it would determine driving force for electron transfer and oxidation state of the electroactive species.

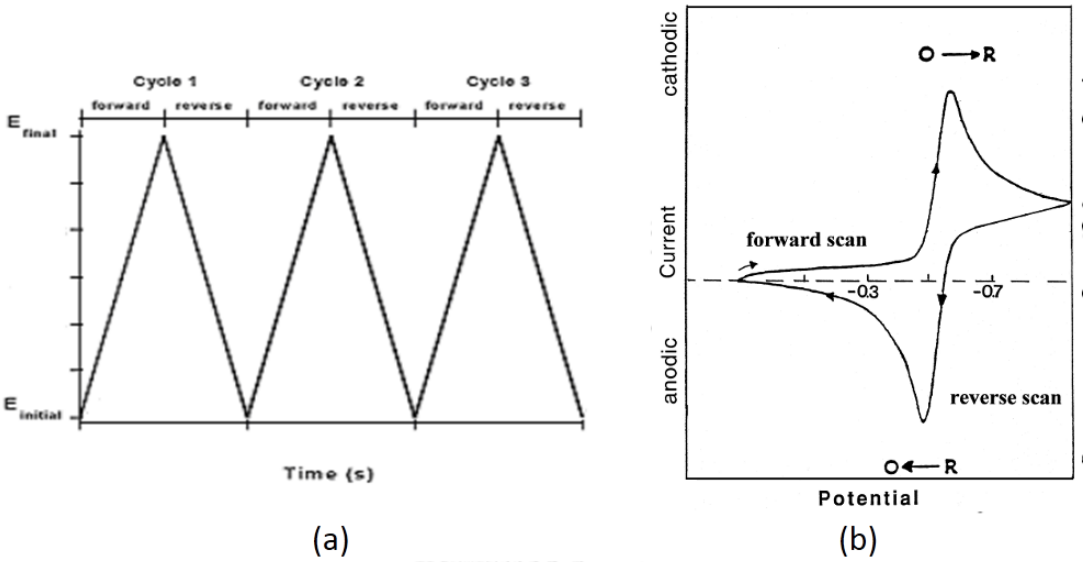

Figure 10 (a,b): Example of (a) potential waveform in cyclic voltammetry with switching potential and (b) response of a reversible redox couple after one scan cycle [54].

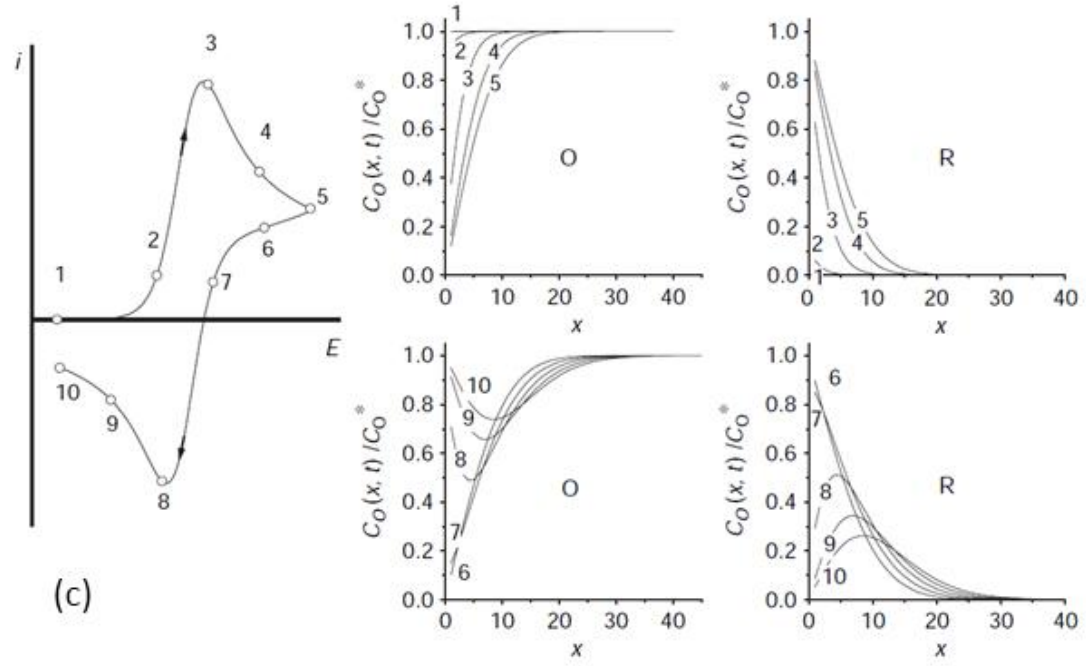

Figure 10 (c): Cyclic voltammogram and corresponding O and R concentration profiles for diffusion to a planar electrode. Numbers on the concentration profiles correspond to the numbered points on the voltammogram [52].

As shown in **figure 10 (c)**, for point 1 to 7, O is consumed to generate R, reduction current is observed. For point 8 to 10, R is consumed to generate O, and oxidation current is observed. Gradient is positive

for point 1 to 7 and negative for point 8 to 10 [52].

One of the key feature of cyclic voltammetry is peak height. For planar diffusion-controlled reaction, the peak current for reversible, diffusion controlled redox process at 25 °C is predictable by the Randles-Sevcik equation [51];

$$i_p = (2.69 \times 10^5)\, n^{3/2} A D^{1/2} v^{1/2} C \tag{10}$$

This equation predicts that peak current is proportional to the square root of sweep rate. This is consistent with inverse square root of time dependence found with potential steps. Therefore a plot of i_p vs $v^{1/2}$ should be linear, pass through origin. And from this equation, active electrode area can also be calculated [55, 56].

There is also two situation for the system, “reversible” and “irreversible”. Reversible system means the system is mass transfer-limited and the surface reaction produces no side products, while irreversible system mean the system is limited by electron-transfer step and/or the surface reaction produces side products. Reversible voltammogram should have characteristics as follows [52]:

$$i_p \propto v^{1/2}$$

$$E_p \text{ is independent of } v$$

$$\Delta E_p = E_{pa} - E_{pc} = \frac{59}{n}\,\text{mV at } 298\,\text{K}$$

$$\left|E_p - E_{p/2}\right| = \frac{59}{n}\,\text{mV at } 298\,\text{K}$$

$$\left|\frac{i_{pa}}{i_{pc}}\right| = 1$$

In irreversible systems, the shape of cyclic voltammogram changes drastically when rate of mass transports exceeds the rate of electron transfer, as in **figure 11**. When mass transfer coefficient is at the same level as electron transfer, the graph would be almost identical to diffusion-controlled graph, but when mass transfer coefficient is increased, the voltammogram will be more drawn out. The peak would become broader, separation increases, and reverse peak would start to disappear.

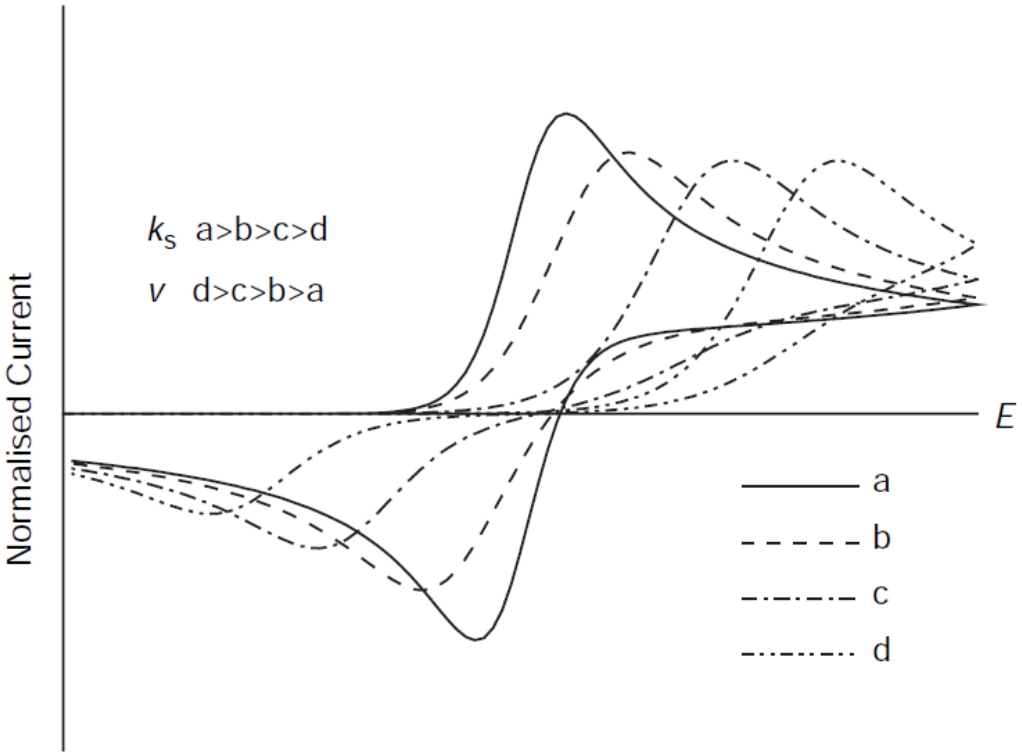

Figure 11: Voltammogram under kinetic control. The current scale is normalized to show effect of changing sweep rate. (a) the mass transfer coefficient is smaller than electron transfer rate constant while in (b-d) mass transfer coefficient is increasingly larger than electron transfer rate constant [52].

Irreversible voltammogram should have characteristics as follows [52]:

$$i_{p,c} \propto v^{1/2}$$

No reverse peak

$E_{p,c}$ shifts to higher overpotentials as v increases

$$|E_p - E_{p/2}| = \frac{48}{\alpha n} \text{mV at } 25^\circ\text{C}$$

Therefore, in order to be able to visualize effect of antigen occlusion effectively, the voltage must be given high enough, and the electron transfer between layers must be fast enough so the graph would show reduction in current (height of *i*) rather than widening of peak shape.

And with the same principle as in amperometry, the influx and efflux of electroactive species would be impeded by antigen occlusion on the electrode surface.

In conclusion, as more antigen are added to the solution, the diffusion rate of the R and O species that generate current via redox reaction would be more obstructed, resulting in lowered diffusion coefficient and, therefore, measurable current.

2.4 Composition of immunosensor

Everything is built from putting together smaller compositions, and immunosensor is no exception. Immunosensor is a combination of entirely different field of biology, physical chemistry, and electronics for the purpose of determining biological particles. When antigen combines to the antibodies to form antigen-antibody complexes, these complexes would generate or impede chemical signals or create changes in properties, which would be later converted into electrical signal by the transducer. Therefore it must be composed of electrodes, biological recognition elements, analyte that contains the antigens to be measured, and a transducer (electrical circuit) for data interpretation and display.

2.4.1 Electrode surface

The specificity and sensitivity of any given biosensor relies almost entirely on its interface on the working electrode which interacts with biological elements, as it is the place where all electrochemical reactions happen.

As for amperometric measurement, current is generated after a redox reaction occurs on the electrode surface. Thus, more redox reaction would lead to more current. The rate of redox reactions can be increased by either increase electrode surface or increase the speed of diffusion.

The most common materials used to fabricate an electrode are inert m*et al*s such as platinum, gold, carbons, epoxy graphite, and glassy carbon. However, these materials also have their own limitations, such as risk of cross-contamination, bulky, and have to go through rigorous washing and scrubbing after each use, making it not appropriate, sometimes not even feasible, for use in point-of-care testing situation [57].

As technological advancement progresses, a solution to this problem arises. Screen printed carbon electrode, as a mass-producible, disposable, portable, inexpensive, simple, easy-to-use working electrode, start gaining more attention in biosensor development as an obviously more practical and promising substitute to conventional electrodes [58-60]

2.4.2 Antibody

Ideal immunosensor interface should be exclusively specific to the target, can recognize the target even at lowest concentration, and binds very strongly to it. One kind of biomolecule that has these characteristic and can be used are antibodies. Antibodies are biomolecules that produced in response to immune reaction in the body to specifically catch its antigen counterpart.

Antibody binds strongly to the antigen via multiple types of bonding (e.g. hydrogen bond, hydrophobic bond) except covalent bonding, and its bonding strength is called avidity. Avidity is influenced by affinity (average constant association of binding sites) multiplied by valence (number of interacting binding sites) of interaction.

There are two categories (polyclonal and monoclonal) and five types (IgA, IgD, IgE, IgG, IgM) of antibodies. Nevertheless, all antibodies have the same basic configuration of two identical light chains (L) and two identical heavy chains (H) (see **figure 12**). The light chain has two forms, lambda (λ) or kappa ($\varkappa$), while the heavy chain has 5 forms of mu (μ), delta (δ), gamma (γ), alpha (α), and epsilon (ε), which determine immunoglobulin type as IgM, IgD, IgG, IgA, and IgE respectively. The most popular and possibly a representative of all antibodies is the IgG, which is responsible for majority of antibody-based immunity against pathogens.

Immunoglobulin G, or IgG, has 4 subclasses and all can be seen as Y-shaped proteins, with the top of the Y formation as antigen binding sites (**f**ragment **a**ntigen **b**inding, Fab) and the base as Fc (**f**ragment **c**rystallizable, as it can be readily crystallized) receptor-binding site for immunosystem to recognize and commence phagocytic operations by white blood cells. At this end of heavy chain contains carboxylic groups which can be exploited and adhere these IgG antibodies on any desired surface. IgG has molecular weight of 150 kDa, and has two binding sites per molecule. IgG is the most abundant type of antibody in the serum, around 80% of total antibody, and would be produced in high titer after secondary stimulation indicating that IgG is the most important isotype for immunological response against antigens.

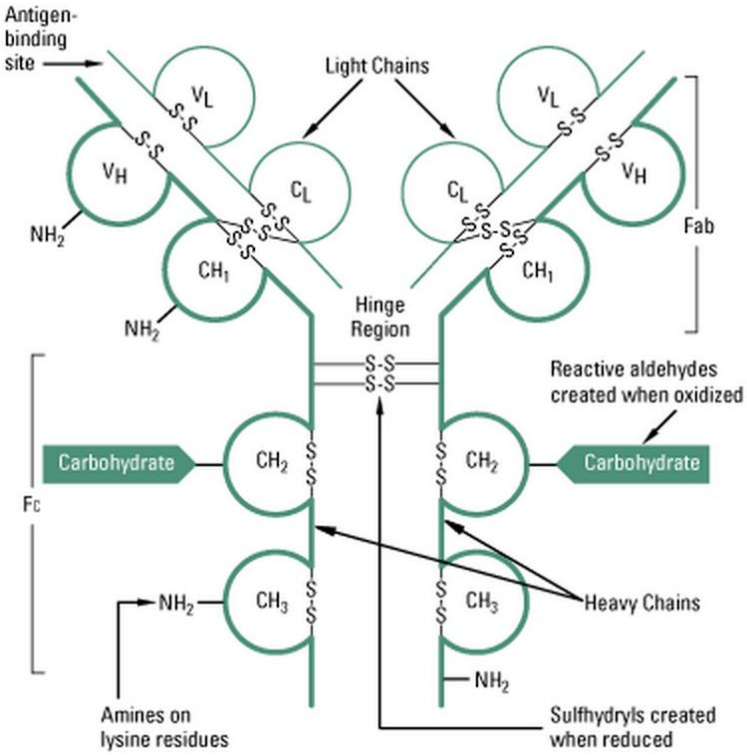

Figure 12: Structure and Functional groups of IgG antibody [61]

2.4.2.1 Antibody immobilization

There are many ways of IgG antibody immobilization, as there are many functional groups on the antibody, as presented in **figure 12**. It can be categorized in to two large types: oriented and non-oriented immobilization.

Oriented immobilization can be accomplished by various means such as via primary antibody, avidin-biotin reaction-based [62], protein A tagging [63], protein G tagging [64], using thiol groups [65, 66], or carbohydrate groups [67].

Another method is non-oriented immobilization. Although obviously giving out less valence (antigen-attaching capacity) than oriented immobilization, it is less complex, easier to accomplish, involves fewer steps, and inexpensive. One of the most common target functional group for this type of immobilization is primary amines (-NH_2) on the antibodies. As amine groups are distributed throughout the antibody as lysine side chain, it can be modified easily with bifunctional cross linkers (such as 0.1% glutaraldehyde) to attach to amine-rich substrate due to less steric hindrance [68]. However, it also has a drawback of attaching antibody to the substrate with its Fab (antigen-binding site), reducing its valence. Also, it cannot be used for immobilization in solution containing substances that contain amine groups. Alternatively, hydroxyl (-OH) and thiol (-SH_2) groups on antibody can also be

joined to amine-rich substrate.

2.4.2.2 Non-reacted electrode surface

Immobilization of antibodies can never achieve perfect coverage, and the electrode surface where no antibody is present must be covered by inert protein in order to prevent non-specific binding of antigen protein to the electrode surface. The most used materials for surface covering is Bovine Serum Albumin (BSA), Non-fat dairy milk (NFDM), normal serum, casein, and fish gelatin [69]. There is a report that BSA is more effective than skimmed milk in application on screen-printed electrode [70].

2.5 Electrode modification

Characters of the working electrode is of the utmost importance factor determining quality of the immunosensor. The optimum electrode condition would bind strongly to the antibody, and have zero total electrical resistance. While that condition cannot be obtained, improving the electrode close to that point would prove beneficial nonetheless. The materials that we found interesting for use in electrode modification are listed as follows:

2.5.1 Screen-printed Carbon Electrode, SPCE

Screen-printed Electrodes (SPEs), was developed with purpose of single-use, with variety of applications ranging from medical to industrial. SPEs fabrication principle is to deposit conductive ink onto desired electrodes, such as glass, ceramic, or plastic, at specific thickness. Its disposability eliminates the possibility of surface fouling, contamination, and the need to be cleaned or re-polished after each use. This leads to high popularity of SPEs in development of electrochemical immunosensors[45]. SPE also offers very low sample and solution consumption as it contains very small area of analysis. Among SPEs, screen-printed carbon electrodes (SPCEs) is one of the most popular due to its simplicity of fabrication and immobilization of reagents on the surface [71].

Nevertheless, bare SPEs and SPCEs alone are not quite qualified for electrochemical applications for detection of low concentration species, thus additional modifications are needed.

2.5.2 Graphene (GR)

Carbon-based materials has always been of some uses to science and technology for a long time.

Many forms of them have been particularly useful due to carbon's unique physical and chemical properties. Recently, discoveries of fullerenes, carbon nanotubes, and graphene has brought many new application opportunities [72]. The latest in the list, Graphene, is a single-layered, hexagon-shaped, allotrope of carbon. Its uniqueness lies in its electrical and mechanical properties [73]. Its theoretical properties of high surface area (2630 m^2/g), Young's modulus(~1 TPa) and charged carrier mobility (~200,000 cm^2/Vs) have been widely accepted and documented [74]. Graphene also promotes electron transfer and facilitate direct electron transfer between the solution and electrode [75]

In the work conducted by Subbiah *et al*. (2009) [76], chemically synthesized graphene electrode was compared to single-walled carbon nanotubes (SWCNT) in terms of electrical conductivity. They found that graphene has 60 times better conductivity than SWCNT (greater sp^2 character), better sensitivity (higher peak current density), signal-to-noise ratio, and stability (28% less decrease in signal after 30 consecutive scans). Additionally, graphene is more responsive to interfering substance(s) in cyclic voltammogram, as one can see between dopamine (153.18 g/mol) and serotonin (176.215 g/mol) in **figure 13B and 13C**

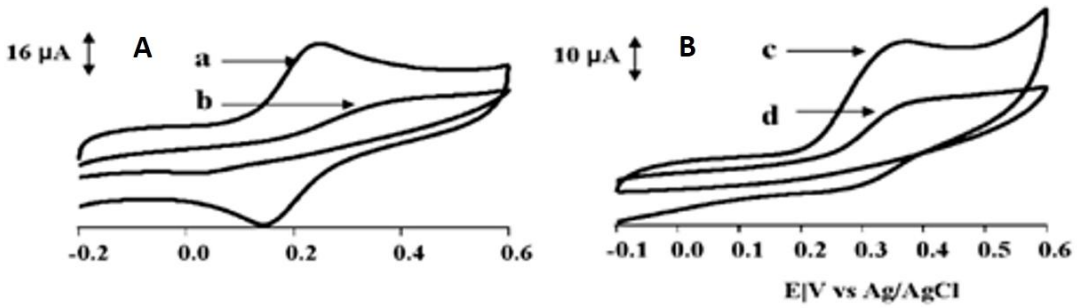

Figure 13: Cyclic voltammogram of graphene electrode in 2.5 mM dopamine (a) and SWCNT in 2.5 mm dopamine (b) (B) graphene electrode in 2.5 mM serotonin (c) and SWCNT in 2.5 mM serotonin (d), no scan rate was mentioned for both graphs. [76]

2.5.3 Poly(3,4-ethylenedioxythiophene) Polystyrene sulfonate(PEDOT:PSS)

Conductive polymers are promising materials for fabrication of electrodes and conducting layers due to their high conductivity, lightweight, low cost, and good industrial processability properties [77]. One of the most interesting materials among them is PEDOT:PSS with a full name of poly(3,4-ethylenedioxythiophene):poly(4-styrenesulfonate). It is even considered as a potential replacement to the already highly-conducting indium tin oxide electrodes because it does not require high-temperature processing, relatively

inexpensive, does not release its content to the analyte, transparent even after full crystallization, and flexible [78, 79].

PEDOT by itself has very interesting qualities such as high electrical conductivity of 300 S/cm [80], oxidized film is near-transparent, easily oxidized, and high stability [81]. Despite its good points, there was one properties that was holding it back from application on wider scale, which is water insolubility.

Later, the problem of insolubility was solved by adding poly(styrene sulfonic acid)(PSS) into it as a charge balancing agent during the forming of the polymer. The highly anionic PSS (negative charge) act as counterion to cationic PEDOT (positive charge), resulting in Polystyrenesulfonate doped poly(3,4-ethylenedioxythiophene) or PEDOT:PSS which is water-soluble, has excellent film-forming capability, high electrical conductivity of estimately 10 S/cm, nearly transparent, and highly stable [82].

PEDOT:PSS can withstand the heat of 100 ℃ more than 1,000 hours without significant changes in electrical conductivity. [83] It can also be mixed with other inert solvents such as Sorbitol or ethylene glycol to increase its conductivity to 80 S/cm [82-85]. PSS are always on the surface of the polymer while the PEDOT remains inside [86]. Thus PEDOT:PSS has been popular in electrode development and frequently used to improve electrical conductivity and performance [77, 87, 88].

Even though PEDOT:PSS has good conductivity of estimately 637 S/cm [77], but it is still far less in comparison with transparent conducting oxides such as the optimized Indium Tin Oxide (ITO) which has the conductivity of ~10^4 S/cm [89], also electrical homogeneity are still a problem [90]. Later it was discovered that inserting graphene into the polymer resulted in a material that has both high conductivity of PEDOT:PSS and the ability of being a catalyst in electrochemical reaction of graphene, which result in large reduction in overall resistance and higher electrical conductivity than normal PEDOT:PSS [90, 91].

PSS act as both a PEDOT dopant and dispersant of graphene [77]. Graphene-PEDOT:PSS, with molecular structure as **figure 14**, has good conductivity properties and has already been applied to make flexible ammonia sensor [92], counter electrode in solar panel [91], flexible organic LEDs [90], and electrochemical enzymatic biosensor [93]. To the best of our knowledge, there is no application of Graphene-PEDOT:PSS as a component in electrochemical immunosensor.

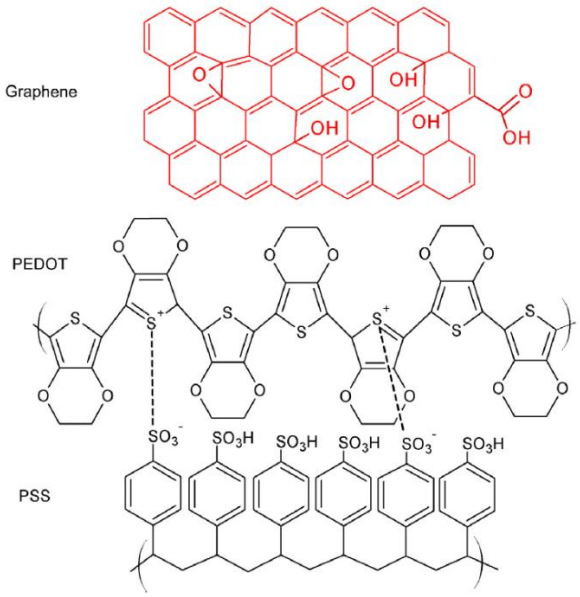

Figure 14: Structure of graphene-PEDOT:PSS[92]

2.5.4 Graphene-PEDOT:PSS

Even though graphene has excellent properties and can be produced to some degree of quality, there is still one problem remaining. Graphene, even in its perfect form, is hard to use due to large surface and strong Van de Walls force makes them aggregate together. It is also chemically inert due to its aromatic, sp-2 bond conjugation between layers (if any) except on the edges and defects, and has to be functionalized in order to attach other materials to it and usable in chemical-based situations. [94-98].

This problems can be overcome altogether by electrochemically exfoliate graphite to graphene in conducting polymers such as PEDOT:PSS, which would both prevent aggregation of graphene layers and assist in conducting electricity. It reportedly increases 41% in conductivity and 93% in power factor than pristine PEDOT:PSS [77].

The given reason was graphene enhances electron transfer via its very high electrical conductivity and large surface area on its edge, resulting in better electrochemical result [99]. This can also be seen in **figure 15,** a result shown in a work by Sriprachuabwong *et al,* below.

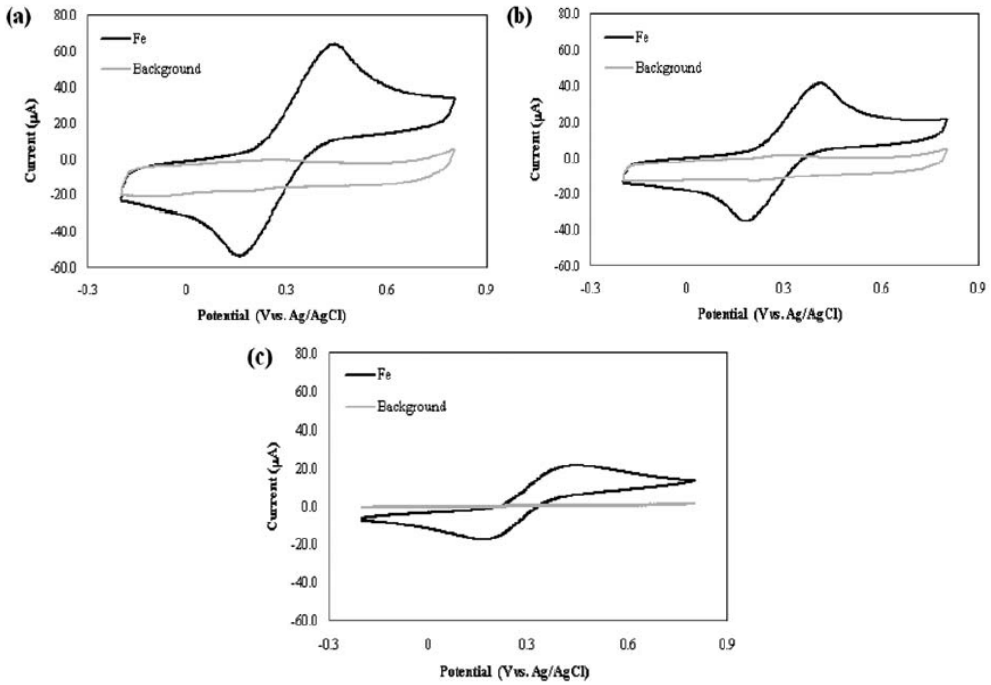

Figure 15: CV response to 320 μM $K_4[Fe(CN)_6]$ of (a) GR-PEDOT:PSS electrode (b) PEDOT electrode and (c) SPCE electrode. Scan rate was 100 mV s^{-1}. Buffer solution was 0.1 M KCl (pH 7.0) [99]

This method of graphene production is promising in electrochemical electrode fabrication because it produces highly conductive, non-aggregated graphene, with high tolerance to heat and flexibility which would be beneficial for real point-of-care application [77, 100, 101].

.

2.5.5 Prussian blue (PB)

Electrical contact between solid phase and another solid phase can be established by introduction of active charge carriers, called “redox mediator”, which would facilitate electron transfer process, as shown in **figure 16.** Redox mediators are capable of transferring electrons in redox reaction, and its presence almost always result in acceleration of reaction rates in most studies, and sometimes it is even a prerequisite for a redox reaction to happen [102].

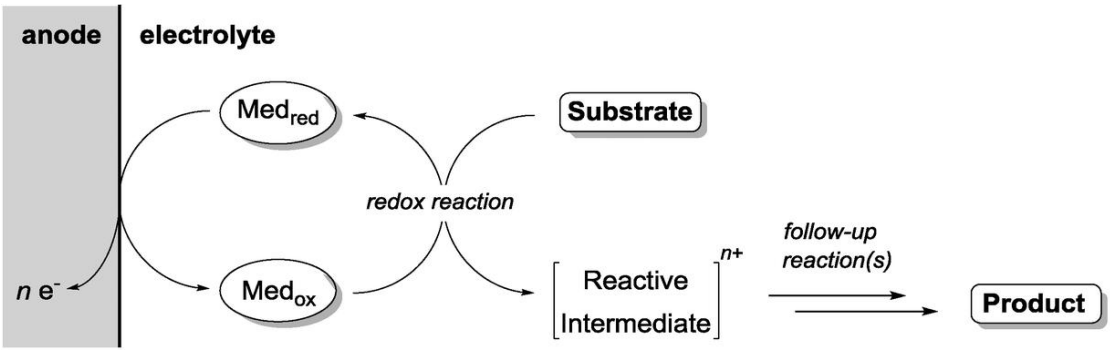

Figure 16: Typical electron shuttling of a redox mediator (Med) in an electrochemical setting [103]

A good redox mediator must not have side reaction during the processes, must have fast reaction with the redox center of both sides, and have reversible chemistry (fast rate constant).

Prussian blue (PB), $Fe_4[Fe(CN)_6]_3$, is a widely used electron transfer mediator for electrochemical analyses. Its duty in electrochemical process is to transfer electrons caused from oxidation of substrate to the anode, while the mediator itself goes through redox reaction [104]. Its changes color according to its oxidation or reduction state. When it is reduced in solution with potassium ions, the film becomes colorless. This form is named Prussian white or Everitt salt (ES). Its redox reaction is presented as in **figure 17** and equation 11.

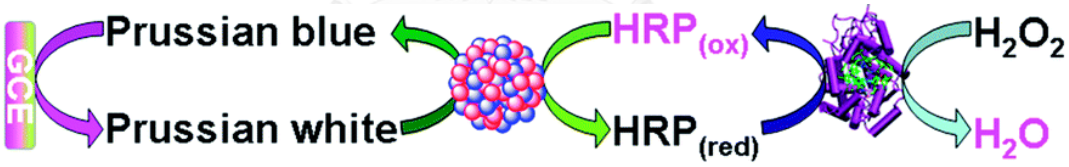

Figure 17: Schematic illustration of Prussian blue/white redox mediator in action in enzymatic electrochemical system [105].

Oxidized form Reduced form

$$Fe_4^{III}[Fe^{II}(CN)_6]_3 + 4e^- + 4K^+ \longleftrightarrow K_4Fe_4^{II}[Fe^{II}(CN)_6]_3 \quad (11)$$

In addition to its easy to prepare, stable, non-hazardous, electrochemically active properties, Prussian blue also reduces resistance of charge transfer [106]. Mostly, Prussian blue as an electron transfer mediator is used to improve sensor's detection capability [107]. Prussian blue is also one of the most popular mediator for biosensor fabrication [108], especially amperometric ones [109]. Lately, Graphene-Prussian blue combination has also been receiving attention, because it is inexpensive, easy to fabricate, and has excellent electrocatalysis properties[110].

Nevertheless, the weak point of Prussian blue is that it is easily soluble in normal and high pH condition and prone to leakage. One of the solution is to coat Prussian blue with polymer to prevent chemical reaction and its leakage to the analyte, which is more practical than other methods [58]. In our work, this would be achieved by coating the Prussian blue layer with either Graphene-PEDOT:PSS or Polyethylenimine.

Although Prussian blue can be deposited on an electrode by various methods, one of the frequently used method for depositing Prussian blue is electrodeposition. It is obviously economical, effective, easy to conduct, and film thickness can be controlled by the time of electrode position[111, 112]. Its electrodeposition can be done via Galvanostatic (constant current)[112, 113], Potentiostatic (constant voltage)[114, 115], and Cyclic Voltammetry (CV) method, as shown in **figure 18 (a) and (b)** [116].

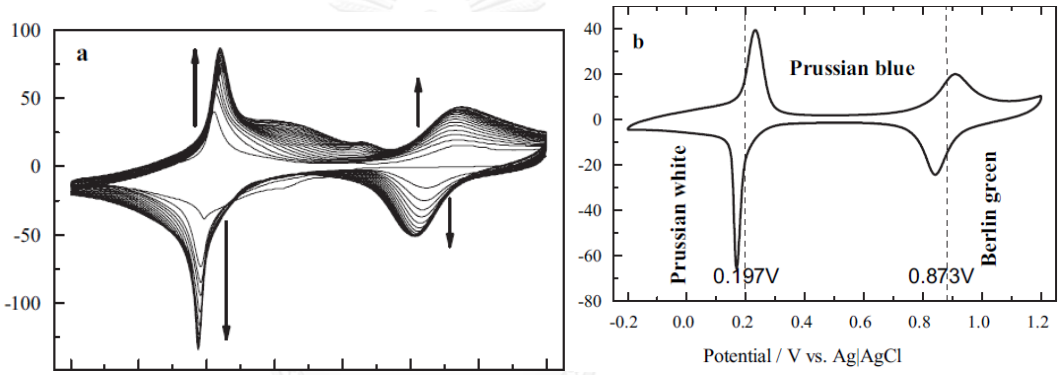

Figure 18: (a) Growth process of PB film on the graphene coated GCE in a solution composed of 2 mM $FeCl_3$, 2 mM $K_3[Fe(CN)_6]$, 0.1 M KCl and 0.01 M HCl. Scan rate: 50mVs−1. (b) Cyclic voltammogram of PB-graphene/GCE in PBS (0.05 M, pH 6.0) containing 0.1 M KCl at 50mVs−1[116].

The film properties can be calculated as follows:

Electrode surface coverage (Γ) in unit of mole/cm^2 of Prussian blue can be estimated using the equation [117]:

$$\Gamma = Q / nAF$$

Where Q is total charge which is current multiplied with time elapsed, n is number of electrons, A is electrode surface in cm^2, F is faraday's constant. Assuming that Prussian blue film has uniform distribution, film thickness can be also determined by equation [117]:

$$\text{Film Thickness (in cm)} = \Gamma \times V_m$$

Where V_m is molar volume, with unit in cm^3/mole, and can be obtained via:

$$V_m = M / \rho$$

Where M is molar mass in g/mole, and ρ is density in g/cm^3, which Prussian blue has 859.23 g/mole molar mass and has density of 1.80 g/cm^3 [118].

After electrodeposition, the PB-deposited electrodes should be treated by cyclic voltammetry around the reduction system of Prussian Blue $\rightleftharpoons$ Prussian White of +0.6 V and -0.2 V vs Ag/AgCl in electrolyte solution at 20 mV/s sweep rate for at least 15 times until stable response is obtained [112]. Its solid film deposition onto the electrode can be verified this way. Successful deposition would result in growth of redox waves at either ~0.10 V or ~0.80 V versus Ag/AgCl cyclic voltammogram**,** indicating that active redox center has successfully been deposited on the electrode surface [116].

Prussian blue layer over Polyethylenimine (PEI) polymer in CEA immunosensor by Zhang *et al* was also created by CV electrodeposition between 0.4 and -0.1 V at scan rate of 50 mV/s for five cycles, then rinsed with double-distilled water and dried under nitrogen [119].

Heat treatment of Prussian blue can also improve or worsen its electronic properties. It reportedly has best conductivity after heat treatment at 100 °C for 1 hour [109] then became worse with increasing temperature, reaching worst conductivity at 250 °C treatment [120]. This phenomenon probably due to elimination of adsorbed water molecules in Prussian blue moiety as presented by Farah *et al*.[121]

Deposition on different substrate with different materials would also yield different surface characteristics. Therefore, tests such as Atomic Force Microscopy (AFM) and Scanning Electron Microscopy (SEM) must be conducted to show more detailed properties of the prepared electrodes such as roughness.

However, it has its own drawback of instability in high pH, which PB would become thermodynamically unstable and prone to break apart into hexacyanoferrate ($Fe(CN)_6^{4-}$) anions and $Fe(OH)_3$ [122].

2.5.6 Chitosan (CS)

However, Prussian blue application as a redox mediator fixated on an electrode surface in biosensor are usually encounter problem regarding its leak into solution and its instability in neutral and high pH [122, 123]. A solution to this problem is to coat Prussian blue with some polymer that has high biocompatibility to protect it from being affected. One of the most popular material used to achieve this is Chitosan, due to it having high mechanical strength, inexpensive, easy to obtain, easy to use, safe, biocompatible, and has good solubility in acidic solutions [123]. Many literature chose CS as polymer of choice when constructing Prussian blue-based sensors [124].

Chitosan, full name poly (b-(1-4)-N-acetyl-D-glucosamine), is a natural polysaccharide derived from

Chitin, which is a polysaccharide commonly found in arthopods and cell walls of yeast and fungi, serving the purpose of reinforcing strength of the structure it is in. CS is soluble in acidic solution due to its $-NH_2$ group on the C-2 position on the D-glucosamine repeat unit, as shown in **figure 19** [125].

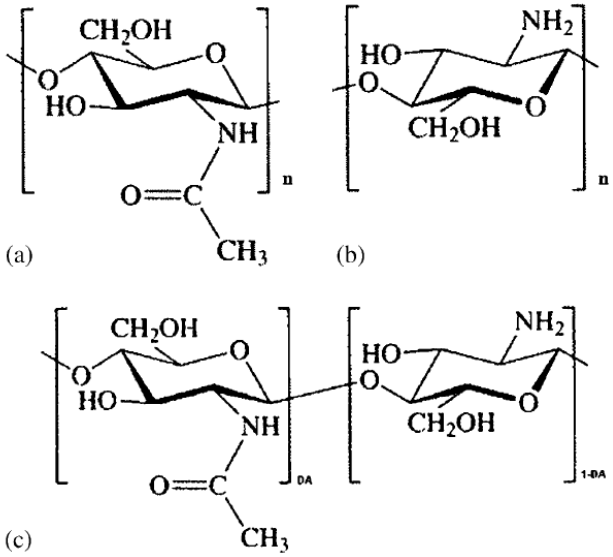

Figure 19: Chemical structure of Chitin (a), D-glucosamine repeat unit (b), and acetylated chitosan, which made up of the two units joining together (c) [125].

Common preparation of Chitosan for application is to dissolve in 0.1 M acetic acid and then adjust the pH of the solution to 7 using 1 M NaOH to deprotonate and make the polymer insoluble at neutral pH. [126]

2.5.7 **Staphylococcal** Protein A (PrA)

Staphylococcal Protein A is a protein derived from cell wall of *Staphylococcus aureus*, having the size of 42 kDa and the capability to bind with antibodies, especially IgGs as it has Fc binding portions, which make it highly useful in biosensing [127]. It was commonly used in biotechnology applications, usually by immobilizing on solid support to segregate IgG antibodies from other proteins in the sample. **Figure 20** shows simplified version of binding chain between cAuNPs-ProteinA-Antibodies-Antigen.

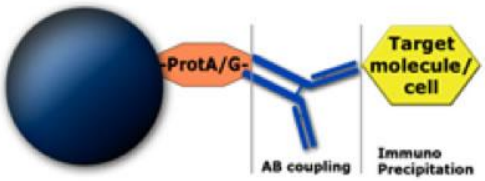

Figure 20: Schematic of binding chain between (from left to right) cAuNPs-ProteinA-Antibodies-Antigen

Due to its high specificity to antibodies and high stability under unfavorable conditions, PrA has also been used in development of many IgG antibody-related researches, biosensors and immunosensors included [128-130]. A genetic study by Moks *et al* in 1986 found that each protein A molecules consists of five IgG-binding domains on its structure [131]. Therefore we apply Protein A per antibody ratio of 1 to 5 in this work.

2.5.8 Gold Nanoparticles

Colloidal gold nanoparticles have been found to be immensely useful in fabrication of diagnostic kits as its capability to be easily liked with proteins not only make it customizable to any specific task, it also increase nanoparticles' stability [132], which is then called conjugated gold nanoparticles. Conjugated gold nanoparticles can be obtained by apply them together with proteins that are positively-charged at neutral pH, which would make them attracted to the negatively-charged gold nanoparticles [133]. The adsorption of proteins on the gold nanoparticle surface is based on three modes of molecular attraction, which are ionic interaction, hydrophobic attraction, and dative bonding between nitrogen and sulfur atom to the gold met al [134].

Stabilizing gold nanoparticles with citrate is one of the most popular choice and has been one of the most frequently used method to prepare gold nanoparticles for immobilization of protein A and IgG antibodies on any given surface due to its excellent stability, chemical properties, and biocompatibility [130, 135]. It was first proposed by Hermanson et al in 2008, which is about reduction of tetrachloroauric acid (HAuCl4) using sodium citrate and heat. Sodium citrate would reduce the gold nanoparticles and act as a capping agent, which would prevent the gold nanoparticles from growing freely or coagulate on themselves [136].

2.6 Antigen-antibody interaction

For fixation on working electrode, biomolecules that are specific to the specified antigen have to be installed on it first in order to "hook" the antigen for electrochemical test. The antibodies are varied in types as mentioned above, but here we will focus only at conditions for optimum application of IgG antibody.

Antigen-antibody interaction is specific and is the primary reaction of the body to protect itself and annihilate invasion of foreign molecules. The forces joining the antigen-antibody complex are not strong covalent bonds but weaker bonds such as electrostatic interactions, hydrogen bonds, Van de Waals forces, and hydrophobic interactions [137, 138]. It is also a reversible reaction, described as;

$$antigen + antibody \leftrightarrows antigen\text{-}antibody\ complex \tag{12}$$

Overall repulsion force of both molecules must be overcame for specific binding to happen. After both molecules come to nanometer proximity of each other, first they would attract each other by long range forces such as ionic and hydrophobic bonds. Then these forces would expel the water molecules, eradicating hydration energy and bring the two molecules closer, which gives way to van der Waals forces to happen. The overall strength depends on the fit of two surfaces and total contact area. This binding between antigen and antibody into a complex involves only a few amino acids with surface area of contact between 0.4 to 8 nm^2 with average of 2.0 nm^2. [139]

2.6.1 Factors affecting antibody-antigen interaction (equilibrium constant)

Antibody-antigen interaction is lock-and-key model, no molecules are altered, and is reversible. According to law of mass action, a chemical reaction first progress only in one direction, but after buildup of the product, the reverse reaction would increase in speed until matched with the forward speed.

$$\frac{[complex]}{[antigen]\times[antibody]} = \frac{k_a}{k_d} = K_{eq} \tag{13}$$

Where K_{eq} is equilibrium constant, k_a is association rate constant, k_d is dissociation rate constant. This equation can be rearranged as;

$$\frac{[complex]}{[antigen]} = K_{eq} \times [antibody] \tag{14}$$

Which shows that in order to improve detection (high complex per antigen ration), either the amount of antibody or equilibrium constant have to be increased. However, the amount of antibody should not be too much, as they would overlap each other and not equally accessible for antigen binding [140].

Therefore, unlike steady environmental condition like bloodstream, physical conditions of immunosensor would significantly affect equilibrium constant of antibody's antigen-binding capability. Hence, optimum condition for antibody-antigen interaction must also be known to properly utilize it.

2.6.1.1 Antibody titer

Optimum antibody titer (concentration) would be the maximum number applicable on the electrode surface without overlapping, which would decrease the valence of the overlapped antibody. This step is of less importance for label-based immunosensor as the signal is produced from the enzyme labels, but is crucial for label-free immunosensor as it directly affects analyte diffusion layer and antigen-immobilization capability.

Thus, antibody titer must depends on electrode's surface area, which can be known by analyzing with Cottrell equation and plots [141].

2.6.1.2 Operating temperature

The thermal optimum would depend on chemical nature of epitope (antigenic site), paratope (antibody site), and the types of bonds involved [142]. Hydrogen bond is exothermic and favors low temperature, while hydrophobic bond strength increases with temperature. However, the overall decrease in association rate with increased temperature is minimal, and can be concluded that optimum temperature for IgG antibodies to operate in is that of mammal body temperature, 30-37°C [143].

2.6.1.3 pH

Due to more restricted molecular structure, monoclonal antibodies are very sensitive to pH and ions. And each type of antibody has different pI. But usually, best reactions of the antibody-antigen reaction are observed from pH 6.5 to 8.4 [144] [145], with recommendation of Buffered saline pH 7.2 for use in immunoassays. At both extremes, such as pH 5.0 or 9.5, the antibody-antigen reaction equilibrium constant become 100-fold lower than pH 6.5 to 7.0 [144], which means the antibody interaction is strongly inhibited. Induced conformational changes in the antibody is a possible cause [146].

2.6.1.4 Incubation time

The higher antibody titer (concentration), the shorter incubation time is needed for optimum result. Incubation time is different for different antibodies, ranging from 10 minutes to 24 hours, depending on the antibody's equilibrium. However, equilibrium is usually not reached during incubation less than 20 minutes, and 24-hours incubation would be a more economical approach as more diluted (higher dilutions) can be used. Thus, 24-hours is advisable, but incubation beyond saturation point is also meaningless [147].

2.6.1.5 Incubation temperature

Although, antigen-antibody equilibrium can be reached more quickly at 37 ℃, it can also be incubated at 4 ℃ overnight or longer. This is also a time-critical process, and all samples must be ensured consistent incubation duration. Samples incubated for prolonged period or at 37 ℃ should also be placed in moist chamber to prevent drying.

2.6.1.6 Antigen-antibody ratio

This usually is a problem in free-floating antibody-antigen solution which involves effect of excess antibody resulting in precipitation and other effect such as Danysz phenomenon which shows potential error when antigen is added in increments rather than a single increment. However, in label-free electrode, this not of concern as the antibodies are immobilized on the electrode. The only concern that involves quantification of antibodies is that of immobilization, which had already been addressed in the topic of antibody titer.

Chapter 3

Literature Review

This chapter is about reviewing past electrochemical-based point-of-care diagnostic electrode fabrication. The main objective of this thesis is to develop a low-cost, high-sensitivity LipL32 detecting electrode for electrochemical measurement; therefore, this review will include discussion of electrochemical biosensors that has interesting sensitivity with potentially diminished costs.

3.1 Existing label-free electrochemical immunosensors

3.1.1 Electrode modification

Due to the fact that electrodes cannot be used as-is, and some modifications are needed, every immunosensor fabrication attempts were about trying to achieve maximum current response with myriad types of conducting materials. The pattern can be classified into two types of monolayer modification and multilayered modification.

3.1.1.1 Monolayer electrode

Most of the immunosensor constructs are in this category. In this type of immunosensor electrode, only one layer of modification was done. There are varieties of materials used in label-free immunosensor development, but most are well-known electrically conductive materials such as Carbon nanotubes [148], Graphene [75, 149], Gold nanoparticles[150], Silver nanoparticles [151], Ionic liquids [152], Prussian blue [153], Arginine [154], Thionine [155], Polydopamine [156], Nafion [157].

However, there are also some application of non-conductive materials such as Chitosan [152, 153, 158-161] and Polyethylenimine [162]. They usually act as a base for antibody immobilization.

3.1.1.2 Multilayered electrode

However, there are some studies which involves multiple layers of the same material. In every cases, multiple layers of redox mediator leads to higher current response. The reason given was that the electron transfer can occur more rapidly, leading to more redox reaction per time on the electrode surface.

The examples are, 10 layers of Prussian blue-Platinum [153], 2 layers of Thionine [160], 5 layers of Prussian blue [119]. Each for detection of antigen of different kind.

3.1.2 Antigen

Due to the fact that there has been no application of LipL32 as a biomarker in electrochemical measurement before, we therefore have to draw assumptions using works of similar models but different biomarkers. Nevertheless, the underlying principles are still the same.

The principle of amperometric immunosensor has firm establishment and its application has already been expanded to various other targets. The type of antigen can roughly be classified into two classes of single-molecule targets and whole-cell targets, as samples shown below.

3.1.2.1 Single-molecule targets

Rabbit IgG antibody [163], mouse IgG [164], goat anti-human IgG [165], goat anti-mouse [166], antibodies to *Salmonella* bacterium [167], alfa-fetoprotein [168-172], Carcinoembryogenic antigen [173-179], Carcinoma antigen 125 [180], Tumor necrosis factor alpha [181], herbicides [182, 183], pesticide [184],polycyclic aromatic hydrocarbons [185], human chorionic gonadotrophin [186], Human serum albumin [187], Breast Cancer Susceptibility Gene [188], milk progesterone [189], biotin [190], shellfish poisoning toxic [191], intracellular protein [192], interleukin-6 [193], egg yolk protein [194] even human immunoglobulin G (IgG) itself [195, 196],

3.1.2.2 Whole-cell targets

Parasitic worm [197, 198], hepatitis B virus [199, 200], fungi *Trichophyton rubrum* [201], *E. coli* O157:H7 [160], *Salmonella typhimurium* [202], *Pseudomonas aeruginosa* [203], and *Campylobacter jejuni* [204].

3.1.3 Electrode compositions in this work

Because our first priorities is to develop a considerable sensitive inexpensive immunosensor for a disease rampant in third-world countries, the main parameters considered are the price of materials, tolerance, toxicity, ease of handling, and reasonable sensitivity.

The material combination to attain these objectives are Graphene-PEDOT:PSS-Prussian blue/PrA combination.

3.1.3.1 Method of antibody immobilization

Antibody immobilization method varies from publication to publication, largely depends on the type of substrate and its functional groups, such as EDC-NHS for carbodiimide crosslinking between carboxylic acids and primary amines, conjugating surface-bound Streptavidin to antibody-bound biotin, activating surface by Maleimide to conjugate with sulfhydryl groups on antibody (-SH), and much more.

One of the most inexpensive, appropriate to the situation at hand, is to use Protein A as base and then immobilize antibodies by dropping them on top. This method is efficient, reagent-less, economical, and non-laborious.

3.1.4 Methods of Detection: Why label-free?

As stated prior, label-based method has been the primary method of detection with both ELISA and immunosensor over the years since the first ELISA in 1960 [205]. Key principle is that either antibodies or antigens got immobilized on the substrate, then after addition of its counterpart to be detected, another antibodies specific to the last layer and tagged with label are added. The most common labels are enzymes, fluorescent, and radioactive markers [206]. Although this method is reportedly more sensitive, but it is obviously also more costly, tedious, complex, and consume more time than direct (label-free) method.

The advantage to label-free (direct) detection in comparison to label-based (indirect) method is that it has significantly lower cost, decreased analysis time, higher portability, easier to be fabricated, less operational complications, and capability of real-time monitoring of antibody-antigen reaction [40]. Its main disadvantage used to be about having less sensitivity than its indirect counterpart, but recent progress in material sciences, such as discovery of graphene and nanoparticles, has already rapidly reducing the sensitivity gap between the two.

Currently, label-free biosensor has vastly improved into a powerful technique and has been applied toward development of new generation of immunoassays [207]. For example, sensitivity of amperometric-based direct immunosensor for detection of Carcinogenic Embryonic antigen (CEA) had dramatically increased from limit of detection (LoD) of 60 pg/ml in 2008 [208] to 0.001 pg/ml in 2013 [209], which is clear that it is more sensitive than enough while commercial ELISA-based detection limit is still around 2.88 pg/ml (USCNLIFE Science & Technology Co., Ltd. (Wuhan,China) according to manufacturer's instructions)

Likewise, the sensitivity of immunosensors for malignant tumor marker alfa-fetoprotein (AFP) had increased from LoD of 2,400 pg/ml in 2005 [161], to 560 pg/ml in 2006 [210], 80 pg/ml in 2008 [153], 40 pg/ml in 2010 [211], 3 pg/ml in 2013[151], and 0.885 pg/ml in 2014 [150], which had very far exceeded the 45,000 pg/ml

threshold of ELISA method [212].

It is obvious that the progress of material science applied in direct method is outpacing indirect method's limit of detection advantage, and using indirect method does not always mean the sensor fabricated will have superior sensitivity to its direct counterpart, as samples shown in **Table 1.**

Although having very low detection limit is a good feature, but for real application it rarely is a primary concern. Key features that will determine a sensor's future are swiftness, ease of use, high reliability, and shallow user learning curve [213].

Thus, label-free diagnostic kit has potential to deliver detection capability as good as its labeled counterparts with potentially longer shelf life, significantly lower cost and complications in application. Also since cost reduction is one of our primary concerns, we decided to apply direct amperometric method to this work.

Table 1: Comparison between label-based immunosensor and label-free immunosensor for AFP

Electrode / Measurement	Surface Mod / Label // Antigen	LoD ($x10^{-12}$ g/ml)	Range ($x10^{-9}$ g/ml)	Ref.
GCE / CV, (indirect)	AuNP-Ab-BSA / Ab-BSA-Ab-HRP-Graphene // AFP	450	1.0-100	[214]
GCE / CV, (indirect)	Au nanowires-Zinc oxide nanorods-Ab1-Antigen / Ab2-HRP // AFP	100	0.5 - 160	[215]
Modified Au / CV, (direct)	([MWCNT-Chitosan]-[Platinum-PrussianBlue])x(1 to 10 layers)-Ab-BSA // AFP	80	0.1-200	[153]
GCE / CV, (direct)	MWCNT-PrussianBlue-AuNP-Ab-BSA // AFP	3	0.01-300	[114]

3.1.5 Performance factors

As it has been proven that label-free can achieve better than label-based immunosensor constructs, we are now going to elaborate further about factors affecting its detection capability and performance. Cross-

validation with gold standard (such as ELISA) must always be conducted to confirm the performance results.

3.1.5.1 Limit of detection

Limit of detection is the lowest amount of target antigen that can be detected and differentiated from the total absence of that analyte. Almost always, an assay cannot accurately measure target antigen concentration down to absolute zero quantity, and sufficient quantity of analyte is needed to generate enough signal larger than the background noise. Noise is fluctuation in the instrument that generates signal even in absence of target antigen. This noise can be constantly present, called background noise, and must also be put to consideration when interpreting results [216].

The factors directly affecting these conditions would be the elements that involve in contact and capture of the target antigen, which are the electrode and the antibody. Unsurprisingly, oriented immobilization of the antibody and utilization of high-affinity antibodies on the electrode surface are critical factors in achieving high sensitivity, specificity, and low limit of detection. [217-219]

Limit of detection, as suggested by Armbruster *et al*. in 2012, can be determined by the following equation;

(I) $$LoD = LoB + 1.645(SD_{low\ concentration\ sample}) \quad (15)$$

Where *LoB* means Limit of Blank, which is given by;

$$LoB = \text{mean blank} + 1.645(SD_{blank}) \quad (16)$$

Both *LoD* and *LoB* are important for discrimination of presence or absence of analyte [220]. Another, more simple formula for determining *LoD* was proposed in 2011 by Borgmann *et al*. [221] as:

(II) $$LoD = SD_{background\ signal} / \text{Sensitivity} \quad (17)$$

3.1.5.2 Sensitivity

Sensitivity is known as true positive rate. High sensitivity mean that sensor is less prone to “overlook” the target analyte and give out false negative signals. It is defined by Borgmann *et al* as slope of change in signal with change in concentration [221]

$$\text{Sensitivity} = \Delta\text{Corrected Signal} / \Delta\text{Concentration} \quad (18)$$

While corrected signal = measured signal – blank signal.

3.1.5.3 Specificity

Specificity is true negative rate. Highly specific means that sensor detects only the target analyte, and not giving out false positive by identifying other interfering substances as analyte. In a work of immunosensor fabrication by Chrouda *et al*, they tested by elaborating different electrodes in the same condition but without antibody immobilization. No significant variation of relative variation of charge transfer resistance should be observable if the assay is specific [222].

3.1.5.4 Linear range (Working range)

Linear range is the range of antigen concentration that the immunosensor can successfully detect, as the sensor's response is inversely proportional to the antigen concentration and the higher limit is due to full occupation of electrode space. This should not be confused with *limit of detection*.

Linear range is determinable by the "method of least squares", which is about drawing the "best" straight line through data obtained from experiments. However, in case of label-free immunosensor, the response would be inversely proportional to the concentration of antigen. But before that, correlation must be determined:

Correlation and regression, to determine whether there is a linear relationship between two variables x_1 and y_1.:

$$r = \frac{n\Sigma x_1 y_1 - \Sigma x_1 \Sigma y_1}{\sqrt{[n\Sigma x_1^2 - (\Sigma x_1)^2][n\Sigma y_1^2 - (\Sigma y_1)^2]}} \quad (19)$$

r is Pearson's correlation coefficient, *n* is the number of data points. The number *r* must lie between +1 and -1. The nearer to the +1 the greater probability that a definite linear relationship exists between the variable *x* and *y*, while *r* tend toward zero means *x* and *y* are not linearly related [223].

Linear Regression, once the linear relationship has been identified as high probability, then the best straight line through data points must be evaluated by the method of least square. The equation of a straight line is

$$y = ax + b \quad (20)$$

Where *y* is dependent variable, plotted as a result of changing independent *x* variable. To obtain the regression line, method of least square must be conducted by the equation of:

$$a = \frac{n\Sigma x_1 y_1 - \Sigma x_1 \Sigma y_1}{n\Sigma x_1^2 - (\Sigma x_1)^2} \quad (21)$$

$$b = \bar{y} - a\bar{x} \quad (22)$$

Examples of label-based immunosensor calibration curve is shown as **figure 21 (a)** while calibration curve of label-free immunosensor is shown as **figure 21 (b).**

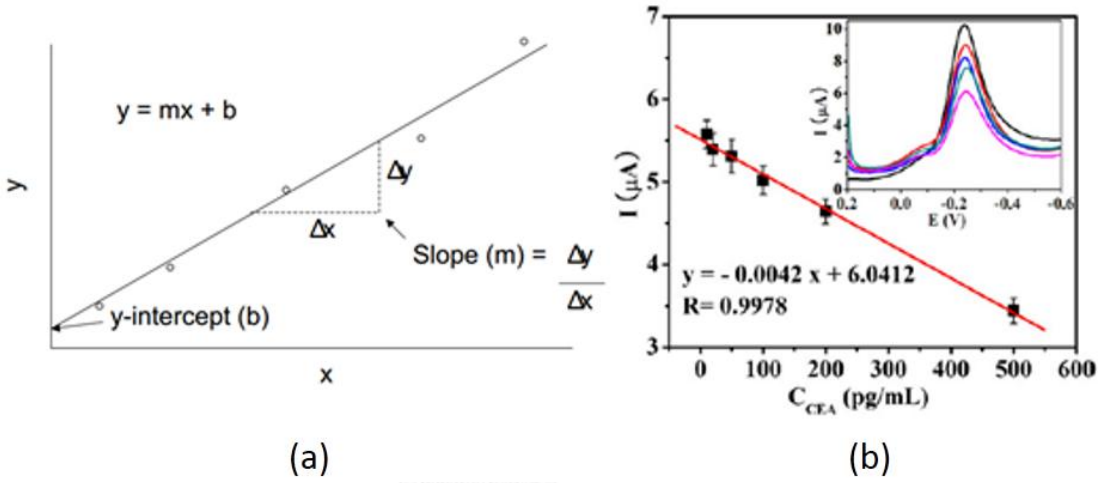

Figure 21: (a) typical calibration curve after method of least squares has been implemented (b) An example of immunosensor calibration curve for CEA detection in a study by Kong *et al*. [224]. Inset is the DPV curves of the immunosensor after incubating with different CEA solutions with concentration of 0, 10, 50, 200, and 500 pg/ml (from top to bottom)

3.1.5.5 Stability

Stability of immunosensor should also be considered as well. Typically, the factor affecting the stability of any immunosensor can be classified into two classes, internal and external.

Internal factors are its compositions' stabilities on its own and stability after assembled together. External factors can be classified as physical (heat, sunlight, moisture), chemical (inadvertent contact with chemicals), and biological factors (sticking of unrelated proteins and contamination).

Because the development objective of this immunosensor is to use in at point-of-care and in the field and chemical and biological factors can only be prevented by protective containment, the parameters to be tested (before application of antibodies) are:

1. Freeze, near-freeze, and thaw stability

Determine if the electrode can functional properly after frozen for 24 hours at **-20°C** (long-term antibody storage temperature), and **4°C** (short-term antibody storage temperature) and thawed unassisted at room temperature for two or three times. This data can be used to evaluate if the electrode can be pre-conjugated with antibody and be ready-to-use.

2. Short-term temperature stability

Determine if the electrode can function properly after kept at room temperature for 24-72 hours in ambience environment (unassisted). This data can be used to determine short-term stability in suitable conditions.

3. Long-term stability

Determine potential degradation of electrode activity over time in long scale. This data can be used to determine prolonged storage of non-conjugated electrode sets at room temperature.

4. Heat and sunlight exposure

Determine potential degradation of electrode activity after prolonged exposure to sunlight, hot/ humid environment, and both for 1-8 hours. This data can be used to determine tolerance for real-situation in-the-field diagnostic.

3.1.5.6 Pretreatment

When the positive potential first applied to the electrode, there will be a surge of current which would decay to zero if no electroactive species are present. This current is called “Charging current”, which creates excess of negative charge on the working electrode and deficiency on another end (i.e. counter electrode). This leads to solution adjacent to the electrodes acquiring an opposing charge, creating electrical double layer.

Pretreatment (activation) of working electrodes reportedly has beneficial results of reducing charging current due to already active surface, which would make the test result more accurate [225].

3.1.5.7 Antigen size

As obstruction of diffusion layer is the key parameter determining the response signal, the size of the obstructing object (antigen) would obviously affect the response. As larger molecules needs more area to occupy, which lead to more electron transfer obstruction than smaller molecules, hence easier to detect as the current will drop more.

Consider a work by Xinle Jia *et al* [150] in **table 2**, they used the same sensor to detect two different antigens. The result provided two different limit of detection. The limit of detection for CEA is 0.650 pg/ml, 0.235 pg lower than the LoD of alfa-fetoprotein (AFP).

Carcinoembryogenic antigen (CEA) has molecular weight of 200,000 Daltons while AFP is 70,000 Daltons. As CEA is larger, this corresponds with the resulting limit of detection in the work. As LipL32 outer membrane protein is 32,000 Daltons, we would expect the limit of detection to be higher than this example

Table 2: An immunosensor for detection of CEA and AFP.

Electrode / Measurement	Surface Mod / Label // Antigen	LoD ($x10^{-12}$ g/ml)	Range ($x10^{-9}$ g/ml)	Ref.
ITO / DPV	Reduced graphene oxide-Thionine-AuNP-Ab-BSA // CEA, α-Fetoprotein (AFP)	0.650 (CEA) 0.885 (AFP)	0.01-300	[150]

Thus, in order to unbiasedly compare label-free electrochemical immunosensor systems, we must compare systems with the same antigen. And as we use graphene as our base material, we shall present the graphene system that have CEA and AFP as target antigens as models for comparison.

3.1.5.8 Redox mediator

Consider the work by Huang *et al*. and works by others, one can spot a little difference. In the work by Huang *et al*, they did not utilized redox mediator as electron shuttle for the immunosensor, while other groups did.

Indeed, the immunosensor can detect the antigen, but with vast difference in limit of detection and linear working range, as can be seen in **table 3**. Hua-Ping P. *et al* utilized Thionine and Polydopamine as redox mediators, Xinle J. *et al* utilized only Thionine as the redox mediator, while Ying Z. *et al* used arginine. These three works, despite having structure not so different from graphene immunosensor by Huang K-J. *et al*, reportedly had much better limit of detection and wider linear working range

Table 3: Comparison between redox mediated and mediator-free immunosensor constructs.

Electrode / Measurement	Surface Mod / Label // Antigen	LoD ($x10^{-12}$ g/ml)	Range ($x10^{-9}$ g/ml)	Ref.
CILE / CV, EIS	[GR-NH_2]-AuNP-Ab-BSA // **α**-1-fetoprotein	100	1-250	[226]
GCE / CV, DPV, UV-vis	GO-**Thionine-Polydopamine**-AuNP-Ab-BSA // **α**-Fetoprotein (AFP)	30	0.1-150	[156]
Bare Au / CV, ECL,UV-vis	Graphene-AuNP-[acid-**arginine**]-Ab-BSA // **α**-1 Fetoprotein (AFP)	0.3	0.001-10	[154]
ITO / DPV	Reduced graphene oxide-**Thionine**-AuNP-Ab-BSA // CEA, **α**-Fetoprotein (AFP)	0.885 (AFP)	0.01-300	[150]

3.1.5.9 Number of conductive layers

Consider the work by Zhang *et al*, presented in **table 4**. The CV response signal increases as they increase the number of MWCNT-PEI-AuNP/Prussian blue bilayers, reaching max value at 5 bilayers. The reason given was that the increased amount of Prussian blue on the electrode surface contributed to the higher response, while stacking the bilayers too high will result in obstruction of electron transfer on the surface of electrode. Therefore, the number of layers (if any) must be considered carefully [119, 227].

Layer-by-layer immunosensor assembly by Ou C. *et al* also confirms this. The peak current reportedly start to slightly decrease after MWCNT/Chitosan-Pt/Prussian blue reached 10^{th} layer [228].

Table 4: Immunosensors with multiple layer assembly.

Electrode / Measurement	Surface Mod / Label // Antigen	LoD ($x10^{-12}$ g/ml)	Range ($x10^{-9}$ g/ml)	Ref.
Au / CV	[MWCNT/Chitosan-Pt/Prussian blue]x10 // AFP	80	0.1-15, 15-200	[228]
GCE / CV	[MWCNT-PEI-AuNP/Prussian blue]x5-Ab-BSA // CEA	800	0.5-160	[119]

3.2 Graphene immunosensors

Graphene has been increasingly popular in many fields, biosensors included, due to its excellent theoretical value of physical strength and electrical conductivity. Currently, the word "Graphene" is being used loosely, not only limited to one-layered carbon atoms, but also few-layered (less than 10 layers) versions of them as well [101, 229, 230].

Application of graphene as a component in immunosensor fabrication varies in type and quality, depends on substrate and resources available to the authors. As state previously, chemically reduced graphene oxide is denoted as rGO, while exfoliated pristine graphene is abbreviated as GR, as these two types have vastly different quality and has to be differently classified.

And as stated prior, the target must be the same antigen for unbiased comparison to be conducted. Here in table and table, we drawn a comparison chart for AFP and CEA immunosensors respectively. From this **table 5**, it can be seen that throughout the years, immunosensor fabricated from graphene and graphene oxide do not differ too much from each other in term of limit of detection and linear range even in different configurations. This can partly prove that graphene is a suitable material for fabrication of immunosensor electrodes.

Table 5: Samples of graphene-based direct voltammetric-amperometric immunosensors for detection of AFP.

Working Electrode / Measurement	Surface Modification // Antigen	LoD ($x10^{-12}$ g/ml)	Linear Range ($x10^{-9}$ g/ml)	Ref.
CILE / CV, EIS	[GR-NH_2]-AuNP-Ab-BSA // **α**-1 Fetoprotein	100	1-250	[226]
GCE / CV, EIS, DPV	GR-PVA-[MPS-TMCS-APTS-CNT-Ab-BSA] // **α**-1 Fetoprotein	60	0.1-100	[231]
Au / CV, Amp	AgNP-GO-Nafion-AuNP-Ab-BSA // **α**-1 Fetoprotein	3	0.01-100	[232]
Bare Au / CV, ECL,UV-vis	Graphene-AuNP-[acid-arginine]-Ab-BSA // **α**-1 Fetoprotein	0.3	0.001-10	[154]
GCE / CV, DPV, UV-vis	GO-Thionine-Polydopamine-AuNP-Ab-BSA // **α**-1 Fetoprotein	30	0.1-150	[156]
ITO / DPV	Reduced graphene oxide-Thionine-AuNP-Ab-BSA // CEA, **α**-1-Fetoprotein	0.885 (AFP)	0.01-300	[150]
GCE / DPV, CV	Dialdehyde cellulose-Ionic liquid-Ab-BSA // **α**-1 Fetoprotein	70	0.1-60	[233]

From this **table 6**, it can be seen that application of graphene alone can even surpass application of graphene with ionic liquid, which is an excellent electron mediator. However, the result by Samanman S. does seem a little bit “too good to be true”, comparing with other similar constructs. Nevertheless, they still shows that graphene plays crucial role in achieving low limit of detection and wide linear range.

Table 6: Samples of graphene-based direct voltammetric-amperometric immunosensors for detection of CEA.

Working Electrode / Measurement	Surface Modification // Antigen	LoD ($x10^{-12}$ g/ml)	Linear Range ($x10^{-9}$ g/ml)	Ref.
GCE / CV, EIS, Amp	[AuNP-GR-Thionine-AuNP]-Ab-BSA // CEA	4	10-500	[224]
CILE / CV, EIS	rGO-poly(L-Arginine)-AuNP-Ab-BSA // CEA	30	0.5-200	[234]
GCE / CV, EIS, Amp	HSO_3-rGO-Thionine-[Chitosan-PdCu]-Ab-BSA // CEA	4.86	0.01-12	[235]
GCE / DPV,	Ionic liquid func. Graphene-AuNP-Ab-BSA // CEA	0.001	0.000001 (1 femto)-100	[209]
Au / CV, EIS, Amp	GR-Chitosan-AuNP-Ab-BSA // CEA	0.0002	0.000001-1	[236]
GCE / CV, DPV, EIS	Au-Pt Nanowire-Thionine-rGO-Ab-BSA // CEA	6	0.005-100	[237]
ITO / DPV	Reduced graphene oxide-Thionine-AuNP-Ab-BSA // CEA, α-Fetoprotein (AFP)	0.650 (CEA)	0.01-300	[150]

From this **table 7**, it can be seen that in non-graphene immunosensors, the limit of detection continually go down (better) throughout the years, representing advancement in material technologies. The best in line that we had is the one by Wen J. *et al* fabricated just from multiwalled carbon nanotubes, Prussian blue, and gold nanoparticles. This became one of the role model of our work due to its simplicity and excellent detection capability. In fact, this work is inspired by the work of Wen J. *et al*. because of its simplicity, low limit of detection, and wide linear range even without application of graphene.

Table 7: Samples of non-graphene direct voltammetric-amperometric immunosensors for detection of AFP

Working Electrode / Measurement	Surface Modification // Antigen /// Redox mediator	LoD ($x10^{-12}$ g/ml)	Linear Range ($x10^{-9}$ g/ml)	Ref.
SPE (Ag ink-graphite) / CV, DPV	HRP-Ab1-Antigen // α-1 Fetoprotein	740	20-150	[238]
Bare Au / CV, EIS	Nafion-Thionine-AuNP-Ab // α-1 Fetoprotein	2400	5.0-200	[161]
Bare Au / CV, EIS	[Nafion-Thionine-AuNP]x(1 to 6)-Ab-HRP // α-1 Fetoprotein	560	1-250	[210]
Modified Au / CV	([MWCNT-Chitosan]-[Platinum-PrussianBlue])x(1 to 10 layers)-Ab-BSA // α-1 Fetoprotein	80	0.1-200	[153]
GCE / CV, EIS	$HAuCl_4$-Au nanolayer-PrussianBlue-[Chitosan-Fe3O4-AuNP]-Au-HRP // α-1 Fetoprotein	20	0.05-300	[159]
GCE / CV	$HAuCl_4$-MWCNT-PDDA-DNA film-Thionine-AuNP-Ab-BSA // α-1 Fetoprotein	40	0.01-200	[211]
GCE / CV	MWCNT-PrussianBlue-AuNP-Ab-BSA // α-1 Fetoprotein	3	0.01-300	[239]
GCE / CV, DPV	PdNP-CO-rGO // α-1 Fetoprotein	5	0.01-12	[240]

Due to the fact that there has been no immunosensor for LipL32 known to us as of date, in order to determine suitable projected limit of detection and linear range for our work we have to rely on immunosensor constructs that employ antigen of similar molecular weight. As LipL32 has molecular weight of 32 kDa [241], the most similar and reasonably popular among immunosensor is Cardiac Troponin T (cTNT), with predicted molecular weight of 33-36 kDa [242, 243]. cTNT immunosensor samples are shown below in **table 8.**

From the table, in order to fully cover potential responses, we projected that the starting point for limit of detection in our work should be a little bit lower than their works, such as 10 pg/ml. For the upper limit, the linear range of the work bu Wen J. *et al* should be used as reference as it is wider, thus the upper limit of linear range should be at 500 ng/ml.

Table 8: Samples of voltammetry-amperometry immunosensors for detection of cTNT

Working Electrode / Measurement	Surface Modification // Antigen /// Redox mediator	LoD ($x10^{-12}$ g/ml)	Linear Range ($x10^{-9}$ g/ml)	Ref.
Bare Au / CV	PEI-MWCNT-COO^--Ab-Glycine // Cardiac Troponin T	33	0.1-10	[162]
SPCE / CV	[Streptavidin-polystyrene]-[Biotin-Ab]-BSA // Cardiac Troponin T	200	0.1-10	[244]

In **Table 9**, it can be seen that the first work, when compared with the work by Samanman S. in the last table, show drastic difference between application of porous nanogold and graphene, with the latter being much superior in term of limit of detection and linear range. Therefore, graphene is suitable and should be used as the conducting layer on the electrode surface.

Table 9: Samples of non-graphene direct voltammetry-amperometry immunosensors for detection of CEA.

Working Electrode / Measurement	Surface Modification // Antigen /// Redox mediator	LoD ($x10^{-12}$ g/ml)	Linear Range ($x10^{-9}$ g/ml)	Ref.
GCE / CV	Porous nanogold-Chitosan-AuNp-Ab-BSA // CEA	60	0.2-120	[208]
Bare Au / CV	HDT-AuNP-StaphylococcalProteinA-Ab-BSA // CEA	0.1	0.001-100	[245]

3.2.1 Graphene-PEDOT:PSS

Graphene-PEDOT:PSS to be used in our study is defined as having 0.5% total Graphene content,

PEDOT-PSS ratio 1:2.5 by weight, with pH of 3-4. According to the manufacture, this is the optimum graphene content in PEDOT:PSS for electrical conductivity. And according to Andrews *et al*, this PEDOT:PSS ratio is the optimum ratio for electrical conductivity, reaching 1 S cm^{-1} [246].

3.2.2 Proposed immunosensor construct

From all the reasons given, our proposed immunosensor construct for LipL32 is BSA/anti-LipL32/PrA/cAuNPs/CS/Graphene-PEDOT:PSS-Prussian blue/SPCE

Chapter 4

Materials and Method

4.1 Materials

- Screen-printed carbon electrode purchased from Qualisense Co., Ltd., Thailand
- 37% M Hydrochloric acid (HCl), Trisodium citrate dihydrate ($Na_3C_6H_5O_7.H_2O$), Potassium ferricyanide ($K_3[Fe(CN)_6]$), Ferric chloride ($FeCl_3$), Chloroauric acid ($HAuCl_4.3H2O$), Bovine Serum Albumin (BSA), Staphylococcal Protein A (PrA), and Chitosan from crab shells (middle viscous) (CS) were purchased from Sigma-Aldrich.
- Sodium hydroxide pellets (NaOH), Potassium Chloride (KCl), Di-potassium Hydrogen Orthophosphate (K_2HPO_4), and Potassium Dihydrogen Orthophosphate (KH_2PO_4) were purchased from Ajax Finechem Pty Ltd.
- Graphene-PEDOT:PSS (Phene X-4011) purchased from Innophene Co., Ltd., Thailand
- Anti-LipL32 antibody (Ab), LipL32 protein (Ag), intact and sonicated *Leptospira interrogans* cells were provided by courtesy of Department of Microbiology, Faculty of Medicine, Chulalongkorn University.

All chemicals are of analytical grade, except Chitosan, Trisodium citrate dihydrate, ferric chloride, and Graphene-PEDOT:PSS which are reagent grade. Solutions were prepared by using deionized water (18MΩ cm) produced by a Thermo Scientific Barnstead EASYpure deionization unit.

4.2 Apparatus

Electrochemical measurements were performed with Metrohm Autolab potentionstat PGSTAT101 (Metrohm, Switzerland) with a conventional three-electrode configuration comprised of a working electrode clamp for use with screen-printed carbon electrode (SPCE), a platinum wire auxiliary electrode, and a silver/silver chloride reference electrode (Ag/AgCl). Every cyclic voltammetry (CV) measurement was performed at a scan rate of 50 mV s-1 at room temperature (25°C).

4.3 Electrode Fabrication Method

5 ml of potassium chloride (KCl) solution of 0.1 M (pH 6) were used in all experiments. The working electrodes were always washed with 0.1 M KCl solution before and after CV measurement or after every

incubation step of any biomolecules. The counter and reference electrodes were always washed with deionized water and wiped dry with clean paper towel after any electrochemical operation was completed.

4.3.1 Fabrication of SPCE modified with Graphene-PEDOT:PSS-Prussian blue (GPB)

Fresh aqueous solution of Prussian blue (PB) was made by mixing various compositions to final concentration of 15 mM $K_3[Fe(CN)_6]$, 15 mM $FeCl_3$, 0.1 M KCl, and 0.1 M HCl in deionized water giving a dark green solution. Then 2.5 ml of GR (Phene X-4011) was pipetted and mixed with 2.5 ml of the prepared PB solution by magnetic stirring, yielding a black solution. The mixture was then continuously magnetic-stirred at a medium speed for 30 minutes. Finally, the solution color was changed from black to blue, which will be specified as a GPB solution. One µL of GPB solution was next drop-casted on the Screen-printed carbon electrode which was then baked at 100 °C for 60 minutes. The GPB electrode was then carefully washed with 0.1 M KCl and activated in a solution of supporting electrolyte containing 0.1 M KCl and 0.1 M HCl by cyclic voltammetry with a scan range from -0.05 V to 0.35 V (50 mV/s, 16 scans) The SPCE with a stable GPB surface layer was then obtained and specified as GPB/SPCE

4.3.2 Preparation of CS/GPB/SPCE

One percent by weight of chitosan solution was made by mixing 0.05 mg Crab shell chitosan with 5 ml of 1% v/v acetic acid and the mixture was then magnetic stirred overnight at room temperature. After the mixture was fully dissolved, the pH of the solution was then slowly adjusted to 6 by using 0.1 M NaOH. Two µL of the pH 6 CS solution was then drop-casted on the GPB/SPCE electrode before being air-dried. This process was repeated three times to generate three layers of CS on the modified electrode surface.

4.3.3 Preparation of cAuNPs/CS/GPB/SPCE

cAuNPs were prepared by reduction of chloroauric acid ($HAuCl_4$) in a trisodium citrate solution known as Fren's method [247]. In brief, 20 ml of a 1 mM $HAuCl_4$ solution was set to the boil, then 2 ml of 1% trisodium citrate (w/v) solution was added. The mixed solution was kept continually stirred and boiled for another 30 minutes, resulting in a wine-red solution. The solution bottle was then wrapped in an aluminum foil and kept in at 4°C before use. This process was reportedly resulted in nanoparticles with an average diameter of 13.9 nm [248].

The immobilization of cAuNP onto the modified electrodes followed the protocol of Bhalla *et al* [249] with some adjustments. Briefly, 1 ml of cAuNP solution was added to 4 ml of 0.1 M KCl solution, the CS-GPB modified electrode was then immersed in this solution and cAuNPs were electrodeposited onto the surface by applying a fixed voltage of +0.65 V for 60 seconds.

4.3.4 Preparation of PrA/cAuNPs/CS/GPB/SPCE

Staphylococcal Protein A was diluted with 0.025 M PBS (pH 6) to concentrations of 0.1, 0.05, 0.01, and 0.002 mg/ml. 10 µl of the diluted solution was then drop-casted on the modified electrodes and was incubated at 4°C for 18 hours, and was washed to eliminate unbound PrA.

4.3.5 Preparation of anti-LipL32 antibody/PrA/cAuNPs/CS/GPB/SPCE

Anti-LipL32 antibody was diluted with 0.025 M PBS (pH 6) to concentrations of 0.5, 0.25, 0.05, and 0.01 mg/ml. 10 µl of the diluted solution were then drop-casted on the modified electrodes and was incubated at 4°C for 18 hours, and was washed to eliminate unbound antibodies.

4.3.6 Preparation of BSA/anti-LipL32 antibody/PrA/cAuNP/CS/GPB/SPCE

Bovine serum albumin (BSA) was diluted to 0.25% by weight, with DI water. 10 µl of the diluted solution was then drop-casted on the modified electrodes. The resulted electrode was then incubated at 25°C for 2 hours and was washed to eliminate unbound BSA

4.3.7 LipL32 detection

After every other modification steps were completed, the antigen is to be added. 10 µl of LipL32 antigen of specified concentrations was then incubated on the BSA/anti-LipL32/PrA/cAuNPs/CS/GPB/SPCE for 1 hour at 25°C. The finished electrodes were then tested with cyclic voltammetry in 0.1 M KCl solution with scan rate of 50 mV s^{-1}

4.4 Optimization of Prussian blue concentration for GPB fabrication

The fabrication process for 2 mM and 40 mM of Prussian blue were the same as the process of 15 mM Prussian blue, except the concentration of $K_3[Fe(CN)_6]$ and $FeCl_3$ were changed to 2 mM and 40 mM accordingly. Likewise, 2.5 mL of the prepared PB solutions were then mixed with 2.5 mL of Graphene-PEDOT:PSS stock

solution using magnetic stirrer at medium speed for 30 minutes. The stirred solutions were then drop-casted on screen-printed carbon electrode at baked at 90°C for 30 minutes. The finished electrodes were then tested with cyclic voltammetry in 0.1 M KCl solution with scan rate of 50 mV s^{-1}.

4.5 Effects of numbers of GPB layers on CV characteristics

For one layer of GPB, the prepared 15 mM GPB solution was drop-casted on SPCE electrode and baked at 90°C for 30 minutes. The same process was then repeated for two and three times to fabricate GPB/SPCE with two and three layers of GPB respectively. The cyclic voltammetric responses were then measured and compared between the electrodes.

4.6 Optimizing number of Chitosan layers

A set of one-layer GPB/SPCE electrodes were then put to test for drop of peak current unrelated to biomolecule adhesion. After 15 mM of GPB was drop-casted on screen-printed carbon electrodes and baked at 100°C for 60 minutes, the GPB electrodes were then drop-casted up to three layers of one percent by weight Chitosan solution and air-dried. The CS/GPB/SPCE electrodes, after measurement of pre-immersion cyclic voltammetric response, were then immersed in 0.025 M PBS (pH 6) solution for 18 hours at 4°C. The cyclic voltammetric response were then measured again after immersion and the drop in peak current due to immersion in 0.025 M PBS (pH 6) were determined.

4.7 Optimizing Protein A and anti-LipL32 antibody concentration (PrA) for antigen detection

The cAuNP/CS/GPB/SPCE modified electrodes were incubated with *Staphylococcal* Protein A solution of different concentrations (0.002 mg/ml, 0.01 mg/ml, 0.05 mg/ml, and 0.1 mg/ml) for 18 hours at 4°C. After the initial cyclic voltammetric measurements were made, the PrA/cAuNP/CS/GPB/SPCE were then incubated further with different concentration of Anti-LipL32 solution (0.010 mg/ml, 0.05 mg/ml, 0.25 mg/ml, and 0.5 mg/ml) for 18 hours at 4°C and the final cyclic voltammetric responses were measured again. The two sets of data were then compared with each other. Lastly, the anti-LipL32/PrA/cAuNP/CS/GPB/SPCE were then incubated further with BSA and LipL32 antigen of single concentration of 250 ng/ml for 2 hours and 1 hour at room temperature respectively. Cyclic voltammetric measurement were then made again after antigen incubation and compared with the second data set of the electrode after antibody incubation.

4.8 Effect of anti-LipL32 antibody incubation time

The cAuNP/CS/GPB/SPCE modified electrodes were incubated with *Staphylococcal* Protein A solution of 0.01 mg/ml for 18 hours at 4°C. After the incubation was completed, cyclic voltammetric measurements were made. Then anti-LipL32 antibody solution of 0.05 mg/ml concentration were then incubated on the electrode at 4°C for different time period (2 hours, 6 hours, and 18 hours). The electrodes were washed with 0.1 M KCl immediately after the incubation period was over to stop the reaction and cyclic voltammetric measurement were conducted.

4.9 Effect of antigen solution pH

The BSA/anti-LipL32/PrA/cAuNP/CS/GPB/SPCE with PrA concentration of 0.01 mg/ml and anti-LipL32 concentration of 0.05 mg/ml were measured for its cyclic voltammetric activity. The electrodes were then incubated with LipL32 of 250 ng/ml concentration with 0.025 M PBS solution with different pH of 4, 5, 6, and 7 for 1 hour at room temperature (25°C). The cyclic voltammetric measurements were then carried out again and compared the data with pre-antigen cyclic voltammogram results.

4.10 CV characteristics

Cyclic voltammetric measurements for every step of modification were done in 0.1 M KCl with scan rate of 50 mV s^{-1} at room temperature. The peak current drop results were then compared to each other, which can be described as:

$$\%\Delta i_{pa} \text{ drop} = (\text{previous } i_{pa} - \text{current } i_{pa})/ \text{previous } i_{pa}] * 100$$

4.11 Calibration curve and limit of detection

The BSA/anti-LipL32/PrA/cAuNP/CS/GPB/SPCE with PrA concentration of 0.01 mg/ml and anti-LipL32 antibody concentration of 0.05 mg/ml were measured for its cyclic voltammetric activity prior to incubation with target LipL32 antigen of 0, 50, 100, 150, 200, 250, 300, 400, 500, and 600 ng/ml for 1 hour at 4°C. After the incubation was completed, the cyclic voltammetric responses of the electrodes were then measured and compared with the pre-incubation data.

4.12 Reproducibility

Ten newly fabricated BSA/anti-LipL32/PrA/cAuNP/CS/GPB/SPCE electrodes were checked for reproducibility by measuring cyclic voltammetric responses and compare against each other for anodic peak current differences, which were then calculated into Relative Standard Deviation (RSD) of the fabricated electrodes.

4.13 Storage stability

The fabricated BSA/anti-LipL32/PrA/cAuNP/CS/GPB/SPCE electrodes were then tested for its storage stability at day 0, 1, 2, 3, 7, 14, and 21 of the same electrodes. The electrodes were always kept at 4°C in dried form, closed container before and after measurement. Prior to measurement, the electrodes were brought to room temperature to establish equilibrium with room temperature for about 20 minutes before conducting any electrochemical measurement.

Chapter 5

Results and Discussion

In order to assemble a workable electrochemical immunosensor, optimization of three components were performed to obtain a working Graphene-Prussian blue composite (GPB) modified screen-printed carbon electrode immunosensor. These steps consisted of subtopics of optimization of Prussian blue (PB) concentration to fabricate GPB composite, numbers of GPB layers, GPB fabricating conditions, number of Chitosan layers, Protein A and antibody incubation time and concentration, and antigen solution pH, which will be discussed sequentially as follows.

5.1 Fabrication of the immunosensor

For a label-free immunosensor, one of the most popular fabrication method is to immobilize a redox couple on the electrode surface for detection of current responses. Detection of antigen concentration could then be achieved by observing a decreased current response due to blockage of charge transfer molecules by antibody-antigen complexes. And because the drop in current is crucial to detection, having high response current would also mean higher sensitivity by default. Thus, label-free immunosensors are largely focused on increasing the base current as high as possible. Usually, this can be accomplished by application of highly conductive materials such as graphene [250], carbon nanotubes [251], copper oxide nanoparticles [252], or gold nanoparticles [253], or many of said materials in tandem with each other [254], and a good redox couple such as Thionine [255], ionic liquid [110, 256], or Prussian blue [114, 153].

In our case, as our focus is on Leptospirosis, the biomarker is thus a protein called LipL32 whose molecules are prevalent on a pathogenic species of the *Leptospira* genus, *Leptospira interrogans* [9]. In order to obtain a sensitive immunosensor for LipL32, this project, therefore, involved fabrication of a working electrode consisted of based layers of PB /GR /CS /cAuNPs on SPCE. Additional layers of PrA, Ab, and BSA were sequentially added before antigen (LipL32) was incubated for its detection.

Prussian blue (PB) is a composition made from mixing potassium ferrocyanide ($K_3[Fe(CN)_6]$) with ferric chloride ($FeCl_3$) , giving out cubic $Fe_3[Fe(CN)_6]$ crystals that have excellent electrochemical activity and can be used as a

redox couple with a molecular structure as presented in **figure 22**. The reaction can be written as:

(Prussian blue)

$$4FeCl_3 + 3K_4Fe(CN)_6 \rightarrow Fe_4[Fe(CN)_6]_3 + 12KCl$$

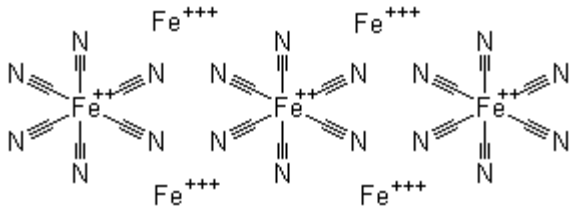

Figure 22: Molecular structure of a Prussian blue molecule [257].

In a cyclic voltammetry, with a voltage respect to Standard Calomel Electrode (SCE), application of electricity towards to anodic potential (positive voltage) would start to change PB to Berlin green (BG) at +0.9 V and change into BG at +1.4 V. Scanning back towards cathode potential (negative voltage), reduction of BG to PB start to occur at +0.9 V, and the transition would complete at +0.6 V. Further reduction of PB to Prussian white (PW) start to occur at +0.2 V, then the process completes at -0.2 V. Scanning forward to anodic potential again, oxidation peak would start to occur at +0.2 V, then completely change into PB at +0.6 V [131, 258-261]. The Prussian blue redox reaction mechanism driven by electrical potential can be described as follows and a typical cyclic voltammogram (CV) of PB-modified electrode is as shown in **figure 23**:

(PB) $Fe_4^{III}[Fe^{II}(CN)_6]_3 + 4K^+ + 4e^- \rightleftharpoons K_4Fe_4^{II}[Fe^{II}(CN)_6]_3$ (PW) V = 0.2 V

(PB) $Fe_4^{III}[Fe^{II}(CN)_6]_3 + 3Cl^- - 3e^- \rightleftharpoons Fe_4^{III}[Fe^{III}(CN)_6]_3 \bullet 3Cl^-$ (BG) V = 0.9 V

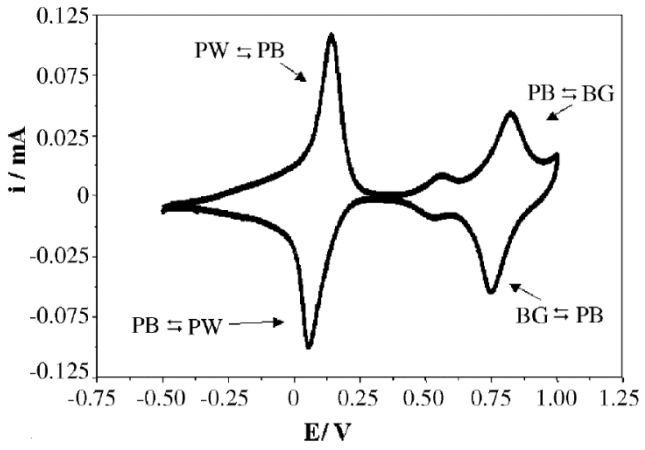

Figure 23: Cyclic voltammogram of a PB modified electrode, showing transition points of PB, BG, and PW [260].

Our redox reaction of interest is the oxidation of PW to PB, which is the reaction occurred at lower potential, thus less tendency to oxidize or reduce unrelated biomolecules. There are two methods that can be used to fabricate a Prussian blue electrode: electrodeposition and drop-casting of the PB solution. Electrodeposition can be done by applying positive voltage higher than +0.2 V usually +0.4 V or +0.7 V (vs SCE) via any conductive surface in a mixed PB solution to drive a reduction reaction of the PB complex and assimilate PB on the anode surface [113]. However, usually the electrodeposition step use only 0.4 V to electrodeposit Prussian blue, as Berlin green is not usually used [114, 262, 263]. Electrochemical behavior of modified electrodes are investigated in a solution of 0.1 M KCl (pH 6) at a scan rate of 50 mV by Cyclic Voltammetry (CV) with voltage range from minimum of -0.35 V to maximum of +0.65 V (vs Ag/AgCl) to prevent over-reduction and changing the PB composition into BG which would give another peak [114, 264, 265].

Prussian blue, however, has its drawbacks of being unstable in under high pH (>6) and prone to leakage into solution. The common approach to counter this problem is to coat the PB surface with Chitosan. Furthermore, application of *Staphylococcal* protein A (PrA) could improve the sensitivity of anti-LipL32 antibody against LipL32 antigen. Therefore, citrate-capped gold nanoparticles (cAuNPs) were used as a base for anchor of PrA over the Chitosan layer. The resulting immunosensor component diagram will be as shown in **figure 24**.

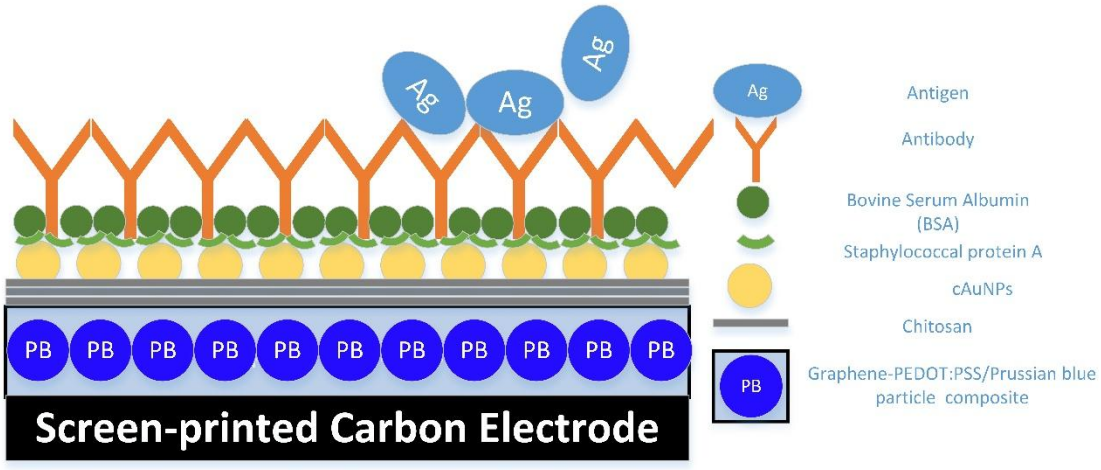

Figure 24: Schematic diagram of the proposed electrochemical immunosensor with antigen. Size not to scale.

5.2 Optimization of the fabrication process: Non-biological

The non-biological part of the immunosensor development is like the foundation of the whole electrode structure. In our case, this part consists of three major components: GPB, Chitosan (CS), and citrate-capped gold nanoparticles (cAuNPs). Each sub-topic will cover the optimization process of each component. Briefly, the GPB layer hosted redox reactions which generated responsive currents for the detection. CS prevented the leak and destabilization of PB to the solution. And finally, cAuNP acted like an anchor for the biological materials of the next section.

5.2.1 Optimizing Prussian blue concentration for GPB fabrication

In our modified electrode, GPB was the primary later drop-casted onto the bare screen-printed electrodes. The amount of PB was varied against the fixed amount of GR. We then conducted CV tests to determine optimum concentration of PB to mix with GR. In this test, we ran CV from +0.2 V to +0.65 V instead of +0.35 V to +0.65 V as in a report about Prussian blue by Karyakin in 2001 stated that electrode working potential should not be lower than 0.2V as ferricyanide ions could be too intensively reduced [261], however we found out later that, compared with +0.35 V to +0.65 V, the change in overall stability of the electrode are not noticeable. Furthermore, other electrochemical immunosensor based on PB also place the reduction limit well past 0.2 V [263, 266]. We then decide to revert back to using +0.35 V in other test as it yields higher current response, making the immunosensor more sensitive. Therefore the peak height in this graph would be lower than other CV graphs in this report although the electrode were all modified with one layer of GPB as same as other tests.

By mixing various concentration of PB with GR, we found that the highest response current achievable was ~100 µA per layer using PB concentration of 15 mM. Higher concentration would lead to a peak shift to higher voltages (higher E_p) while the peak current (i_p) stay the same, indicating impediment to electron transfer kinetic (the electron transfer process becomes slower), and higher overpotential is needed for the PB to be oxidized or reduced, possibly due to PB's crystal stacking on each other, which could impede electron transfer [267]. GPB with lower concentration (2 mM) has significantly less peak current values, possibly due to the fact that there are much less PB particles. The CV graphs are shown in **figure 25**.

In a research we reviewed, PB concentration of 15 mM was also used to mix with Graphene oxide (GO), creating GPB-like solution, which was used to drop-cast on Glassy carbon electrode surface to make hydrogen peroxide sensor. The sensor reportedly has excellent electrochemical activity due to synergistic effect between GO and PB [268], which is in agreement with our test result. Therefore we implement PB concentration of 15mM for the fabrication of GPB.

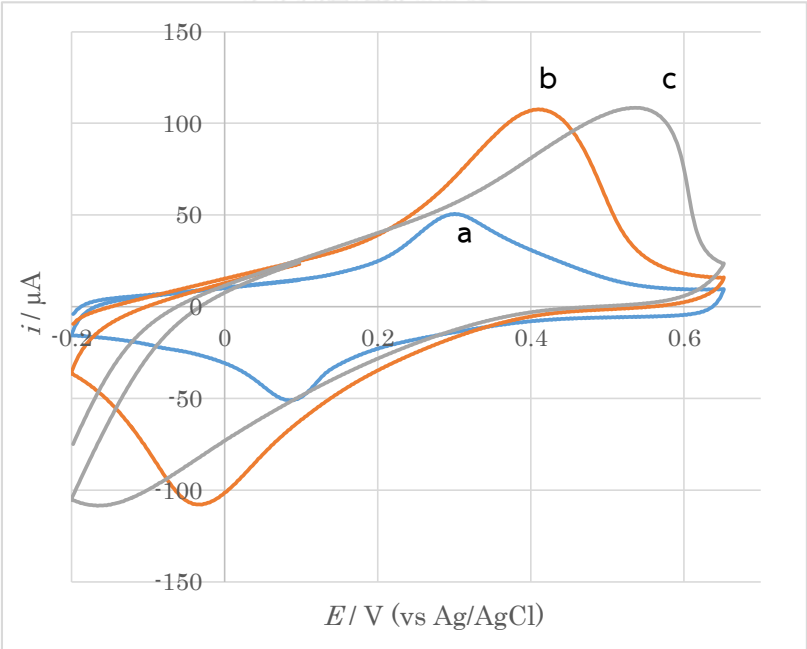

Figure 25: Cyclic voltammogram of different Prussian blue concentration after mixing with constant concentration of GR: 2 mM (a), 15 mM (b), 40 mM (c). All the tests were conducted in in 0.1 m KCL with scan rate of 50 mV s^{-1}

5.2.2 Effects of numbers of GPB layers on CV characteristics

The maximum number of GPB layers is three, as more than three layers results in E_{pc} and E_{pa} exceeding -0.35 V and +0.65 V which is the defined CV voltage boundary respectively. And as expected, more number of GPB layers led to higher response current, due to higher amount of PB on the surface. However, *E*p also became increasingly higher and peak sharpness also lessened with the number of layers, as shown in **figure 26**. This phenomena indicates slower rate of electron transfer as total thickness increases. Eventhough higher response current is favorable, it would be meaningless if the peak current cannot be clearly determined. Furthermore, the rise of peak potential needed to generate oxidation peaks also increase the risk of oxidizing unrelated biomolecules in the samples. Therefore, tests were conducted using single-layered configuration as it shows sharpest peak shape within the set boundaries.

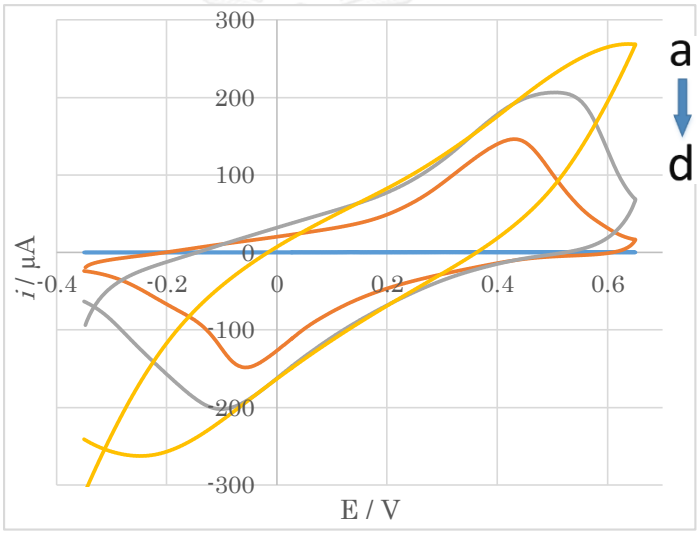

Figure 26: CV of electrodes with (a) single, (b) double, (c) triple layers of GPB, (d) and zero (blank SPCE) in 0.1 M KCL and scan rate of 50 mV S^{-1}

5.2.3 Optimizing number of Chitosan layers (CS)

As presented in many literatures, PB is prone to leak into the test solution if it is not properly covered with some other materials [124, 269]. One of the most common method to overcome this particular problem, especially in immunosensor fabrication is to use Chitosan (CS) as a protective matrix as it does not only prevent PB leakage, but also adds biocompatibility and film-forming properties [234, 270-273].

In our experiments, tremendous drop of peak current was observed after immersing the uncovered GPB modified SPCE in a PBS solution. We theorized that this was supposedly occurred from PB leakage as was

previously mentioned.

In order to optimize the numbers of CS layers on the fabricated electrode, different CS covered electrodes were immersed in 0.025 M PBS (pH 6) at 4 °C for 18 hours and tested by the CV technique. The identified electrode immersion conditions were specified based on the conditions for incubation of the fabricated electrodes with Protein A and anti-LipL32 antibodies.

The results obtained consistently showed that higher number of CS layer led to more protection against the drop of peak current (**figure 27**). After 18 hours in 0.025 M PBS (pH 6), GPB electrode without CS retained only about half of pre-immersion i_{pa}, while GPB electrodes with single, double, and triple layers of CS on top retained as much as 83.22%, 90.43%, and 95.99% peak current respectively.

As three layers of Chitosan are seemed sufficient to decrease the effect of PB leakage of the electrodes and adding more layer would mean lower CV response current, we chose this amount for later experiments. To the best of our knowledge, although there are a lot of research papers utilizing CS as a protective matrix for PB, reports regarding protection value of CS in quantitative number has not yet been found anywhere.

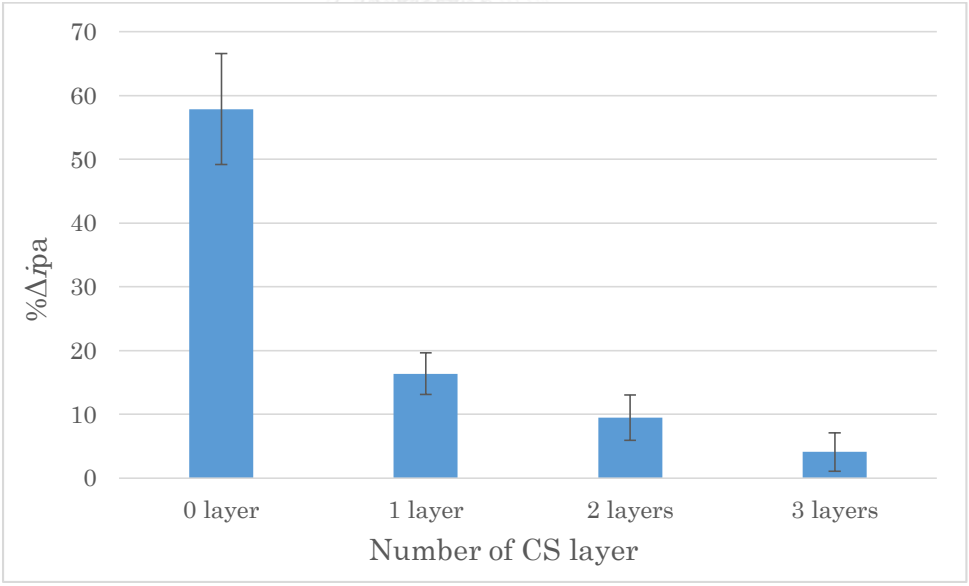

Figure 27: %drop of oxidation peak after 18 hrs immersion in 0.025 M PBS (pH 6) at 4°C with different number of Chitosan (CS) layers on the GPB modified electrodes. The scans were done in 0.1 m KCL with scan rate of 50 mV s^{-1} vs Ag/AgCl.

5.2.4 Citrate-capped gold electrodeposition (cAuNPs)

As reported earlier in section 2.6, citrate-capped gold nanoparticles has been an object of interest in

medical applications for a long time due to its inertness, non-toxicity, and biocompatible nature. It has been heavily used in immunosensor and biosensor development to immobilize immunoproteins such as antibodies and staphylococcal protein A [130, 135]. Due to the fact that application of Protein A on citrate-capped gold nanoparticles are commonplace [130, 274], we decided to synthesize cAuNPs before electrodepositing them on the modified GPB-CS electrodes for Protein A immobilization.

The resulting GPB-CS-cAuNPs electrode performed an oxidation current around ~75 µA, reducing from ~81.5 µA before cAuNPs addition, as shown in **figure 28**. This indicates that even though cAuNPs are themselves electroactive, adding them on layers of relatively non-conductive CS resulted in further insulation of the electrode. This effect of insulating cAuNPs is also reported elsewhere [234, 275]. This is in contrast to cases where cAuNPs were deposited onto a conductive layer which enhancement of electron transfer was postulated as a result of higher current responses obtained [276].

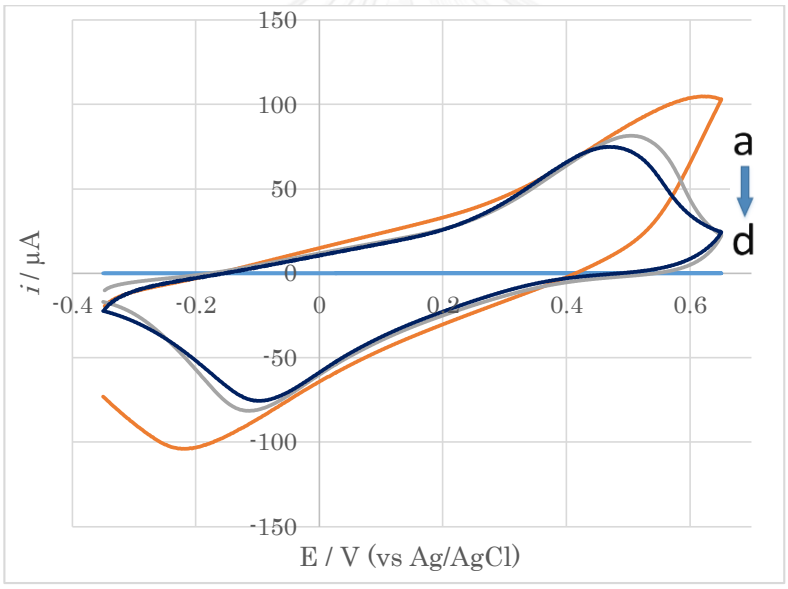

Figure 28: Cyclic voltammogram of electrodes with: GPB (a), CS-GPB (b), cAuNP-CS-GPB (c) modification and bare SPCE (d). The scans were done in 0.1 m KCL with scan rate of 50 mV s^{-1} vs Ag/AgCl.

In this section, we reported optimization of electrode fabrication steps and their effects in electrochemical response. The electrode that we obtained as optimized in this section composed of 1 layer of GPB (15mM, 1:1 ratio) with 3 layers of Chitosan and 1 layer of electrodeposited citrate-capped gold nanoparticles. The electrode displayed a peak current of around ~75 µA while its peak voltage was at ~0.44 V, which was ready for the next step of fabrication.

5.3 Optimization of the fabrication process: Biological

The biological part is the most crucial part to any biosensor since it contains biological sensing elements which are delicate yet largely influence effective measurements. This part of the electrode consists of four components: Staphylococcal protein A (PrA), anti-LipL32 antibodies (Ab), Bovine Serum Albumin (BSA), and LipL32 antigen (Ag).

Objective of PrA application on the electrode is to increase the sensitivity of antibodies using Fc portion-specific binding properties of PrA to immobilize antibodies in "standing" stance with two antigen-binding sites fully expose outwards on the PrA instead of laying down on the cAuNPs layer [127]. If the antibodies are to be immobilized on cAuNPs without using PrA, the binding capacity of immobilized antibodies might diminish as much as half of its original capacity due to its antigen-binding site (F_{ab} portion) lying side down on the electrode surface [277], as shown in **figure 29**. It also has been reported that PrA has five IgG binding domains [278], therefore the application of PrA and antibodies in this work was set at a constant weight ratio of 1:5.

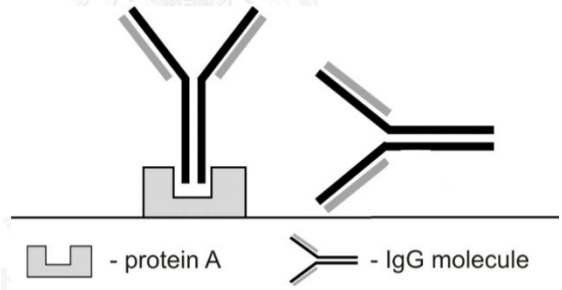

Figure 29: Simplified drawing of Ab attachment to the electrode surface with and without PrA. Adapted from [279].

As the target protein to be detected was LipL32, the anti-LipL32 antibody was hence used for the analysis. This antibody is of IgG subclass and was applied in various concentrations to determine the optimum mass ratio concentration for the fabrication of the immunosensor. However, the concentration was always in fixed at a ratio of five parts of antibodies per one part of PrA.

Bovine serum albumin (BSA) is a type of protein commonly applied on ELISA test kits and immunosensors to coat unreacted electrode surface after the application of antibodies in order to prevent non-specific binding. However, if the BSA layer is too thick it could also impeded the ionic charge transfer to the electrode surface.

Therefore, the concentration of BSA used in this work was fixed at 0.25% w/v, which is the concentration used in many immunosensor researches, electrochemical immunosensor included [280, 281].

5.3.1 Optimizing Protein A and anti-LipL32 antibody concentration (PrA)

5.3.1.1 Effect of antibody incubation time

The incubation time clearly affects the amount of antibody immobilized on the electrode surface since the soluble antibody requires time for its mass transfer to reach the solid electrode phase. With PrA concentration of 0.01 mg/ml and Ab concentration of 0.05 mg/ml, the incubation time of 2, 6, and 18 hours yielded peak current drop of ~7.8%, 16.3%, and 23.5% respectively, as shown in **figure 30**, indicating that more Ab attached to the electrode surface with time. Also, from the graph, it is evident that the amount of Ab attached on the electrode surface was approaching its equilibrium value. Thus, longer incubation time would not result in a significant change in i_{pa} response. As more Ab would supposedly improve the limit of detection and more incubation time would lead to more specific attachment of the antibodies, we then chose 18 hours incubation period to be the standard incubation time for both PrA and Ab as this is also the amount of time commonly used in antibody immobilization in other works [282-284].

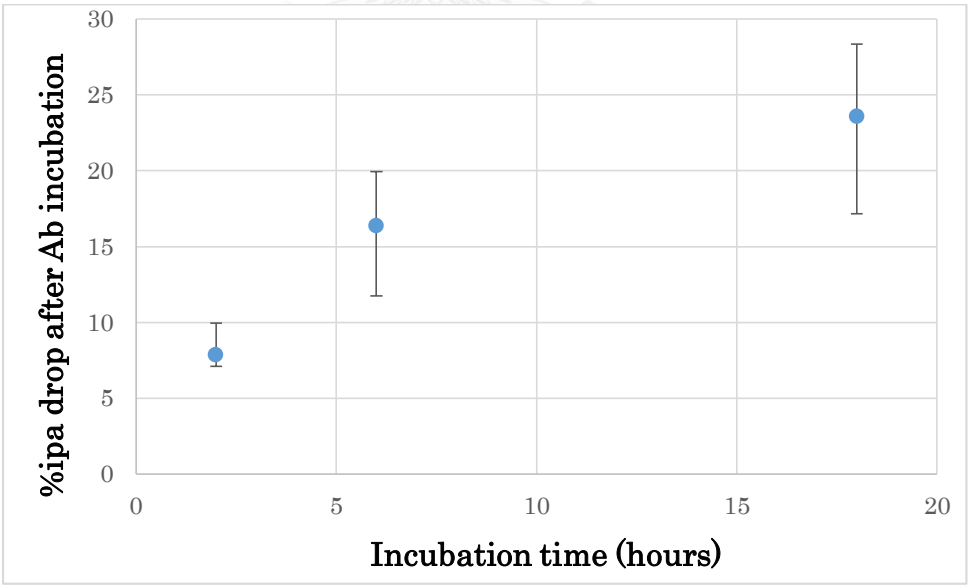

Figure 30: Percent drop of peak current under different antibody incubation time at 4 °C. The solution was 0.025 M PBS (pH 6) with antibody concentration of 0.05 mg/ml.

5.3.1.2 Effect of PrA concentration on antibody immobilization

For protein A incubation, high concentration of PrA consequentially led to further drop in response current after antibody incubation. As shown in **figure 31**, PrA concentration of 0.1 mg/ml led to 38% drop in current after Ab incubation, while 0.05, 0.01, and 0.002 mg/ml led to only 11.11%, 10.98%, and 1.37% drop respectively. This result indicated that high amount of PrA also led to higher adsorption of Ab on the electrode surface, thus impeding the charge transfer more than the low-concentration ones. The large difference in peak current drop occurred even though the ratio between PrA/Ab was identical, as one unit of PrA can optimally hold as many as five IgG antibody units, two fold difference in the amount of PrA can lead to ten times of difference in current drop after immobilization of Ab.

However, this information alone was not enough to determine the optimum concentration for detection of antigen, therefore experiments with antigen were then followed.

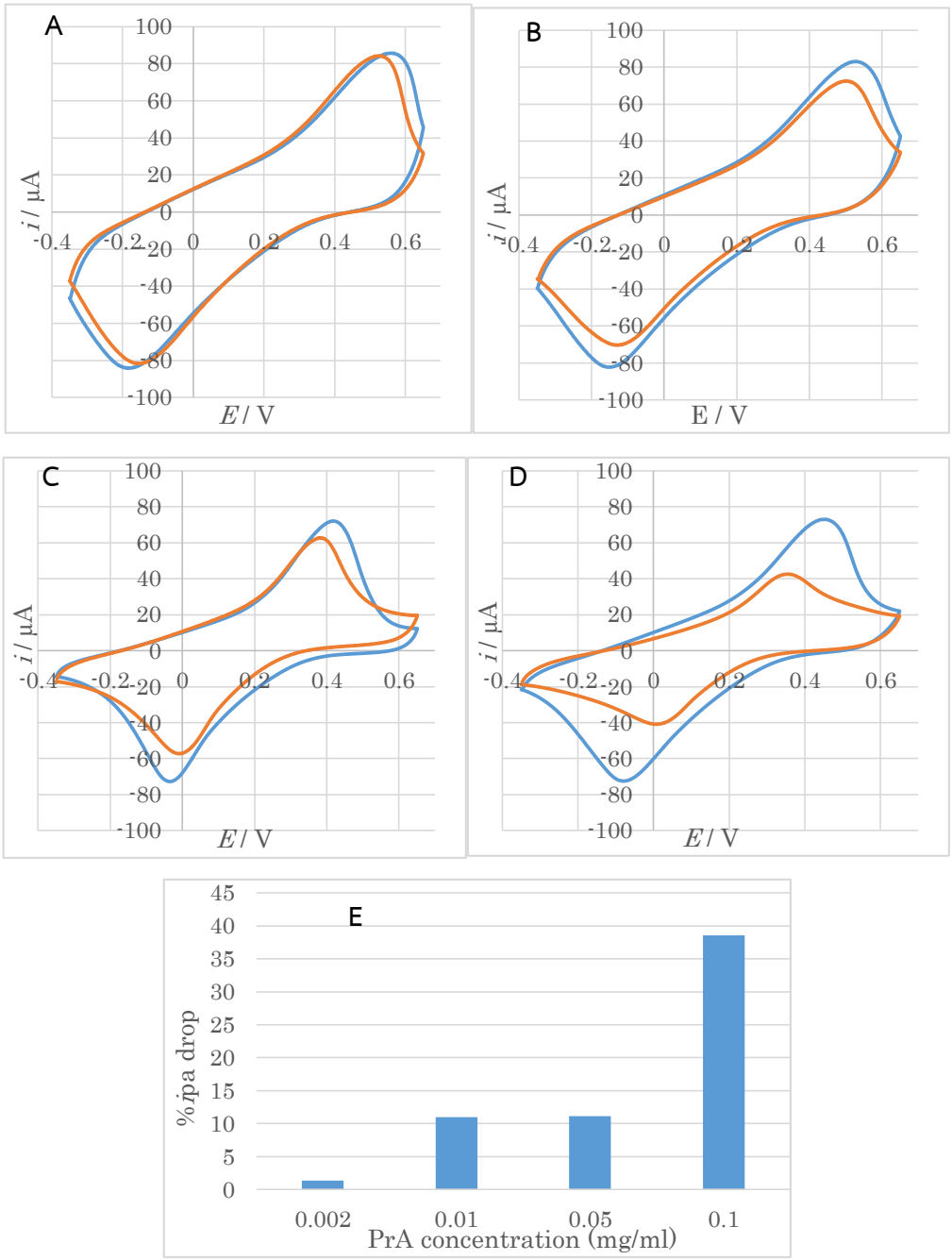

Figure 31: CV responses showing the effect of Protein A/antibody of various concentrations: 0.002/0.010 mg/ml (A), 0.01/0.05 mg/ml (B), 0.05/0.25 mg/ml (C), and 0.1/0.5 mg/ml (D), with the CV after Protein A immobilization in blue line color, and CV after immobilization of antibody in red line color. The bar graph summarizes the peak current drop of all the four graphs (E). The scan was done in 0.1 M KCl at the scan rate of 50 mV s^{-1} vs Ag/AgCl

5.3.1.3 Effect of PrA concentration on antigen detection

Modified electrodes with different PrA-Ab concentrations were then incubated with BSA and antigen (LipL32 protein, 250 ng/ml) to test for their analytical capabilities. Surprisingly, the electrodes with a relatively high PrA-Ab concentration produced much less drop in peak current comparing to those with lower concentrations after immunosensor reaction. With high PrA and Ab concentrations, the electrode surface might already be densely occupied with PrA and Ab, generating high current drop on its own. When the antigen was applied, the low concentration of antigen would add just a minuscule fraction of charge transfer obstruction to the already highly obstructed electrode. On the other hand, with appropriate density of PrA and Ab, the antigen added would contribute more noticeable charge transfer obstruction to the electrode.

The results show that, the optimum PrA concentration for detection of antigen was 0.01 mg/ml and Ab concentration of 0.05 mg/ml, which produced ~18% drop in the current, while PrA concentration of 0.1 mg/ml, 0.05 mg/ml, and 0.002 mg/ml gave CV peak current drop of only 0.2%, 4.7%, and 16.1% accordingly, as shown in **figure 32**.

Therefore, as larger drop of current after incubation of antigen is favorable due to being more sensitive, the fixed concentration of 0.01 mg/ml for PrA and 0.05 mg/ml Ab were then used in all later tests.

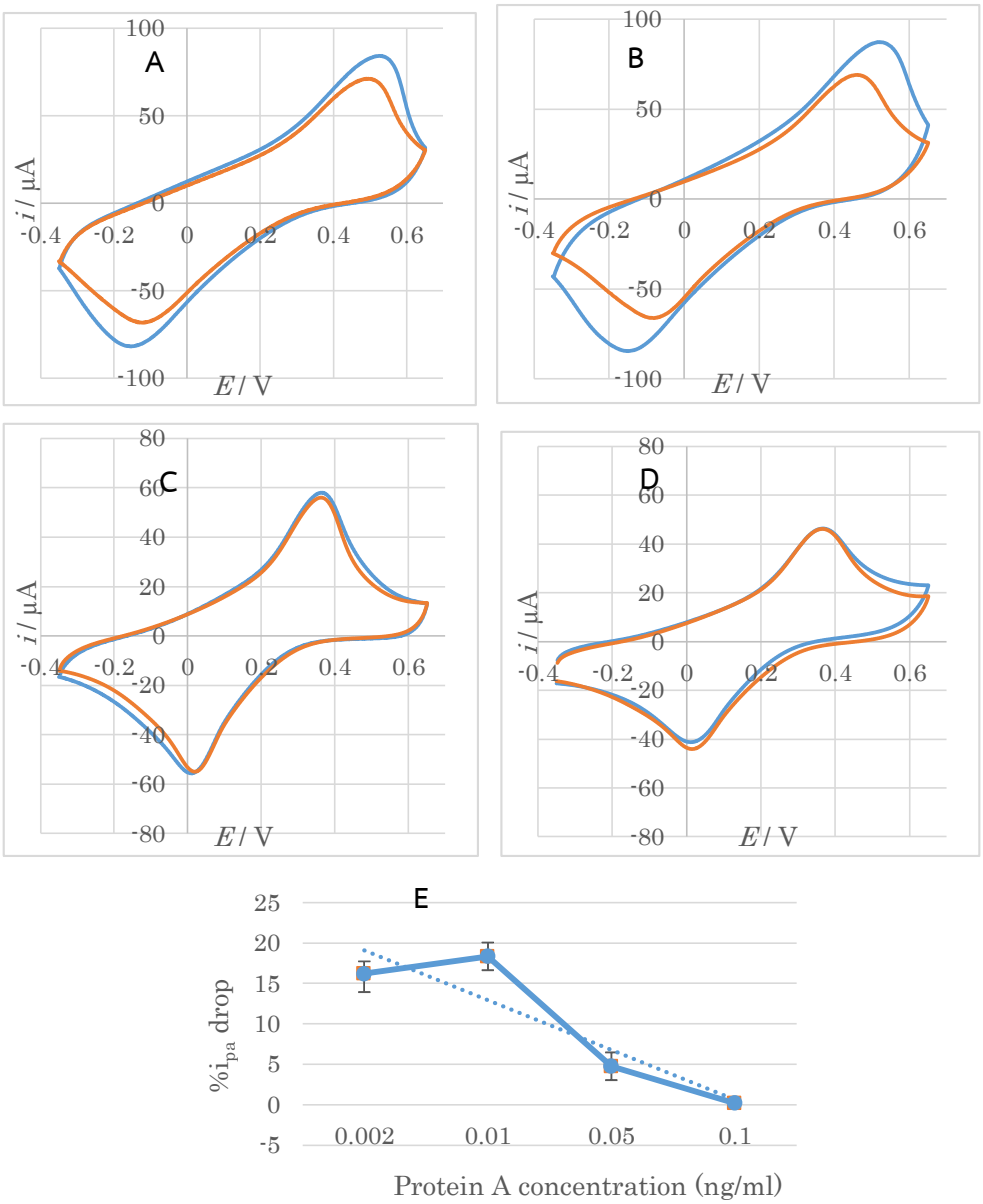

Figure 32: CV responses showing the effect of Protein A/antibody of concentrations on reduction of peak current upon addition of 250 ng/ml antigen: 0.002/0.010 mg/ml (A), 0.01/0.05 mg/ml (B), 0.05/0.25 mg/ml (C), and 0.1/0.5 mg/ml (D), with the CV after antibody immobilization in blue line color, and CV after immobilization of antigen in red line color. The line graph summarizes the result of peak current reduction before and after addition of antigen in percent with error bars (E). The scan was done in 0.1 M KCL and scan rate of 50 mV s^{-1} vs Ag/AgCl

5.3.1.4 Effect of antigen (LipL32) solution pH

The pH of the antigen solution also plays a role in the detection sensitivity, as antigen-antibody

binding kinetics are built from mixtures of weak interactions such as Van der Waals and hydrophobic bonding, which are not affected by pH, and electrostatic interactions and hydrogen bonds which can be affected by pH of the solution they are in [285]. In order to obtain optimal sensitivity against LipL32, LipL32 in different pH solutions was investigated on the response of the BSA/anti-LipL32/PrA/cAuNPs/Chitosan/GPB/SPCE by cyclic voltammetry. The effect of pH was tested in a series of PBS with pH ranged from 4 to 7. **Figure 33** shows the change of anodic peak current (i_{pa}) in each electrode's cyclic voltammogram with different pH under constant LipL32 concentration (250 ng/ml). The highest response current was obtainable at pH 6.0, with averaged $\%i_{pa}$ drop of 24.11%. The reason contributing to gradual peak current drop in pH lower and higher than 6 was supposedly because antibody-antigen reaction are usually inhibited at low pH [286], and at both low and high pH the antigen-antibody complex tends to dissociate from each other [287, 288]. In fact, low and high pH treatment (generally of order 2 to 4 and 9 to 10) has been used as a common practice to dissociate antibodies from viruses and bacteria by disrupting electrostatic interactions [289].

Furthermore, as both Prussian blue and Prussian white are unstable in neutral and alkaline solutions, it might contribute to a significant drop in response at pH 7.0. This occurrence was also commonly reported in other PB-related researches [290, 291]. Therefore, pH of 6.0 was chosen as the optimum pH for the antigen solution.

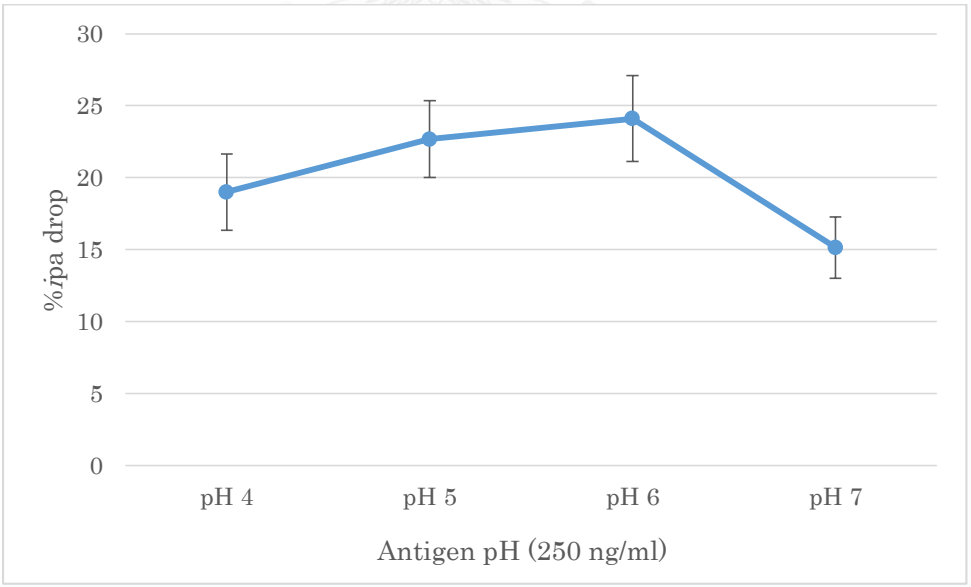

Figure 33: Graph derived from $\%i_{pa}$ drop of multiple fully modified electrodes (BSA/anti-LipL32/PrA/cAuNPs/Chitosan/GPB/SPCE) incubated with antigen in different pH solutions from 4 to 7. The CV scan was done in 0.1 M KCL with scan rate of 50 mV s^{-1} vs Ag/AgCl.

5.4 Electrochemical Characteristics

5.4.1 CV characteristics

The modified working electrodes resulted in CV characteristics of each stage from the start to the end of modifications as presented in **figure 34**. All the electrodes were modified under room temperature, except the immobilization steps which were carried out at 4°C, and scanned in 0.1 M KCl with scan rate of 50 mV S^{-1} vs Ag/AgCl reference electrode. No redox peak is observable with bare SPCE (curve a). After the application GPB, a redox peak appears (curve b). From then, each modification decreases the redox peak level sequentially, starting from Chitosan (curve c), cAuNPs (curve d), PrA (curve e), IgG (curve f), BSA (curve g), and antigen (curve h). This shows incremental resistivity or hindrances of charged molecule diffusion towards the electrode surface.

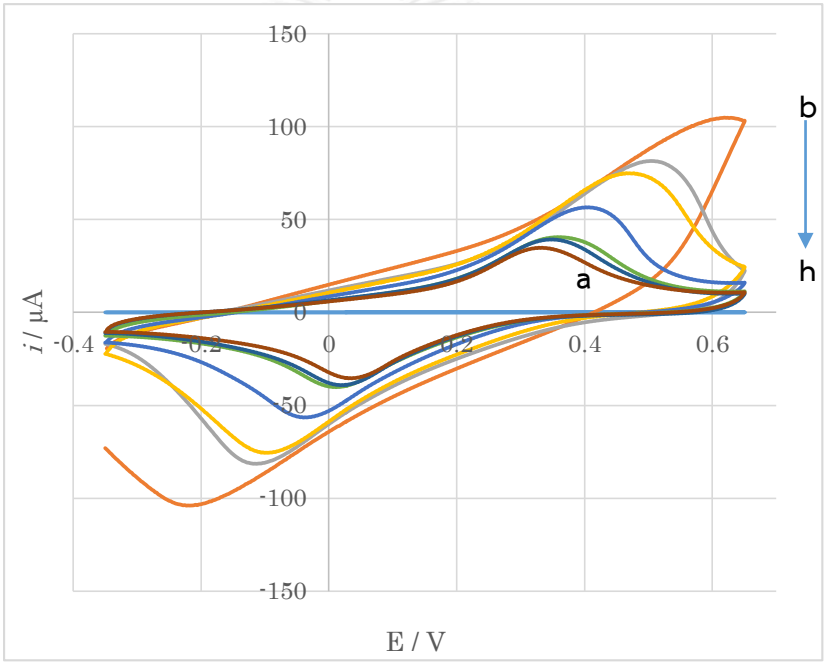

Figure 34: The CV responses for each stage of modification. Blank SPCE (a), One layer of GPB (b), three layers of Chitosan (c), cAuNP (d), PrA (e), Ab (f), BSA (g), Ag (250 ng/ml, pH 6). The tests was conducted in 0.1 M KCL at scan rate of 50 mV S^{-1}

5.4.2 Effects of scan rate on CV

A fully modified electrode (modified to the BSA step) was then tested in 0.1 M KCL solution under different scan rates and the result are presented in **figure 35**. The anodic peaks shifted to higher positive voltages while cathodic peaks shifted to higher negative voltages. Plot of *E*p vs. square root of scan rate shows that the

separation between cathodic and anodic peak potential increases with scan rate. This phenomenon indicates that the electrode processes are diffusion controlled [267, 292] which means the electron transfer in the electrode is quasi-reversible. Quasi-reversible is the state where rate constant of the electrode is in intermediate range, neither electrochemically reversible nor irreversible [293]. The determining numerical factor for this is the magnitude of rate constant values called "standard heterogeneous rate constant" or k_s. High k_s means the equilibrium between oxidized and reduced form can be achieved quickly at the given potential and vice versa. The common commonly accepted ranges of k_s to determine the electrode's electrochemical reversibility are [54, 294]:

$k_s > 0.020$ cm/s	Reversible
$0.020 > k_s > 5.0 \times 10^{-5}$ cm/s	Quasi-reversible
$k_s < 5.0 \times 10^{-5}$ cm/s	Irreversible

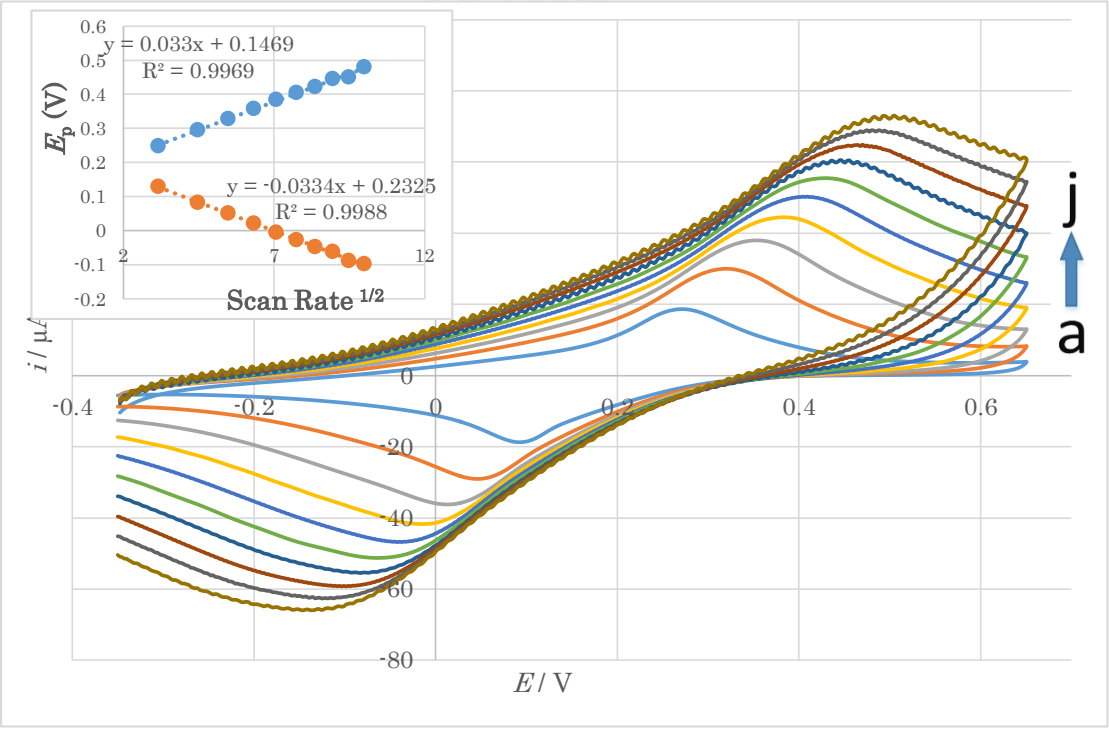

Figure 35: CVs of the modified electrode at different scan rates (from a to j): 10, 20, 30, 40, 50, 60, 70, 80, 90, 100 mV s^{-1} in 5 mL 0.1 mol L^{-1} KCl solution (pH 6) at 25°C. All potentials are given vs Ag/AgCl. The inset shows the dependence of redox peak currents on the potential sweep rates (the working surface was 2×3 mm^2).

5.4.3 Calibration curve and Limit of Detection (LoD)

To evaluate the performance of the fabricated immunosensor, the GPB-CS-cAuNP-PrA/anti-LipL32-BSA

modified electrode was tested in various LipL32 concentrations. The CVs of the test were shown in **figure 37**. The peak currents obtained showed the peak current decreased with increased LipL32 concentration, which was due to increased hindrance occurred from the formation of the antigen–antibody complex to the access of the redox probe to the outer electrode surface. The calibration curve for LipL32 immunosensor under the optimal conditions is shown in the inset of **figure 36**

As a result, a linear relationship between the oxidation peak currents and LipL32 concentrations ranging from 50 to 200 ng ml^{-1} and 250 to 600 ng ml^{-1} was obtained, with a linear equation of y = 0.0198x + 13.815 (R^2 = 0.9889) and y = 0.0108x + 15.192 (R^2 = 0.9653) respectively. Limit of Detection can be calculated as follows

$$LoD = 3(S.D)/sensitivity \quad ($$

The detection limit was then calculated to be of 54.98 ng ml^{-1}. Note that with a blank solution (without antigen), there was already estimately ~12% drop in the oxidation peak current, indicating that something in the PBS other than the antigen caused some obstructions to the charge transfer to the electrode surface.

Figure 37 B and C shows the detection results for intact and sonicated *L. interrogans* cells. The linear ranges obtained were 10 to 100 ng ml^{-1}, with linear equation of y = 0.0833x + 11.944 (R^2 = 0.9916) and y = 0.0886x + 14.29 (R^2 = 0.9192), with detection limits of 44.29 cell ml^{-1} and 77.25 cell ml^{-1} respectively.

For solution with 500 cell ml^{-1} or higher, in the case of intact cells the $\%i_{pa}$ drop became steady, while in the case of sonicated cells the $\%i_{pa}$ drop became lower. The reason might be due to saturated Ab sites on the electrode surface.

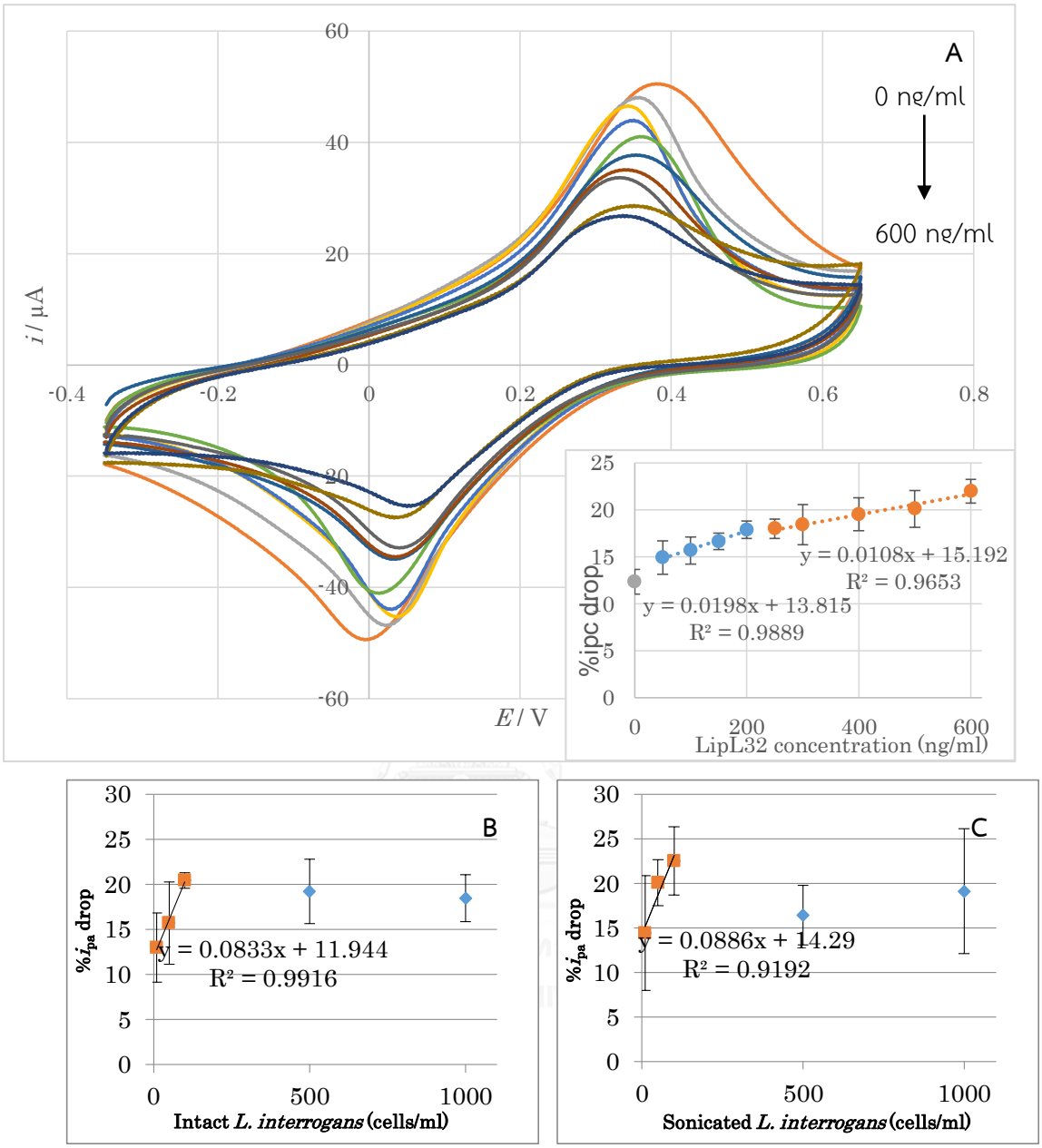

Figure 36: $\%i_{pa}$ drop of peak currents of immunosensors incubated with different concentrations of LipL32 protein and *L. interrogans* spp. bacterium: (A) the concentrations of solubilized LipL32 are pre-antigen, 0, 50, 100, 150, 200, 250, 300, 400, 500, 600 ng/ml. The inset is the calibration curve based on the change of the CV peak currents vs. the concentrations. (B) the concentration of intact *L. interrogans* bacterium are 10, 50, 100, 500, 1000 cells/ml. (C) the concentration of sonicated *L. interrogans* bacterium are 10, 50, 100, 500, 1000 cells/ml. The tests was conducted in 0.1 M KCL at scan rate of 50 mV S^{-1} vs Ag/AgCl

5.4.4 Reproducibility

The reproducibility of each fabrication process of the immunosensor was also tested. As the RSDs are in the range of 5 to 8 (n=10), it can be concluded that the fabrication is fairly reproducible. The RSDs for each step of modification are listed in **table 11**.

Table 10: RSDs for each step of modification

Modification step	**RSD**
Citrate gold nanoparticles	6.232
Protein A (0.01 mg/ml)	5.237
Antibody (0.05 mg/ml)	8.525
Bovine Serum Albumin	8.254

5.4.5 Storage stability

Finally, the stability of the fabricated electrodes were tested. The electrodes were fabricated to the BSA step using new SPCEs, stored at 4 °C in a closed container, and then were tested for the CV responses every week for three weeks. In relation to CV response collected at day 0, we found that our electrode's CV response swung higher for average of 1.53% in the first day, then continuously lost its response up to -7.74% by average at day 14th, then swung back to -6.79% at day 21th, possibly indicate that the electrode response drop has stabilized, as presented in **figure 37** This result fits almost perfectly to a Prussian blue immunosensor stability report by Zhang *et al* in 2015, which fabricated Au-PDA-PB-GO electrode has no obvious decrease of CV current response during the first 10 days, then -6.8% after day 21th. [295]

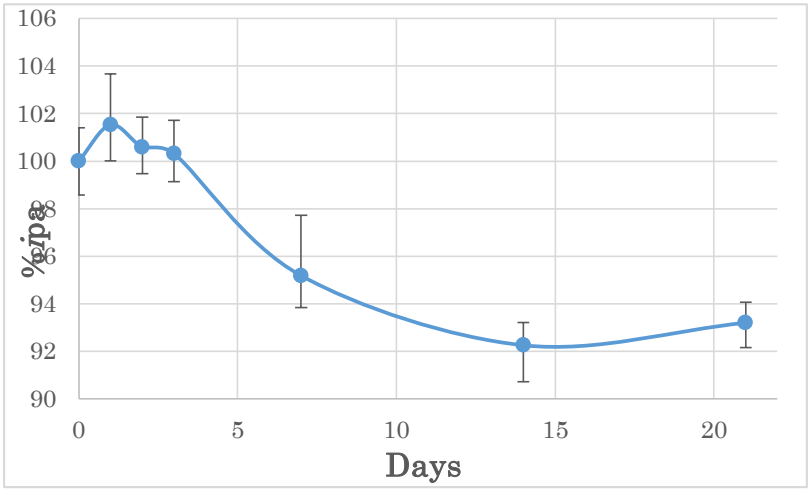

Figure 37: Storage stability of the fabricated immunosensors. The measurements were taken at day 1, 2, 3, 7, 14, and 21. The tests was conducted in 0.1 M KCL at scan rate of 50 mV S^{-1} vs Ag/AgCl

5.5 GPB electrode surface physiology characterization by Scanning Electron Microscrope (SEM)

The following **figure 38** to **43** show the surface morphology of the modified electrode step-wise using Scanning Electron Microscope (SEM). In **figure 38**, the screen-printed carbon electrode was examined. The pictures show irregular, porous surface of the screen-printed carbon on the electrode. The bare electrode seemingly composed of large carbon grain (~0.1 μM) formed together into cake-like matrix. This rough surface could be advantageous as it would increase surface area for the electron transfer

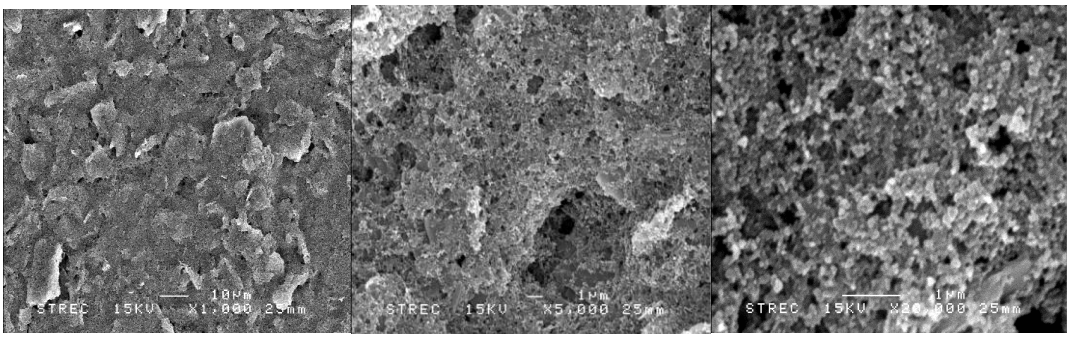

Figure 38: SEM images of screen-printed electrode surface at different magnifications of: x1000, x5000, and x20000.

In figure 39, after application of a layer of GPB on SPCE, we found that the GPB matrix did not fully

cover the electrode surface, and the PB microparticles in the matrix were not well dispersed.

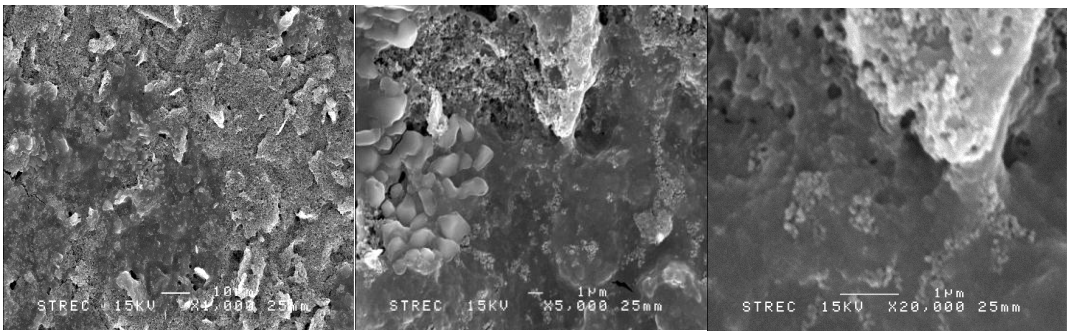

Figure 39: SEM images of GPB-modified SPCE electrode at different magnifications of: x1000, x5000, and x20000.

In figure 40, shows the images of modified electrode at 3 layers addition of CS. The surface and also the submerged layers were riddled by microparticles with size of ~10 μm which is suspected to be undissolved Chitosan particles. Some has strange, irregular shape possibly due to only partial dissolution. These large blocks of Chitosan were expected to add additional blockage against electron transfer to and from the electrode.

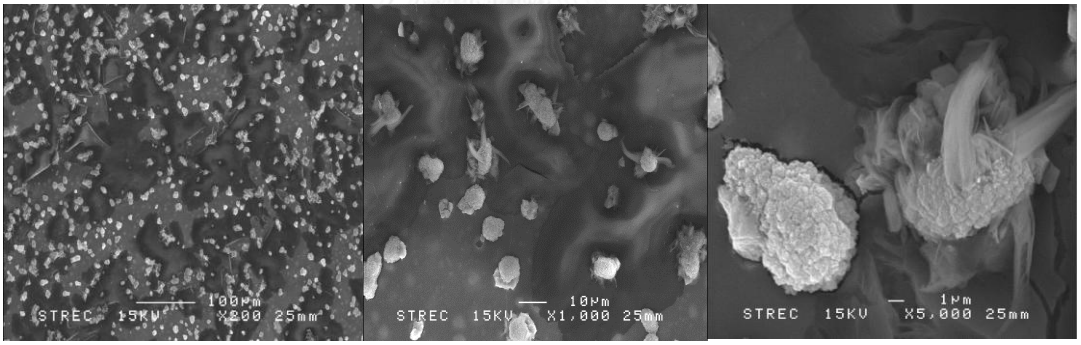

Figure 40: SEM images of CSx3-GPB-modified SPCE electrode at different magnifications of: x200, x1000, and x5000

In figure 41, electrodeposition of citrate gold nanoparticles seemingly cleared out loosely-attached Chitosan particles on the surface and smoothed the surface. Some of the electrodeposited gold nanoparticles can be seen dispersed on the surface, as these groups of gold nanoparticles might lost some of its citrate capping and formed clusters of gold nanoparticles. However, its biocompatibility would still be retained as both citrate-capped and bare gold are biocompatible and can be used to adhere staphylococcal Protein A [296].

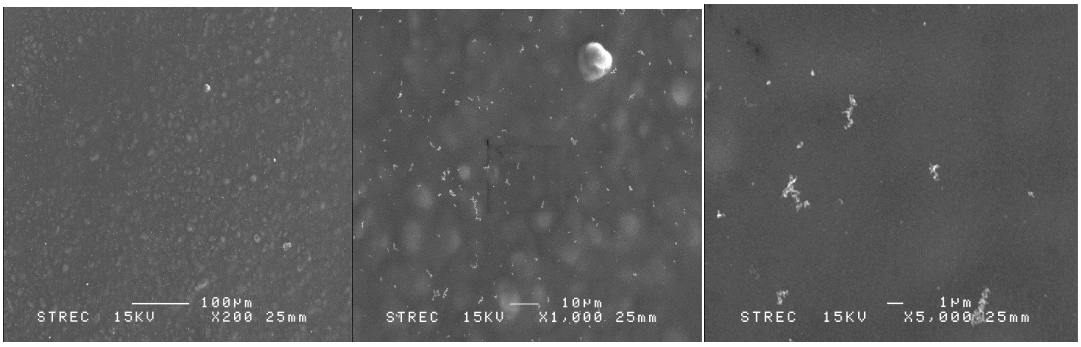

Figure 41: SEM images of cAuNP-CSx3-GPB-modified SPCE electrode at different magnifications of: x200, x1000, and x5000

In figure 42, after incubation of the previously modified electrode with Protein A solution (0.01 mg/ml) for 18 hours, the electrode surface totally transformed from smooth to rough surface full of particles with high density. As IgG antibody which has molecular weight of 150 kDa [137] has estimated size of 11.5 ± 0.5 nm [297], Protein A which has molecular weight of 42 kDa [298] should be estimately 3.5 fold smaller, or about 3.2 nm if to use molecular weight as reference, and thus should be too small to be seen in the SEM pictures. Therefore, the object seen in this step might be a mixture of PrA agglomeration together with the salt crystals attached to the electrode surface. However, more experiments are needed to confirm this assumption.

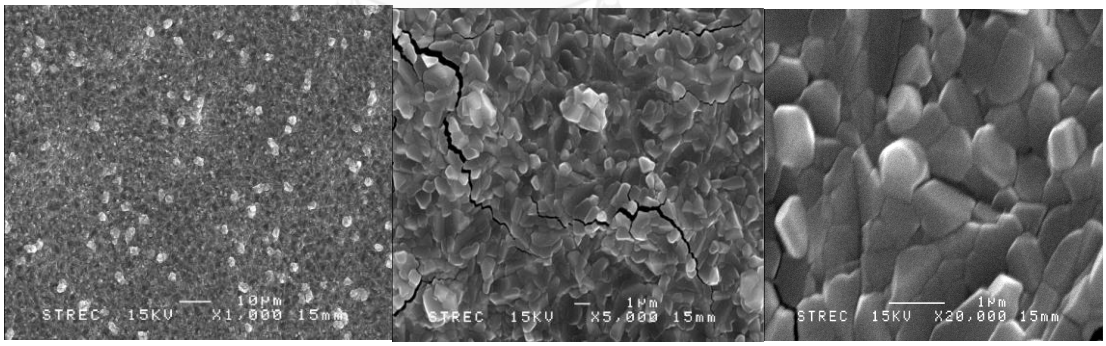

Figure 42: PrA-cAuNP-CSx3-GPB-modified SPCE electrode at different magnifications of: x1000, x5000, and x20000

In **figure 43**, further incubation of the electrode in anti-LipL32 IgG antibodies solution resulted in the surface character similar to that of the previous step. However, the electrode surface with Ag seemed to be rougher than the one without, possibly indicating antigen adhesion on PrA on the electrode surface.

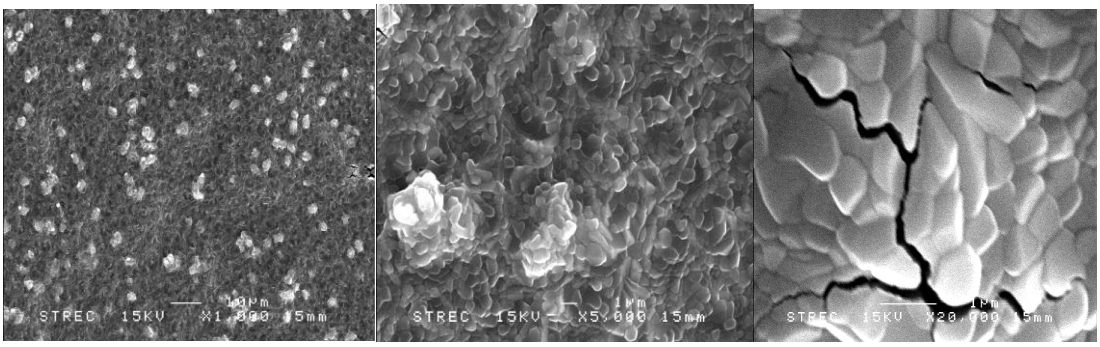

Figure 43: Ab-PrA-cAuNP-CSx3-GPB-modified SPCE electrode at different magnifications of x1000, x5000, and x20000.

5.6 Conclusions

This thesis reports a fabrication of an electrochemical immunosensor for detection of LipL32 protein based on immobilization of anti-LipL32 antibodies electrode configuration of Protein A/Gold Nanoparticles/3xChitosan/Graphene -Prussian blue/Screen-printed carbon electrode. Every modification step was optimized, which results can be summarized as follows:

- The best concentration of Prussian blue to be used to make GPB was 15 mM, as lower PB concentration provided less response, while higher concentration decreased reaction rate constant while having as same response level as 15 mM.
- The optimum number of GPB layer was one layer, as more potential was needed to drive the reaction of electrodes with higher GPB layers number.
- The optimum number of Chitosan layers was three, as its protection capability against Prussian blue leakage seemed proportional to the number of its layers.
- Suitable antibody incubation time was 18 hours (overnight), as equilibrium between the phases seemed to be almost established, maximizing the number of adsorbed antibody on the electrode surface.
- The optimum Protein A and antibody concentration was 0.01 mg ml^{-1} and 0.05 mg ml^{-1} respectively. Lower concentration provides lower current drop after incubation with antigen, as there were less antibody to bind with antigen. Conversely, higher concentration would block the electrode surface to higher degree, decreasing the effect of antigen addition on peak current drop.
- The optimum antigen solution pH was 6. Lower solution pH slightly affected peak current drop as the low pH possibly affected antibody-antigen reaction, while higher pH might interfere or destabilized Prussian blue, resulting in less peak current drop.

After the optimization experiments were done, freshly optimized electrodes were tested with LipL32 protein, and later with sonicated and intact *Leptospira interrogans* cells. The limit of detection obtained for LipL32, intact and sonicated *L. interrogans* cells were 54.98 ng ml^{-1}, 44.29 cells ml^{-1}, and 77.25 cells ml^{-1} respectively. There were two linear ranges for LipL32 protein detection, which were 50-200 ng ml^{-1} and 250-600 ng ml^{-1}. The linear range for detection of intact intact and sonicated *L. interrogans* cells was 10-100 cells ml^{-1}.

In conclusion, the fabricated immunosensor shows good performance, reproducibility, and sensitivity although it could be better. This model can be used as a base for "upgraded" versions in the future.

References

1. Langston, C.E. and K.J. Heuter, *Leptospirosis: A re-emerging zoonotic disease.* Veterinary Clinics of North America: Small Animal Practice, 2003. **33**(4): p. 791-807.
2. Wuthiekanun, V., et al., *Clinical diagnosis and geographic distribution of leptospirosis, Thailand.* Emerging infectious diseases, 2007. **13**(1): p. 124.
3. Kishimoto, M., et al., *Leptospirosis misdiagnosed as pulmonary-renal syndrome.* American Journal of the Medical Sciences, 2004. **328**(2): p. 116-120.
4. Kreetha, T., S. Khachornsakdi, and B. Baralee, *Leptospirosis and its pulmonary complications.* Respirology, 2005. **10**: p. 656-659.
5. Z., T., R. D., and S. K., *Global Epidemiological Overview of Leptospirosis.* International Journal of Microbiological Research, 2013. **4**(1): p. 09-15.
6. Epidemiology, B.o., *National Disease Surveillance (Report 506), Leptospirosis, 2012*, D.o.D. Control, Editor. 2012, Ministry of Public Health. p. 1.
7. Al-shere, T.A., et al., *Outbreak of leptospirosis after flood, the Philippines, 2009.* Emerging infectious diseases, 2012. **18**(1): p. 91.
8. Lau, C.L., et al., *Climate change, flooding, urbanisation and leptospirosis: fuelling the fire?* Transactions of the Royal Society of Tropical Medicine and Hygiene, 2010. **104**(10): p. 631-638.
9. Vasconcellos, F.A., et al., *Testing different antigen capture ELISA formats for detection of Leptospira spp. in human blood serum.* Transactions of the Royal Society of Tropical Medicine and Hygiene, 2010. **104**(4): p. 259-264.
10. Shah, I., et al., *Leptospirosis-an under-diagnosed clinical condition.* Journal of postgraduate medicine, 1999. **45**(3): p. 93-94.
11. Wuthiekanun, V., et al., *Maintenance of Leptospira Species in Leptospira Vanaporn Wuthiekanun Agar.* Journal of clinical microbiology, 2014. **52**(12): p. 4350-4352.
12. Wuthiekanun, V., et al., *Rapid Isolation and Susceptibility Testing of Leptospira spp. Using a New Solid Medium, LVW Agar.* Antimicrobial agents and chemotherapy, 2013. **57**(1): p. 297-302.
13. Organization, W.H., *Human leptospirosis: guidance for diagnosis, surveillance and control*. 2003, World

Health Organization Malta.

14. Humberd, C.M., et al., *Enumerating leptospires using the Coulter Counter.* The American journal of tropical medicine and hygiene, 2005. **73**(5): p. 962-963.

15. Evans, A.S. and P.S. Brachman, *Bacterial Infections of Humans: Epidemiology and Control*. 1998: Plenum Medical Book Company.

16. Vijayachari, P., A. Sugunan, and S. Sehgal, *Evaluation of microscopic agglutination test as a diagnostic tool during acute stage of leptospirosis in high & low endemic areas.* The Indian journal of medical research, 2001. **114**: p. 99-106.

17. Smythe, L.D., et al., *The microscopic agglutination test (MAT) is an unreliable predictor of infecting Leptospira serovar in Thailand.* The American journal of tropical medicine and hygiene, 2009. **81**(4): p. 695-697.

18. Ahmad, S. and S. Shah, *Laboratory diagnosis of leptospirosis.* Journal of postgraduate medicine, 2005. **51**(3): p. 195.

19. Rogers, K.R., *Principles of affinity-based biosensors.* Molecular biotechnology, 2000. **14**(2): p. 109-129.

20. Castillo, M., A. Oubina, and D. Barceló, *Evaluation of ELISA kits followed by liquid chromatography-atmospheric pressure chemical ionization-mass spectrometry for the determination of organic pollutants in industrial effluents.* Environmental science & technology, 1998. **32**(14): p. 2180-2184.

21. Leon, F., et al., *Anti-transglutaminase IgA ELISA: clinical potential and drawbacks in celiac disease diagnosis.* Scandinavian journal of gastroenterology, 2001. **36**(8): p. 849-853.

22. Edwards, R., *Immunodiagnostics: A Practical Approach: A Practical Approach*. 1999: Oxford University Press.

23. Li, X., et al. *Paper-based electrochemical ELISA*. in *Proc. Micro Total Analysis Systems*. 2010.

24. Gruhl, F.J., B.E. Rapp, and K. Länge, *Biosensors for diagnostic applications*, in *Molecular Diagnostics*. 2013, Springer. p. 115-148.

25. IUPAC., *Compendium of Chemical Terminology, 2nd ed. (the "Gold Book")*, ed. M. A. D and W. A. Vol. 64. 1992: Blackwell Scientific Publications, Oxford (1997).

26. Fleisher, M. and M.K. Schwartz, *Automated approaches to rapid-response testing. A comparative evaluation of point-of-care and centralized laboratory testing.* Am J Clin Pathol, 1995. **104**(4 Suppl 1): p. S18-25.

27. Kuila, T., et al., *Recent advances in graphene-based biosensors.* Biosensors and Bioelectronics, 2011.

26(12): p. 4637-4648.

28. Shao, Y., et al., *Graphene based electrochemical sensors and biosensors: a review.* Electroanalysis, 2010. **22**(10): p. 1027-1036.
29. Ghindilis, A.L., et al., *Immunosensors: electrochemical sensing and other engineering approaches.* Biosensors and Bioelectronics, 1998. **13**(1): p. 113-131.
30. Abdel-Hamid, I., et al., *Fast amperometric assay for E. coli O157: H7 using partially immersed immunoelectrodes.* Electroanalysis, 1998. **10**(11): p. 758-763.
31. Vonderschmitt, D.J., *Laboratory Organization. Automation*. Vol. 4. 1991: Walter de Gruyter.
32. Stedtfeld, R.D., et al., *Gene-Z: a device for point of care genetic testing using a smartphone.* Lab on a Chip, 2012. **12**(8): p. 1454-1462.
33. Cabera, H., *A comprehensive evaluation of pregnancy tests.* American journal of obstetrics and gynecology, 1969. **103**(1): p. 32-38.
34. Von Lode, P., *Point-of-care immunotesting: approaching the analytical performance of central laboratory methods.* Clinical biochemistry, 2005. **38**(7): p. 591-606.
35. Mabey, D., et al., *Tropical infectious diseases: diagnostics for the developing world.* Nature Reviews Microbiology, 2004. **2**(3): p. 231-240.
36. Yager, P., G.J. Domingo, and J. Gerdes, *Point-of-care diagnostics for global health.* Annu. Rev. Biomed. Eng., 2008. **10**: p. 107-144.
37. Merriam-Webster, *immunosorbent*, in *Merriam-Webster.com*. 2014: Web.
38. Crowther, J.R. and J.M. Walker, *The ELISA guidebook*. Vol. 149. 2009: Springer.
39. Ricci, F., G. Adornetto, and G. Palleschi, *A review of experimental aspects of electrochemical immunosensors.* Electrochimica acta, 2012. **84**: p. 74-83.
40. Morgan, C.L., D.J. Newman, and C. Price, *Immunosensors: technology and opportunities in laboratory medicine.* Clinical Chemistry, 1996. **42**(2): p. 193-209.
41. Tothill, I.E., *Biosensors developments and potential applications in the agricultural diagnosis sector.* Computers and Electronics in Agriculture, 2001. **30**(1): p. 205-218.
42. Bertold, H., *Antibodies for immunosensors A review* Analytica Chimica Acta, 1997. **347**: p. 177-186.
43. Tokarskyy, O. and D.L. Marshall, *Immunosensors for rapid detection of< i> Escherichia coli</i> O157: H7—Perspectives for use in the meat processing industry.* Food microbiology, 2008. **25**(1): p. 1-12.
44. Polo, E., S. Puertas, and P. Batalla, *Biosensors Based on Nanoparticles and Electrochemical Detection.*

Inorganic Nanoparticles vs Organic Nanoparticles, 2012: p. 247.

45. Ilaria, P. and M. Marco, *Electroanalytical biosensors and their potential for food pathogen and toxin detection.* Analytical and Bioanalytical Chemistry, 2008. **391**(2): p. 455-471.

46. Rai, V., J. Deng, and C.S. Toh, *Electrochemical nanoporous alumina membrane-based label-free DNA biosensor for the detection of Legionella sp.* Talanta, 2012. **98**: p. 112-7.

47. Gooding, J.J., *Electrochemical DNA hybridization biosensors.* Electroanalysis, 2002. **14**(17): p. 1149-1156.

48. Warsinke, A., A. Benkert, and F. Scheller, *Electrochemical immunoassays.* Fresenius' journal of analytical chemistry, 2000. **366**(6-7): p. 622-634.

49. Yunlei, Z., et al., *Electrochemical immunoassay platform for high sensitivity detection of indole-3-acetic acid.* Electrochimica Acta, 2013. **96**: p. 66-73.

50. Yan, W., et al., *Fabrication of a label-free electrochemical immunosensor of low-density lipoprotein.* The Journal of Physical Chemistry B, 2008. **112**(4): p. 1275-1281.

51. Pletcher, D., *A first course in electrode processes*. 2009: Royal Society of Chemistry.

52. Zoski, C.G., *Handbook of electrochemistry*. 2007: Elsevier.

53. SKLÁDAL, P., *Electrochemical detection for biological identification.* Biological Identification: DNA Amplification and Sequencing, Optical Sensing, Lab-On-Chip and Portable Systems, 2014: p. 131.

54. Wang, J., *Analytical electrochemistry*. 2006: John Wiley & Sons.

55. Trasatti, S. and O. Petrii, *Real surface area measurements in electrochemistry.* Pure and applied chemistry, 1991. **63**(5): p. 711-734.

56. Yao, Y., et al., *Electrochemical recognition and trace-level detection of bactericide carbendazim using carboxylic group functionalized poly (3, 4-ethylenedioxythiophene) mimic electrode.* Analytica chimica acta, 2014. **831**: p. 38-49.

57. St-Louis, P., *Status of point-of-care testing: promise, realities, and possibilities.* Clinical biochemistry, 2000. **33**(6): p. 427-440.

58. Dequaire, M. and A. Heller, *Screen Printing of Nucleic Acid Detecting Carbon Electrodes.* Analytical Chemistry, 2002. **74**(17): p. 4370-4377.

59. Zen, J.-M., et al., *Photoelectrochemical Oxygen Sensor Using Copper-Plated Screen-Printed Carbon Electrodes.* Analytical Chemistry, 2002. **74**(23): p. 6126-6130.

60. Yan, M., et al., *A disposable electrochemical immunosensor based on carbon screen-printed electrodes for the detection of prostate specific antigen.* Biosensors and Bioelectronics, 2012. **38**(1): p. 355-361.

61. Hermanson, G.T., *Bioconjugate techniques*. 2013: Academic press.

62. Cui, X., et al., *Layer-by-layer assembly of multilayer films composed of avidin and biotin-labeled antibody for immunosensing.* Biosensors and Bioelectronics, 2003. **18**(1): p. 59-67.

63. Ikeda, T., et al., *Oriented immobilization of antibodies on a silicon wafer using Si-tagged protein A.* Analytical biochemistry, 2009. **385**(1): p. 132-137.

64. Jung, Y., et al., *Self-directed and self-oriented immobilization of antibody by protein G-DNA conjugate.* Analytical chemistry, 2007. **79**(17): p. 6534-6541.

65. Karyakin, A.A., et al., *Oriented immobilization of antibodies onto the gold surfaces via their native thiol groups.* Analytical chemistry, 2000. **72**(16): p. 3805-3811.

66. YoungáJeong, J. and B. HyunáChung, *Recent advances in immobilization methods of antibodies on solid supports.* Analyst, 2008. **133**(6): p. 697-701.

67. Turkova, J., *Oriented immobilization of biologically active proteins as a tool for revealing protein interactions and function.* Journal of Chromatography B: Biomedical Sciences and Applications, 1999. **722**(1): p. 11-31.

68. Albarghouthi, M., et al., *Immobilization of antibodies on alginate-chitosan beads.* International journal of pharmaceutics, 2000. **206**(1): p. 23-34.

69. Gerstein, A.S., *Molecular Biology Problem Solver: A Laboratory Guide*. 2004: Wiley.

70. Suresh, S., et al., *Detection of Ricin in Water Samples using DisposableScreen-printed Electrodes.* Defence Science Journal, 2007. **57**(6): p. 839-844.

71. Jan, D., et al., *Utilization of Unmodified Screen-Printed Carbon Electrodes in Electroanalysis of Organinc Compounds.* Sensing in Electroanalysis, 2011. **6**: p. 129-138.

72. Gao, L., J.R. Guest, and N.P. Guisinger, *Epitaxial graphene on Cu (111).* Nano letters, 2010. **10**(9): p. 3512-3516.

73. Ruoff, R., *Graphene: Calling all chemists.* Nature Nanotechnology, 2008. **3**(1): p. 10-11.

74. Lee, J.-U., D. Yoon, and H. Cheong, *Estimation of Young's modulus of graphene by Raman spectroscopy.* Nano letters, 2012. **12**(9): p. 4444-4448.

75. Changsheng, S., et al., *Direct Electrochemistry of Glucose Oxidase and Biosensing for Glucose Based on Graphene.* Anal. Chem, 2009(81): p. 2378–2382.

76. Subbiah, A., et al., *Probing the Electrochemical Properties of Graphene Nanosheets for Biosensing Applications.* Journal of Physical Chemistry, 2009(113): p. 8853-8857.

77. Yoo, D., J. Kim, and J.H. Kim, *Direct synthesis of highly conductive PEDOT: PSS/graphene composites and their applications in energy harvesting systems.* 2014.

78. Cui, J., et al., *Indium Tin Oxide Alternatives—High Work Function Transparent Conducting Oxides as Anodes for Organic Light‐Emitting Diodes.* Advanced materials, 2001. **13**(19): p. 1476-1480.

79. Na, S.I., et al., *Efficient and Flexible ITO‐Free Organic Solar Cells Using Highly Conductive Polymer Anodes.* Advanced Materials, 2008. **20**(21): p. 4061-4067.

80. Lock, J.P., et al., *Electrochemical investigation of PEDOT films deposited via CVD for electrochromic applications.* Synthetic Metals, 2007. **157**(22): p. 894-898.

81. Herzer, N., et al., *Fabrication of PEDOT–OTS-patterned ITO substrates.* Journal of Materials Chemistry, 2010. **20**(32): p. 6618-6621.

82. Kirchmeyer, S. and K. Reuter, *Scientific importance, properties and growing applications of poly (3, 4-ethylenedioxythiophene).* Journal of Materials Chemistry, 2005. **15**(21): p. 2077-2088.

83. Crispin, X., et al., *The origin of the high conductivity of poly (3, 4-ethylenedioxythiophene)-poly (styrenesulfonate)(PEDOT-PSS) plastic electrodes.* Chemistry of Materials, 2006. **18**(18): p. 4354-4360.

84. Groenendaal, L., et al., *Poly (3, 4‐ethylenedioxythiophene) and its derivatives: past, present, and future.* Advanced Materials, 2000. **12**(7): p. 481-494.

85. W. H. KIM, et al., *Effect of Annealing on the Electrical Properties and Morphology of a Conducting Polymer used as an Anode in Organic Light-Emitting Devices.* Journal of Polymer Science: Part B: Polymer Physics, 2003. **41**: p. 2522-2528.

86. G. Greczynski, Th. Kugler, and W.R. Salaneck, *Characterization of the PEDOT-PSS system by means of X-ray and ultraviolet photoelectron spectroscopy.* Thin Solid Films, 1999. **354**: p. 129-135.

87. Shi, H., et al., *Facile Fabrication of PEDOT: PSS/Polythiophenes Bilayered Nanofilms on Pure Organic Electrodes and Their Thermoelectric Performance.* ACS applied materials & interfaces, 2013. **5**(24): p. 12811-12819.

88. Shi, H., et al., *Electrochemical Fabrication and Thermoelectric Performance of the PEDOT: PSS Electrode Based Bilayered Organic Nanofilms.* Int. J. Electrochem. Sci, 2014. **9**: p. 7629-7643.

89. Kim, M., S. Lai, and R.M. Laine, *Combinatorial Nanopowder Synthesis Along the ZnO–Al2O3 Tie Line Using Liquid‐Feed Flame Spray Pyrolysis.* Journal of the American Ceramic Society, 2011. **94**(10): p. 3308-3318.

90. Wu, X., et al., *Flexible organic light emitting diodes based on double-layered graphene/PEDOT: PSS*

conductive film formed by spray-coating. Vacuum, 2014. **101**: p. 53-56.

91. Hong, W., et al., *Transparent graphene/PEDOT–PSS composite films as counter electrodes of dye-sensitized solar cells.* Electrochemistry Communications, 2008. **10**(10): p. 1555-1558.

92. Seekaew, Y., et al., *Low-cost and flexible printed graphene–PEDOT: PSS gas sensor for ammonia detection.* Organic Electronics, 2014. **15**(11): p. 2971-2981.

93. A. Wisitsoraat, et al., *Graphene–PEDOT:PSS on screen printed carbon electrode for enzymatic biosensing.* Journal of Electroanalytical Chemistry, 2013. **704**: p. 208–213.

94. Jiang, D.-e., B.G. Sumpter, and S. Dai, *How do aryl groups attach to a graphene sheet?* The Journal of Physical Chemistry B, 2006. **110**(47): p. 23628-23632.

95. Cao, Y. and K. Houk, *Computational assessment of 1, 3-dipolar cycloadditions to graphene.* Journal of Materials Chemistry, 2011. **21**(5): p. 1503-1508.

96. Kuila, T., et al., *Chemical functionalization of graphene and its applications.* Progress in Materials Science, 2012. **57**(7): p. 1061-1105.

97. Georgakilas, V., et al., *Functionalization of graphene: covalent and non-covalent approaches, derivatives and applications.* Chemical reviews, 2012. **112**(11): p. 6156-6214.

98. Zheng, W., B. Shen, and W. Zhai, *Surface Functionalization of Graphene with Polymers for Enhanced Properties.* 2013.

99. Sriprachuabwong, C., et al., *Inkjet-printed graphene-PEDOT: PSS modified screen printed carbon electrode for biochemical sensing.* J. Mater. Chem., 2012. **22**(12): p. 5478-5485.

100. Parvez, K., et al., *Electrochemically exfoliated graphene as solution-processable, highly conductive electrodes for organic electronics.* ACS nano, 2013. **7**(4): p. 3598-3606.

101. Karuwan, C., et al., *Inkjet-printed graphene-poly (3, 4-ethylenedioxythiophene): poly (styrene-sulfonate) modified on screen printed carbon electrode for electrochemical sensing of salbutamol.* Sensors and Actuators B: Chemical, 2012. **161**(1): p. 549-555.

102. Van der Zee, F.P. and F.J. Cervantes, *Impact and application of electron shuttles on the redox (bio) transformation of contaminants: a review.* Biotechnology advances, 2009. **27**(3): p. 256-277.

103. Francke, R. and R.D. Little, *Redox catalysis in organic electrosynthesis: basic principles and recent developments.* Chemical Society Reviews, 2014. **43**(8): p. 2492-2521.

104. Delaney, G.M., et al., *Electron - transfer coupling in microbial fuel cells. 2. performance of fuel cells containing selected microorganism—mediator—substrate combinations.* Journal of chemical technology

and biotechnology. Biotechnology, 1984. **34**(1): p. 13-27.

105. Li, Q., F. Lou, and D. Tang, *Biofunctional nanogold microsphere doped with Prussian blue nanoparticles for sensitive electrochemical immunoassay of cancer marker.* Analytical Methods, 2014. **6**(10): p. 3442-3448.

106. XUE Fang-qin, et al., *Performance and mechanism of Prussian blue (PB) modified carbon felt electrode.* Transactions of Nonferrous Metals Society of China, 2009. **19**: p. s594-s599.

107. Ling-Yan, Z. and L. Yan-Jun, *Label-free amperometric immunosensor based on prussian blue as artificial peroxidase for the detection of methamphetamine.* Analytica Chimica Acta, 2014. **806**: p. 204-209.

108. Pyrasch, M. and B. Tieke, *Electro-and photoresponsive films of Prussian blue prepared upon multiple sequential adsorption.* Langmuir, 2001. **17**(24): p. 7706-7709.

109. Ricci, F., et al., *Prussian Blue based screen printed biosensors with improved characteristics of long-term lifetime and pH stability.* Biosensors and Bioelectronics, 2003. **18**(2): p. 165-174.

110. Qi, G., L. Na, and M. Zhanfang, *Prussian blue–gold nanoparticles-ionic liquid functionalized reduced graphene oxide nanocomposite as label for ultrasensitive electrochemical immunoassay of alpha-fetoprotein.* Analytica Chimica Acta, 2014. **829**: p. 15-21.

111. Agnihotry, S., et al., *Electrodeposited Prussian blue films: Annealing effect.* Electrochimica acta, 2006. **51**(20): p. 4291-4301.

112. Garcia-Jareno, J., et al., *Electrochemical Behavior of Electrodeposited Prussian Blue Films on ITO Electrode: An Attractive Laboratory Experience.* Journal of chemical education, 1998. **75**(7): p. 881.

113. Itaya, K., T. Ataka, and S. Toshima, *Spectroelectrochemistry and electrochemical preparation method of Prussian blue modified electrodes.* Journal of the American Chemical Society, 1982. **104**(18): p. 4767-4772.

114. Jiang, W., et al., *Amperometric immunosensor based on multiwalled carbon nanotubes/Prussian blue/nanogold-modified electrode for determination of α-fetoprotein.* Analytical biochemistry, 2010. **407**(1): p. 65-71.

115. Shan, Y., et al., *Prussian blue nanoparticles potentiostatically electrodeposited on indium tin oxide/chitosan nanofibers electrode and their electrocatalysis towards hydrogen peroxide.* Electrochimica Acta, 2008. **53**(26): p. 7751-7755.

116. Jiang, Y., et al., *Functionalization of graphene with electrodeposited Prussian blue towards amperometric sensing application.* Talanta, 2011. **85**(1): p. 76-81.

117. Hazen, R., et al., *Electrochemistry in thin solid films of prussian blue: A model demonstration on reversible behavior.* American Journal of Undergraduate Research, 2002. **2**: p. 27-36.

118. Weaver, J. and H. Frederikse, *Crc handbook of chemistry and physics.* Journal of the American Chemical Society, 2007. **129**(3): p. 724.

119. Zhang, Y., et al., *A novel immunosensor based on an alternate strategy of electrodeposition and self-assembly.* Biosensors and Bioelectronics, 2012. **35**(1): p. 277-283.

120. Inoue, H., et al., *Characterization of Prussian blue and its thermal decomposition products.* Hyperfine Interactions, 1989. **46**(1-4): p. 723-731.

121. A. M. Farah, et al., *Synthesis of Prussian Blue and Its Electrochemical Detection of Hydrogen Peroxide Based on Cetyltrimethylammonium Bromide (CTAB) Modified Glassy Carbon Electrode.* International Journal of Electrochemical Science, 2012. **8**: p. 12132-12146.

122. Bust, P.D. and P.T. McCabe, *Contemporary Ergonomics 2005: Proceedings of the International Conference on Contemporary Ergonomics (CE2005), 5-7 April 2005, Hatfield, UK*. 2005: Taylor & Francis.

123. Kumar, M.N.R., *A review of chitin and chitosan applications.* Reactive and functional polymers, 2000. **46**(1): p. 1-27.

124. Gao, Z.-D., et al., *Development of Amperometric Glucose Biosensor Based on Prussian Blue Functionlized TiO2 Nanotube Arrays.* Scientific reports, 2014. **4**.

125. Rinaudo, M., *Chitin and chitosan: properties and applications.* Progress in polymer science, 2006. **31**(7): p. 603-632.

126. Aiba, S.-i., *Studies on chitosan: 2. Solution stability and reactivity of partially N-acetylated chitosan derivatives in aqueous media.* International journal of biological macromolecules, 1989. **11**(4): p. 249-252.

127. Forsgren, A. and J. Sjöquist, *"Protein A" from S. aureus I. Pseudo-immune reaction with human* γ*-globulin.* The Journal of Immunology, 1966. **97**(6): p. 822-827.

128. Derkus, B., et al., *Protein A immunosensor for the detection of immunoglobulin G by impedance spectroscopy.* Bioprocess and biosystems engineering, 2014. **37**(5): p. 965-976.

129. Majumdar, T., R. Chakraborty, and U. Raychaudhuri, *Development of PEI-GA modified antibody based sensor for the detection of S. aureus in food samples.* Food Bioscience, 2013. **4**: p. 38-45.

130. Sun, X., Y. Zhu, and X. Wang, *Amperometric immunosensor based on a protein A/deposited gold nanocrystals modified electrode for carbofuran detection.* Sensors, 2011. **11**(12): p. 11679-11691.

131. Yang, D.-J., et al., *Fast switching Prussian blue film by modification with cetyltrimethylammonium*

bromide. Solar Energy Materials and Solar Cells, 2012. **99**: p. 129-134.

132. Wangoo, N., et al., *Synthesis and capping of water-dispersed gold nanoparticles by an amino acid: bioconjugation and binding studies.* Journal of colloid and interface science, 2008. **323**(2): p. 247-254.

133. Norde, W., *Adsorption of proteins from solution at the solid-liquid interface.* Advances in colloid and interface science, 1986. **25**: p. 267-340.

134. Thobhani, S., et al., *Bioconjugation and characterisation of gold colloid-labelled proteins.* Journal of immunological methods, 2010. **356**(1): p. 60-69.

135. Ríos-Corripio, M., et al., *UV–Visible intensity ratio (aggregates/single particles) as a measure to obtain stability of gold nanoparticles conjugated with protein A.* Journal of nanoparticle research, 2013. **15**(5): p. 1-7.

136. Hermanson, G., *Avidin-biotin systems in bioconjugate techniques*. 2008, San Diego: Academic Press Inc.

137. Janeway, C.A., et al., *Immunobiology: the immune system in health and disease*. Vol. 2. 2001: Churchill Livingstone.

138. Watson, J.D., *Molecular biology of the gene.* Molecular biology of the gene., 1970(2nd edn).

139. Van Oss, C., *Hydrophobic, hydrophilic and other interactions in epitope-paratope binding.* Molecular immunology, 1995. **32**(3): p. 199-211.

140. Andreu, D. and P. Gomes, *Binding of Small Peptides to Immobilized Antibodies: Kinetic Analysis by Surface Plasmon Resonance.* Current Protocols in Immunology, 2002: p. 18.9. 1-18.9. 22.

141. Fragkou, V., et al., *Determination of the Real Surface Area of a Screen-Printed Electrode by Chronocoulometry.* Int. J. Electrochem. Sci, 2012. **7**: p. 6214-6220.

142. Hughes-Jones, N., *Red-cell antigens, antibodies and their interaction.* Clinics in haematology, 1975. **4**(1): p. 29.

143. Reverberi, R. and L. Reverberi, *Factors affecting the antigen-antibody reaction.* Blood Transfusion, 2007. **5**(4): p. 227.

144. Hughes-Jones, N., B. Gardner, and R. Telford, *The effect of pH and ionic strength on the reaction between anti-D and erythrocytes.* Immunology, 1964. **7**(1): p. 72.

145. Karush, F., *Immunologic specificity and molecular structure.* Advances in Immunology, 1963. **2**: p. 1-40.

146. Barnes, A.E., *The specificity of pH and ionic strength effects on the kinetics of the Rh (D)-anti-Rh (D) system.* The Journal of Immunology, 1966. **96**(5): p. 854-864.

147. Boenisch, T., *| Antibodies.* Education Guide Immunohistochemical Staining Methods Fifth Edition, 2009: p.

1.

148. Ning, G., et al., *A Non-enzyme Amperometric Immunosensor for Rapid Determination of Human Immunodeficiency Virus p24 Based on Magnetism Controlled Carbon Nanotubes Modified Printed Electrode.* Chinese Journal of Analytical Chemistry, 2010. **38**(11): p. 1556–1562.

149. Eissa, S., et al., *Electrochemical immunosensor for the milk allergen b-lactoglobulin based on electrografting of organic film on graphene modified screen-printed carbon electrodes.* Biosensors and Bioelectronics, 2012(38): p. 308 - 313.

150. Xinle, J., et al., *A label-free immunosensor based on graphene nanocomposites for simultaneous multiplexed electrochemical determination of tumor markers.* Biosensors and Bioelectronics, 2014. **53**: p. 160 - 166.

151. Yongmei, W., et al., *Silver–graphene oxide nanocomposites as redox probes for electrochemical determination of -1-fetoprotein.* Electrochimica Acta, 2013. **88**: p. 135-140.

152. Changsheng, S., et al., *Electrochemical determination of NADH and ethanol based on ionic liquid-functionalized graphene.* Biosensors and Bioelectronics, 2010. **25**: p. 1504-1508.

153. Chaofeng, O., et al., *Layer-by-layer self-assembled multilayer films of multi-walled carbon nanotubes and platinum–Prussian blue hybrid nanoparticles for the fabrication of amperometric immunosensor.* Journal of Electroanalytical Chemistry, 2008. **624**: p. 287-292.

154. Ying, Z., et al., *Supramolecular assembly of perylene derivatives on Au functionalized graphene for sensitivity enhancement of electrochemiluminescent immunosensor.* Journal of Electroanalytical Chemistry, 2013(709): p. 106 - 110.

155. Wei, Q., et al., *Ultrasensitive detection of kanamycin in animal derived foods by label-free electrochemical immunosensor.* Food Chemistry, 2012(134): p. 1601 - 1606.

156. Peng, H.-P., et al., *Label-free electrochemical immunosensor based on multi-functional gold nanoparticles–polydopamine–thionine–graphene oxide nanocomposites film for determination of alpha-fetoprotein.* Journal of Electroanalytical Chemistry, 2014(712): p. 89 - 95.

157. Tessy Theres, B., et al., *Metal decorated graphene nanosheets as immobilization matrix for amperometric glucose biosensor.* Sensors and Actuators B, 2010. **145**: p. 71-77.

158. Changsheng, S., et al., *Graphene/AuNPs/chitosan nanocomposites film for glucose biosensing.* Biosensors and Bioelectronics, 2010. **25**: p. 1070-1074.

159. Zhongju, S., et al., *Dual amplification strategy for the fabrication of highly sensitive amperometric*

immunosensor based on nanocomposite functionalized interface. Sensors and Actuators B, 2010. **145**: p. 817-825.

160. Yan, L., et al., *Amperometric immunosensor for the detection of Escherichia coli O157:H7 in food specimens.* Analytical Biochemistry, 2012(421): p. 227 - 233.

161. Ying, Z., et al., *A reagentless amperometric immunosensor based on gold nanoparticles/thionine/Nafion-membrane-modified gold electrode for determination of a-1-fetoprotein.* Electrochemistry Communications, 2005. **7**: p. 355-360.

162. Gomes-Filho, S.L.R., et al., *A carbon nanotube-based electrochemical immunosensor for cardiac troponin T.* Microchemical Journal, 2013(109): p. 10-15.

163. Darain, F., S.-U. Park, and Y.-B. Shim, *Disposable amperometric immunosensor system for rabbit IgG using a conducting polymer modified screen-printed electrode.* Biosensors and Bioelectronics, 2003. **18**(5): p. 773-780.

164. Wu, Y., et al., *A novel reagentless amperometric immunosensor based on gold nanoparticles/TMB/Nafion-modified electrode.* Biosensors and Bioelectronics, 2009. **24**(5): p. 1389-1393.

165. Liu, Z.-M., et al., *Core–shell magnetic nanoparticles applied for immobilization of antibody on carbon paste electrode and amperometric immunosensing.* Sensors and Actuators B: Chemical, 2006. **113**(2): p. 956-962.

166. Preechaworapun, A., et al., *Development of amperometric immunosensor using boron-doped diamond with poly (o-aminobenzoic acid).* Analytical chemistry, 2008. **80**(6): p. 2077-2083.

167. Rao, V.K., et al., *Amperometric immunosensor for detection of antibodies of< i> Salmonella typhi</i> in patient serum.* Analytica chimica acta, 2005. **531**(2): p. 173-177.

168. Zhuo, Y., et al., *A reagentless amperometric immunosensor based on gold nanoparticles/thionine/Nafion-membrane-modified gold electrode for determination of* **α***-1-fetoprotein.* Electrochemistry communications, 2005. **7**(4): p. 355-360.

169. Lin, J., et al., *Sensitive amperometric immunosensor for* **α***-fetoprotein based on carbon nanotube/gold nanoparticle doped chitosan film.* Analytical biochemistry, 2009. **384**(1): p. 130-135.

170. Yu, H., et al., *A disposable amperometric immunosensor for* **α***-1-fetoprotein based on enzyme-labeled antibody/chitosan-membrane-modified screen-printed carbon electrode.* Analytical biochemistry, 2004. **331**(1): p. 98-105.

171. Xu, Y.Y., et al., *A microelectronic technology based amperometric immunosensor for* **α***-fetoprotein using*

mixed self-assembled monolayers and gold nanoparticles. Analytica chimica acta, 2006. **561**(1): p. 48-54.

172. Lu, X., et al., *A reagentless amperometric immunosensor for α-1-fetoprotein based on gold nanowires and ZnO nanorods modified electrode.* Analytica chimica acta, 2008. **615**(2): p. 158-164.

173. Dai, Z., et al., *Novel amperometric immunosensor for rapid separation-free immunoassay of carcinoembryonic antigen.* Journal of immunological methods, 2004. **287**(1): p. 13-20.

174. Ou, C., et al., *A novel amperometric immunosensor based on layer-by-layer assembly of gold nanoparticles–multi-walled carbon nanotubes-thionine multilayer films on polyelectrolyte surface.* Analytica chimica acta, 2007. **603**(2): p. 205-213.

175. He, X., et al., *A sensitive amperometric immunosensor for carcinoembryonic antigen detection with porous nanogold film and nano-Au/chitosan composite as immobilization matrix.* Journal of biochemical and biophysical methods, 2008. **70**(6): p. 823-829.

176. Li, X., et al., *Amperometric immunosensor based on toluidine blue/nano-Au through electrostatic interaction for determination of carcinoembryonic antigen.* Journal of biotechnology, 2006. **123**(3): p. 356-366.

177. Zhuo, Y., et al., *Nanostructured conductive material containing ferrocenyl for reagentless amperometric immunosensors.* Biomaterials, 2008. **29**(10): p. 1501-1508.

178. Li, N., et al., *An amperometric immunosensor with a DNA polyion complex membrane/gold nanoparticles-backbone for antibody immobilisation.* Electrochimica Acta, 2008. **54**(2): p. 235-241.

179. Shi, W. and Z. Ma, *A novel label-free amperometric immunosensor for carcinoembryonic antigen based on redox membrane.* Biosensors and Bioelectronics, 2011. **26**(6): p. 3068-3071.

180. Wu, L., F. Yan, and H. Ju, *An amperometric immunosensor for separation-free immunoassay of CA125 based on its covalent immobilization coupled with thionine on carbon nanofiber.* Journal of immunological methods, 2007. **322**(1): p. 12-19.

181. Weng, S., et al., *Label-free electrochemical immunosensor based on K< sub> 3</sub>[Fe (CN)< sub> 6</sub>] as signal for facile and sensitive determination of tumor necrosis factor-alpha.* Sensors and Actuators B: Chemical, 2013. **184**: p. 1-7.

182. Kalab, T. and P. Skládal, *A disposable amperometric immunosensor for 2, 4-dichlorophenoxyacetic acid.* Analytica chimica acta, 1995. **304**(3): p. 361-368.

183. Grennan, K., et al., *Atrazine analysis using an amperometric immunosensor based on single-chain antibody fragments and regeneration-free multi-calibrant measurement.* Analytica Chimica Acta, 2003.

500(1): p. 287-298.

184. Bäumner, A.J. and R.D. Schmid, *Development of a new immunosensor for pesticide detection: a disposable system with liposome-enhancement and amperometric detection.* Biosensors and Bioelectronics, 1998. **13**(5): p. 519-529.

185. Fähnrich, K., M. Pravda, and G. Guilbault, *Disposable amperometric immunosensor for the detection of polycyclic aromatic hydrocarbons (PAHs) using screen-printed electrodes.* Biosensors and Bioelectronics, 2003. **18**(1): p. 73-82.

186. Chen, J., et al., *Reagentless amperometric immunosensor for human chorionic gonadotrophin based on direct electrochemistry of horseradish peroxidase.* Biosensors and Bioelectronics, 2005. **21**(2): p. 330-336.

187. Elham, A., et al., *Multiwall carbon nanotube-ionic liquid electrode modified with gold nanoparticles as a base for preparation of a novel impedimetric immunosensor for low level detection of human serum albumin in biological fluids.* Journal of Pharmaceutical and Biomedical Analysis, 2014(92): p. 74 - 81.

188. Haixia, F., et al., *Construction of label-free electrochemical immunosensor on mesoporous carbon nanospheres for breast cancer susceptibility gene.* Analytica Chimica Acta, 2013(770): p. 62 - 67.

189. Pemberton, R., et al., *A comparison of 1-naphthyl phosphate and 4 aminophenyl phosphate as enzyme substrates for use with a screen-printed amperometric immunosensor for progesterone in cows' milk.* Biosensors and Bioelectronics, 1999. **14**(5): p. 495-503.

190. Lu, B., et al., *Development of an "electrically wired" amperometric immunosensor for the determination of biotin based on a non-diffusional redox osmium polymer film containing an antibody to the enzyme label horseradish peroxidase.* Analytica chimica acta, 1997. **345**(1): p. 59-66.

191. Campàs, M., et al., *Enzymatic recycling-based amperometric immunosensor for the ultrasensitive detection of okadaic acid in shellfish.* Biosensors and Bioelectronics, 2008. **24**(4): p. 716-722.

192. Wang, S.-F. and Y.-M. Tan, *A novel amperometric immunosensor based on Fe3O4 magnetic nanoparticles/chitosan composite film for determination of ferritin.* Analytical and bioanalytical chemistry, 2007. **387**(2): p. 703-708.

193. Wang, G., et al., *Dual amplification strategy for the fabrication of highly sensitive interleukin-6 amperometric immunosensor based on poly-dopamine.* Langmuir, 2010. **27**(3): p. 1224-1231.

194. Darain, F., et al., *A separation-free amperometric immunosensor for vitellogenin based on screen-printed carbon arrays modified with a conductive polymer.* Biosensors and Bioelectronics, 2005. **20**(9): p. 1780-1787.

195. Campanella, L., et al., *New amperometric and potentiometric immunosensors for anti-human immunoglobulin G determinations.* Sensors and Actuators B: Chemical, 1999. **55**(1): p. 23-32.

196. Liu, K., et al., *Graphene-assisted dual amplification strategy for the fabrication of sensitive amperometric immunosensor.* Biosensors and Bioelectronics, 2011. **26**(8): p. 3627-3632.

197. Liu, G.-D., et al., *Renewable amperometric immunosensor for Schistosoma japonium antibody assay.* Analytical chemistry, 2001. **73**(14): p. 3219-3226.

198. Lei, C.-X., et al., *Amperometric immunosensor for< i> Schistosoma japonicum</i> antigen using antibodies loaded on a nano-Au monolayer modified chitosan-entrapped carbon paste electrode.* Sensors and Actuators B: Chemical, 2003. **96**(3): p. 582-588.

199. Liang, R., J. Qiu, and P. Cai, *A novel amperometric immunosensor based on three-dimensional sol–gel network and nanoparticle self-assemble technique.* Analytica chimica acta, 2005. **534**(2): p. 223-229.

200. Qiu, J.-D., et al., *A label-free amperometric immunosensor based on biocompatible conductive redox chitosan-ferrocene/gold nanoparticles matrix.* Biosensors and Bioelectronics, 2009. **25**(4): p. 852-857.

201. E.P., M., et al., *Amperometric enzyme immunosensor for the determination of the antigen of the pathogenic fungi Trichophyton rubrum.* Analytica Chimica Acta, 2000. **411**: p. 13-18.

202. Dong, J., et al., *A label-free electrochemical impedance immunosensor based on AuNPs/PAMAM-MWCNT-Chi nanocomposite modified glassy carbon electrode for detection of Salmonella typhimurium in milk.* Food Chemistry, 2013(141): p. 1980–1986.

203. El Ichi, S., et al., *Microconductometric immunosensor for label-free and sensitive detection of Gram-negative bacteria.* Biosensors and Bioelectronics, 2014. **54**: p. 378-384.

204. Huang, J., et al., *An electrochemical impedimetric immunosensor for label-free detection of< i> Campylobacter jejuni</i> in diarrhea patients' stool based on O-carboxymethylchitosan surface modified Fe< sub> 3</sub> O< sub> 4</sub> nanoparticles.* Biosensors and Bioelectronics, 2010. **25**(5): p. 1204-1211.

205. Yalow, R.S. and S.A. Berson, *Immunoassay of endogenous plasma insulin in man.* Obesity research, 1996. **4**(6): p. 583-600.

206. Miyai, K. and C. Price, *Problems for improving performance in immunoassay.* Journal of the International Federation of Clinical Chemistry/IFCC, 1992. **4**(4): p. 154-163.

207. O'Malley, S., *Recent advances in label-free biosensors applications in protein biosynthesis and hts screening.* Protein Biosynthesis (TE Esterhouse and LB Petrinos, eds.), Nova Science Publishers, Inc, 2008.

208. Xiulan, H., et al., *A sensitive amperometric immunosensor for carcinoembryonic antigen detection with porous nanogold film and nano-Au/chitosan composite as immobilization matrix.* J. Biochem. Biophys. Methods, 2008(70): p. 823-829.

209. Na, L., C. Xia, and M. Zhanfang, *Ionic liquid functionalized graphene/Au nanocomposites and its application for electrochemical immunosensor.* Biosensors and Bioelectronics, 2013. **48**: p. 33 - 38.

210. Ying, Z., et al., *Amperometric enzyme immunosensors based on layer-by-layer assembly of gold nanoparticles and thionine on Nafion modified electrode surface for alpha-1-fetoprotein determinations.* Sensors and Actuators B, 2006. **114**: p. 631-639.

211. Xiao-Qi, R., et al., *A sensitive amperometric immunosensor for alpha-fetoprotein based on carbon nanotube/DNA/Thi/nano-Au modified glassy carbon electrode.* Colloids and Surfaces B: Biointerfaces, 2010. **79**: p. 421-426.

212. Huang, K.-W., et al., *Feasibility studies for assaying alpha-fetoprotein using antibody-activated magnetic nanoparticles.* International journal of nanomedicine, 2012. **7**: p. 1991.

213. Petr, S., *Advances in Electrochemical Immunosensors.* Electroanalysis, 1997. **9**(10): p. 737-806.

214. Shen, G., X.H. , and S.Z. , *A signal-enhanced electrochemical immunosensor based on dendrimer functionalized-graphene as a label for the detection of a-1-fetoprotein.* Journal of Electroanalytical Chemistry, 2014(717-718): p. 172 - 176.

215. Xuxiao, L., et al., *A reagentless amperometric immunosensor for alpha-1-fetoprotein based on gold nanowires and ZnO nanorods modified electrode.* Analytica Chimica Acta, 2008(615): p. 158-164.

216. Biermann, H.W., *Important Factors that Influence the Determination of Detection Limits*. 1989: Environmental Hazards Assessment Program.

217. Yuan, Y., H. He, and L.J. Lee, *Protein A - based antibody immobilization onto polymeric microdevices for enhanced sensitivity of enzyme - linked immunosorbent assay.* Biotechnology and bioengineering, 2009. **102**(3): p. 891-901.

218. Cavalcanti, I.T., et al., *A label-free immunosensor based on recordable compact disk chip for early diagnostic of the dengue virus infection.* Biochemical Engineering Journal, 2012. **67**: p. 225-230.

219. Parkash, O., C.Y. Yean, and R.H. Shueb, *Screen Printed Carbon Electrode Based Electrochemical Immunosensor for the Detection of Dengue NS1 Antigen.* Diagnostics, 2014. **4**(4): p. 165-180.

220. Armbruster, D.A. and T. Pry, *Limit of blank, limit of detection and limit of quantitation.* Clin Biochem Rev, 2008. **29**(Suppl 1): p. S49-S52.

221. Borgmann, S., et al., *Amperometric biosensors.* Advances in Electrochemical Science and Engineering, 2011.

222. Chrouda, A., et al., *An Immunosensor for Pathogenic Staphylococcus aureus Based on Antibody Modified Aminophenyl-Au Electrode.* ISRN Electrochemistry, 2013. **2013**.

223. Mendham, J., *Vogels textbook of quantitative chemical analysis*. 2006: Pearson Education India.

224. Kong, F.-Y., et al., *A novel lable-free electrochemical immunosensor for carcinoembryonic antigen based on gold nanoparticles–thionine–reduced graphene oxide nanocomposite film modified glassy carbon electrode.* Talanta, 2011. **85**(5): p. 2620-2625.

225. Cui, R., et al., *Horseradish peroxidase-functionalized gold nanoparticle label for amplified immunoanalysis based on gold nanoparticles/carbon nanotubes hybrids modified biosensor.* Biosensors and bioelectronics, 2008. **23**(11): p. 1666-1673.

226. Huang, K.-J., et al., *An electrochemical amperometric immunobiosensor for label-free detection of α-fetoprotein based on amine-functionalized graphene and gold nanoparticles modified carbon ionic liquid electrode.* Journal of Electroanalytical Chemistry, 2011. **656**(1): p. 72-77.

227. Bellezza, F., et al., *Zirconium phosphate and modified zirconium phosphates as supports of lipase. Preparation of the composites and activity of the supported enzyme.* Langmuir, 2002. **18**(23): p. 8737-8742.

228. Ou, C., et al., *Layer-by-layer self-assembled multilayer films of multi-walled carbon nanotubes and platinum–Prussian blue hybrid nanoparticles for the fabrication of amperometric immunosensor.* Journal of Electroanalytical Chemistry, 2008. **624**(1): p. 287-292.

229. Park, H.J., et al., *Growth and properties of few-layer graphene prepared by chemical vapor deposition.* Carbon, 2010. **48**(4): p. 1088-1094.

230. Yoo, K., et al., *Direct physical exfoliation of few-layer graphene from graphite grown on a nickel foil using polydimethylsiloxane with tunable elasticity and adhesion.* Nanotechnology, 2013. **24**(20): p. 205302.

231. Lin, J., et al., *Sensitive immunosensor for the label-free determination of tumor marker based on carbon nanotubes/mesoporous silica and graphene modified electrode.* Biosensors and Bioelectronics, 2013. **41**: p. 342-347.

232. Wu, Y., et al., *Silver–graphene oxide nanocomposites as redox probes for electrochemical determination of α-1-fetoprotein.* Electrochimica Acta, 2013. **88**: p. 135-140.

233. Shen, G., et al., *One-step immobilization of antibodies for α-1-fetoprotein immunosensor based on*

dialdehyde cellulose/ionic liquid composite. Analytical biochemistry, 2014.

234. Yu, S., X. Cao, and M. Yu, *Electrochemical immunoassay based on gold nanoparticles and reduced graphene oxide functionalized carbon ionic liquid electrode.* Microchemical Journal, 2012. **103**: p. 125-130.

235. Cai, Y., et al., *Electrochemical immunoassay for carcinoembryonic antigen based on signal amplification strategy of nanotubular mesoporous PdCu alloy.* Biosensors and Bioelectronics, 2012. **36**(1): p. 6-11.

236. Samanman, S., et al., *Highly-sensitive label-free electrochemical carcinoembryonic antigen immunosensor based on a novel Au nanoparticles–graphene–chitosan nanocomposite cryogel electrode.* Analytica chimica acta, 2015. **853**: p. 521-532.

237. Lu, W., et al., *Large-scale synthesis of ultrathin Au-Pt nanowires assembled on thionine/graphene with high conductivity and sensitivity for electrochemical immunosensor.* Electrochimica Acta, 2014. **130**(0): p. 335-343.

238. Hua, Y., et al., *A disposable amperometric immunosensor for alpha-1-fetoprotein based on enzyme-labeled antibody/chitosan-membrane-modified screen-printed carbon electrode.* Analytical Biochemistry, 2004. **331**: p. 98-105.

239. Wen, J., et al., *Amperometric immunosensor based on multiwalled carbon nanotubes/Prussian blue/nanogold-modified electrode for determination of a-fetoprotein.* Analytical Biochemistry, 2010. **407**: p. 65-71.

240. TingTing, Q., et al., *Label-free alpha fetoprotein immunosensor established by the facile synthesis of a palladium–graphene nanocomposite.* Biosensors and Bioelectronics, 2014. **61**: p. 245-250.

241. Haake, D.A., et al., *The leptospiral major outer membrane protein LipL32 is a lipoprotein expressed during mammalian infection.* Infection and immunity, 2000. **68**(4): p. 2276-2285.

242. Michielsen, E.C., et al., *Interpretation of cardiac troponin T behaviour in size-exclusion chromatography.* Clinical Chemical Laboratory Medicine, 2006. **44**(12): p. 1422-1427.

243. Kajioka, S., et al., *Endogenous Cardiac Troponin T Modulates Ca2+-Mediated Smooth Muscle Contraction.* Scientific reports, 2012. **2**.

244. Silva, B.V., et al., *Disposable immunosensor for human cardiac troponin T based on streptavidin-microsphere modified screen-printed electrode.* Biosensors and Bioelectronics, 2010. **26**(3): p. 1062-1067.

245. Jie, Z., et al., *An ultrasensitive electrochemical immunosensor for carcinoembryonic antigen detection based on staphylococcal proteinA—Au nanoparticle modified gold electrode.* Sensors and Actuators B,

2014(197): p. 220 - 227.

246. Andrews, D., G. Scholes, and G. Wiederrecht, *Comprehensive Nanoscience and Technology, Five-Volume set: Online Version*. 2010: Elsevier Science.

247. Frens, G., *Controlled nucleation for the regulation of the particle size in monodisperse gold suspensions.* Nature, 1973. **241**(105): p. 20-22.

248. Shi, X., et al., *Spectroscopic investigation of the interactions between gold nanoparticles and bovine serum albumin.* Chinese Science Bulletin, 2012. **57**(10): p. 1109-1115.

249. Bhalla, V., et al., *Gold nanoparticles mediated label-free capacitance detection of cardiac troponin I.* Sensors and Actuators B: Chemical, 2012. **161**(1): p. 761-768.

250. Eissa, S., et al., *Electrochemical immunosensor for the milk allergen β-lactoglobulin based on electrografting of organic film on graphene modified screen-printed carbon electrodes.* Biosensors and Bioelectronics, 2012. **38**(1): p. 308-313.

251. Dou, W., W.T. , and G.Z. , *A disposable electrochemical immunosensor arrays using 4-channel screen-printed carbon electrode for simultaneous detection of Escherichia coli O157:H7 and Enterobacter sakazakii.* Electrochimica Acta, 2013(97): p. 79-85.

252. Taher, A. and M. Shabnam, *A Nafion-free non-enzymatic amperometric glucose sensor based on copper oxide nanoparticles - graphene nanocomposite.* Sensors and Actuators B, 2014(198): p. 438–447.

253. Jia, X., et al., *A label-free immunosensor based on graphene nanocomposites for simultaneous multiplexed electrochemical determination of tumor markers.* Biosensors and Bioelectronics, 2014. **53**: p. 160-166.

254. Han, J., J. Ma, and Z. Ma, *One-step synthesis of graphene oxide–thionine–Au nanocomposites and its application for electrochemical immunosensing.* Biosensors and Bioelectronics, 2013. **47**: p. 243-247.

255. Ran, X.-Q., et al., *A sensitive amperometric immunosensor for alpha-fetoprotein based on carbon nanotube/DNA/Thi/nano-Au modified glassy carbon electrode.* Colloids and Surfaces B: Biointerfaces, 2010. **79**(2): p. 421-426.

256. Lifang, Z., et al., *Ionic liquid functionalized graphene based immunosensor for sensitive detection of carbohydrate antigen 15-3 integrated with Cd2p-functionalized nanoporous TiO2 as labels.* Biosensors and Bioelectronics, 2014. **59**: p. 75-80.

257. Buser, H., et al., *The crystal structure of Prussian blue: Fe4 [Fe (CN) 6] 3. xH2O.* Inorganic Chemistry, 1977. **16**(11): p. 2704-2710.

258. Ataka, T.S.I.E.L. and K.S.I.E.L. Iwasa, *Secondary cell*. 1985, Google Patents.

259. Padigi, P., et al., *Prussian Green: A High Rate Capacity Cathode for Potassium Ion Batteries.* Electrochimica Acta, 2015. **166**: p. 32-39.

260. Ricci, F. and G. Palleschi, *Sensor and biosensor preparation, optimisation and applications of Prussian Blue modified electrodes.* Biosensors and Bioelectronics, 2005. **21**(3): p. 389-407.

261. Karyakin, A.A., *Prussian blue and its analogues: electrochemistry and analytical applications.* Electroanalysis, 2001. **13**(10): p. 813-819.

262. Matlosz, M. and E.S.E. Division, *Fundamental Aspects of Electrochemical Deposition and Dissolution: Proceedings of the International Symposium*. 2000: Electrochemical Society.

263. Bai, X., G. Chen, and K.-K. Shiu, *Electrochemical biosensor based on reduced graphene oxide modified electrode with Prussian blue and poly (toluidine blue O) coating.* Electrochimica Acta, 2013. **89**: p. 454-460.

264. Huang, K.-J., et al., *Label-free amperometric immunobiosensor based on a gold colloid and Prussian blue nanocomposite film modified carbon ionic liquid electrode.* Analytical and bioanalytical chemistry, 2010. **397**(8): p. 3553-3561.

265. Guan, J.-G., Y.-Q. Miao, and J.-R. Chen, *Prussian blue modified amperometric FIA biosensor: one-step immunoassay for α-fetoprotein.* Biosensors and Bioelectronics, 2004. **19**(8): p. 789-794.

266. Zonghua, W., et al., *Facile preparation of a Pt/Prussian blue/graphene composite and its application as an enhanced catalyst for methanol oxidation.* Electrochimica Acta, 2014. **121**: p. 245-252.

267. Shaikh, A., et al., *Cyclic voltammetric studies of the redox behavior of iron (III)-vitamin B6 complex at carbon paste electrode.* Russian Journal of Electrochemistry, 2006. **42**(6): p. 620-625.

268. Liu, X.-W., et al., *Graphene oxide sheet–prussian blue nanocomposites: Green synthesis and their extraordinary electrochemical properties.* Colloids and Surfaces B: Biointerfaces, 2010. **81**(2): p. 508-512.

269. Xue, M.-H., et al., *In situ immobilization of glucose oxidase in chitosan–gold nanoparticle hybrid film on Prussian Blue modified electrode for high-sensitivity glucose detection.* Electrochemistry communications, 2006. **8**(9): p. 1468-1474.

270. Knowles, K.R., et al., *Layer-by-layer assembled multilayers of polyethylenimine-stabilized platinum nanoparticles and PEDOT: PSS as anodes for the methanol oxidation reaction.* ACS applied materials & interfaces, 2012. **4**(7): p. 3575-3583.

271. Song, Z., et al., *Dual amplification strategy for the fabrication of highly sensitive amperometric*

immunosensor based on nanocomposite functionalized interface. Sensors and Actuators B: Chemical, 2010. **145**(2): p. 817-825.

272. Yao, Z., et al., *Electrochemical sensing based on graphene oxide/Prussian blue hybrid film modified electrode.* Electrochimica Acta, 2011. **56**: p. 1239-1245.

273. Chen, S., et al., *A new antibody immobilization technique based on organic polymers protected Prussian blue nanoparticles and gold colloidal nanoparticles for amperometric immunosensors.* Sensors and Actuators B: Chemical, 2008. **135**(1): p. 236-244.

274. Thanh, N.T.K. and Z. Rosenzweig, *Development of an aggregation-based immunoassay for anti-protein A using gold nanoparticles.* Analytical chemistry, 2002. **74**(7): p. 1624-1628.

275. Yang, H., et al., *Electrochemically deposited nanocomposite of chitosan and carbon nanotubes for detection of human chorionic gonadotrophin.* Colloids and Surfaces B: Biointerfaces, 2011. **82**(2): p. 463-469.

276. Zhao, H., et al., *An ultra-sensitive acetylcholinesterase biosensor based on reduced graphene oxide-Au nanoparticles-β-cyclodextrin/Prussian blue-chitosan nanocomposites for organophosphorus pesticides detection.* Biosensors and Bioelectronics, 2015. **65**: p. 23-30.

277. Babacan, S., et al., *Evaluation of antibody immobilization methods for piezoelectric biosensor application.* Biosensors and Bioelectronics, 2000. **15**(11): p. 615-621.

278. MOKS, T., et al., *Staphylococcal protein A consists of five IgG - binding domains.* European Journal of Biochemistry, 1986. **156**(3): p. 637-643.

279. Tatlybaeva, E.B., et al., *Atomic force microscopy recognition of protein A on Staphylococcus aureus cell surfaces by labelling with IgG–Au conjugates.* Beilstein journal of nanotechnology, 2013. **4**(1): p. 743-749.

280. Deng, S., et al., *Electrocatalytic reduction of coreactant by highly loaded dendrimer-encapsulated palladium nanoparticles for sensitive electrochemiluminescent immunoassay.* Chemical Communications, 2012. **48**(73): p. 9159-9161.

281. Yao, C., et al., *Development of a quartz crystal microbalance biosensor with aptamers as bio-recognition element.* Sensors, 2010. **10**(6): p. 5859-5871.

282. Xiong, P., et al., *An ultrasensitive electrochemical immunosensor for alpha-fetoprotein using an envision complex-antibody copolymer as a sensitive label.* Materials, 2012. **5**(12): p. 2757-2772.

283. Kemmegne-Mbouguen, J.C., et al., *Carcinoembryonic Antigen Immunosensor Developed with Organoclay Nanogold Composite Film.* Int. J. Electrochem. Sci, 2014. **9**: p. 478-492.

284. Geng, P., et al., *Self-assembled monolayers-based immunosensor for detection of Escherichia coli using electrochemical impedance spectroscopy.* Electrochimica Acta, 2008. **53**(14): p. 4663-4668.

285. Janeway, C.A., et al., *The interaction of the antibody molecule with specific antigen.* 2001.

286. Li, Y., et al., *Disposable amperometric immunosensor based on layer-by-layer electro-depositing of the nanogold particles, prussian blue-modified indium tin oxide for determination of α-fetoprotein.* Journal of Chemical Sciences, 2009. **121**(6): p. 1069-1076.

287. Li, Q., et al., *Improvement of a low pH antigen-antibody dissociation procedure for ELISA measurement of circulating anti-Aβ antibodies.* BMC neuroscience, 2007. **8**(1): p. 22.

288. Kress-Rogers, E. and C.J.B. Brimelow, *Instrumentation and Sensors for the Food Industry*. 2001: Woodhead.

289. Atassi, M.Z., C.J. Van Oss, and D.R. Absolom, *Molecular Immunology: A Textbook*. 1984: Taylor & Francis.

290. Pasta, M., et al., *Full open-framework batteries for stationary energy storage.* Nature communications, 2014. **5**.

291. Zhong, X., R. Yuan, and Y.-Q. Chai, *Synthesis of chitosan-Prussian blue-graphene composite nanosheets for electrochemical detection of glucose based on pseudobienzyme channeling.* Sensors and Actuators B: Chemical, 2012. **162**(1): p. 334-340.

292. Hasan, M.M., et al., *Study of redox behavior of Cd (II) and interaction of Cd (II) with proline in the aqueous medium using cyclic voltammetry.* Journal of Saudi Chemical Society, 2012. **16**(2): p. 145-151.

293. Avaca, L., et al., *Theory of Cyclic Voltammetry for Quasi - Reversible Electrodeposition Reactions with insoluble Products.* Berichte der Bunsengesellschaft für physikalische Chemie, 1993. **97**(1): p. 70-76.

294. Gosser, D.K., *Cyclic voltammetry: simulation and analysis of reaction mechanisms*. 1993: VCH New York.

295. Zhang, R.-z., et al., *Polydopamine and graphene oxide synergistically modified Prussian blue electrochemical immunosensor for the detection of alpha-fetoprotein with enhanced stability and sensibility.* RSC Advances, 2015. **5**(48): p. 38176-38182.

296. James, A.E. and J.D. Driskell, *Monitoring gold nanoparticle conjugation and analysis of biomolecular binding with nanoparticle tracking analysis (NTA) and dynamic light scattering (DLS).* Analyst, 2013. **138**(4): p. 1212-1218.

297. Gagnon, P., et al., *Transient conformational modification of immunoglobulin G during purification by protein A affinity chromatography.* Journal of Chromatography A, 2015. **1395**: p. 136-142.

298. Nguyen, T., B. Ghebrehiwet, and E.I. Peerschke, *Staphylococcus aureus protein A recognizes platelet gC1qR/p33: a novel mechanism for staphylococcal interactions with platelets.* Infection and immunity,

2000. **68**(4): p. 2061-2068.

Appendix

1. Prussian blue concentration optimization

Table 11: Peak anodic current value for each type of PB concentration (unit in amps)

	2mM	15mM	40mM
Max i_{pa}	51.0E-05	1.08E-04	1.08E-04

2. Chitosan layers

Table 12: Numerical details of $\%\Delta i_{pa}$ after immersing CS-covered electrode in 0.025 M PBS for 18 hours

	elec01	elec02	elec03	$\bar{x}\Delta i_{pa}$ (%)	%RSD
0 layer	58.43285	63.74197	51.47416	57.88299	8.678516
1 layer	15.94904	17.15256	16.08941	16.39701	3.276965
2 layers	9.068807	9.566267	9.896138	9.510404	3.575647
3 layers	4.112676	3.975762	4.279644	4.122694	3.014075

3. Effect of antibody incubation time

Table 13: %difference in anodic peak of each electrode after incubate with antibody for different time period (unit in amps)

	No.	Pre-Ab i_{pa}	Post-Ab i_{pa}	%Difference	%Diff.Average	%RSD
2 hrs	1	7.59E-05	7.03E-05	7.318057	7.336236	2.8164
	2	7.83E-05	7.28E-05	7.092753		
	3	7.00E-05	6.47E-05	7.597898		
6 hrs	4	7.61E-05	6.29E-05	17.39487	16.36254	4.4809
	5	7.39E-05	6.23E-05	15.76226		
	6	6.59E-05	5.54E-05	15.93049		
18 hrs	7	5.60E-05	4.13E-05	26.22585	23.56949	10.3487
	8	5.69E-05	4.31E-05	24.14706		
	9	7.28E-05	5.8E-05	20.33556		

4. Effect of PrA concentration on antibody immobilization

Table 14: %difference anodic peak of electrode with different concentrations of PrA after antibody incubation (unit in amps)

PrA	preAb	postAb	%i_{pa} drop
0.002	8.66E-05	8.54E-05	1.374224
0.01	8.36E-05	7.45E-05	10.9814
0.05	7.28E-05	6.47E-05	11.11103
0.1	7.34E-05	4.51E-05	38.553

5. Effect of PrA concentration on antigen detection

Table 15: %difference in anodic peak of each electrode with different concentration of PrA after incubation of antigen

PrA	elec01	elec02	elec03	Average	Max	Min
0.002	-14.6481	-18.4485	-15.4466	16.18104	1.5329	2.2675
0.01	-20.0489	-16.6403	N/A	18.34459	1.7043	1.7043
0.05	-3.02399	-6.4762	N/A	4.750098	1.72611	1.72611
0.1	-0.06076	0.441004	-0.96751	0.195753	0.245254	0.77176

6. Effect of antigen solution pH

Table 16: %difference in anodic peak of each electrode after incubation of antigen with different pH

pH	name	%Diff	Average %ipa drop	%RSD
	elec01	17.79213		
	elec02	20.26307	19.00427	5.310903
pH 4	elec03	18.9576		
	elec04	21.30976		
	elec05	24.24177	22.68109	5.310393
pH 5	elec06	22.49173		
pH 6	elec07	25.26572		

	elec08	22.07328	24.10905	5.989297
	elec09	24.98817		
	elec10	16.00365		
	elec11	14.99173	15.15099	4.231687
pH 7	elec12	14.4576		

7. CV characteristics

Table 17: peak anodic current of each CV in figure 34, unit in amps

	Blank SPCE	**PPBx1**	**CSx3**	**cAuNP**	**PrA**	**Ab**	**BSA**	**Ag(250 ng/ml pH6)**
i_{pa}	2.56E-07	1.05E-04	8.15E-05	7.50E-05	5.66E-05	4.05E-05	3.93E-05	3.48E-05

8. Effect of scan rate

Table 18: Current, potential, peak potential separation, and peak current ratio of the antigen-ready electrodes of figure 35

v (V s^{-1})	$v^{1/2}$	E_{pa}(+) (V)	E_{pc}(-) (V)	i_{pa}(+) (μA)	i_{pc}(-) (μA)	$\Delta E_p = E_{pa} - E_{pc}$ (V)	i_{pa}/i_{pc}
0.01	3.162	0.248108	0.128479	18.6615	-18.7256	0.119629	0.996577
0.02	4.472	0.294495	0.082092	30.011	-29.0436	0.212403	1.033309
0.03	5.477	0.328674	0.050354	37.9944	-36.2183	0.27832	1.049039
0.04	6.324	0.357971	0.021057	44.4794	-41.7328	0.336914	1.065814
0.05	7.071	0.384827	-0.0058	50.2899	-46.8018	0.390625	1.074529
0.06	7.745	0.404358	-0.02777	55.4718	-51.2482	0.432129	1.082415
0.07	8.366	0.421448	-0.0473	60.6079	-55.484	0.46875	1.092349
0.08	8.944	0.445862	-0.06195	64.8804	-59.2621	0.507813	1.094804
0.09	9.486	0.450745	-0.08881	68.9392	-62.6526	0.539551	1.100341
0.10	10	0.480042	-0.09857	73.0591	-65.9485	0.578614	1.10782

v = scan rate, $v^{1/2}$ = SQRT of scan rate, E_{pa} = anodic peak potential, E_{pc} = cathodic peak potential, i_{pa} = anodic peak current, i_{pc} = cathodic peak current, ΔE_p = peak potential separation, ipa/ipc = peak current ratio.

9. Calibration curve

Table 19: Averaged %ipa drop of each electrode in LipL32 calibration curve

Ag.conc (ng/ml)	elec1	elec2	elec3	Average %ipa drop	RSD
0	12.06474	12.26066	12.76789	12.36443	2.39633
50	14.25484	14.91965	15.6811	14.95186	3.897276
100	15.10587	16.25467	15.39761	15.58605	3.128159
150	15.92897	16.44425	17.59875	16.65733	4.191171
200	18.20538	17.12507	17.34626	17.55891	2.653703
250	18.24171	17.62915	18.15258	18.00782	1.500549
300	18.90879	18.45891	17.97391	18.4472	2.069427
400	18.95743	19.6667	19.95913	19.52775	2.153735
500	20.28314	19.25765	20.82785	20.12288	3.234992
600	21.2171	22.11407	22.67843	22.0032	2.73468

Table 20: Averaged %ipa drop of each electrode in intact *Leptospira spp.* calibration curve

Ag.conc (ng/ml)	elec1	elec2	elec3	Int.drop% average	RSD
10	14.29822	11.85331	12.84308	12.9982	7.725217
50	17.33344	13.83719	15.96382	15.71149	9.155375
100	19.96561	20.74876	20.64322	20.45253	1.696567
500	19.70231	20.63111	17.36118	19.23153	7.153993
1000	17.46074	19.77967	18.17458	18.47166	5.249808

Table 21: Averaged %ipa drop of each electrode in sonicated *Leptospira spp.* calibration curve

Ag.conc (ng/ml)	elec1	elec2	elec3	Soc.drop% average	RSD

10	16.82743	13.89155	12.33403	14.351	12.98145
50	20.12798	18.79895	21.32839	20.08511	5.143548
100	23.83163	23.69757	20.09908	22.54276	7.669023
500	18.01161	15.60141	15.74319	16.45207	6.712096
1000	20.88515	21.15177	15.33197	19.12296	14.02945

10. Storage stability

Table 22: %Change in peak anodic current after stored at 4 °C for different time period

Days	1	2	3	7	14	21
elctrd01	-2.14779	-1.70432	-1.49525	3.611476	8.319164	5.759469
elctrd02	0.606511	0.675359	1.08168	7.359893	8.698111	7.660075
elctrd03	-3.05189	-0.74225	-0.53446	3.473502	6.210589	6.97074
Average%	-1.53105	-0.5904	-0.31601	4.814957	7.742621	6.796761
errMax	2.137565	1.265762	1.39769	2.544936	0.95549	0.863314
errMin	1.520834	1.113914	1.179239	1.341455	1.532032	1.037292

REFERENCES

[1]

APPENDIX

VITA

Zunpitch Kwanyuen: born 1988, April 29th. Taurus. Love to take on challenges but sometimes knowingly bitten off more than he can chew, so he thought M.Sc. in Biomedical engineering would be able to help teach him about how to limit frameworks, and it did excellently.